



LEHIGH
UNIVERSITY

PITA Project PIT-457-04

Comparative Performance of
High Early Strength and Self Consolidating Concrete
For Use in Precast Bridge Beam Construction

FINAL REPORT

By

Clay Naito, Principal Investigator
Geoffrey Brunn, Undergraduate Researcher
Greg Parent, Graduate Student Researcher
Tyler Tate, Graduate Student Researcher

May 2005

ATLSS REPORT NO. 05-03

**ATLSS is a National Center for Engineering Research
on Advanced Technology for Large Structural Systems**

117 ATLSS Drive
Bethlehem, PA 18015-4729

Phone: (610)758-3525

Fax: (610)758-5902

www.atlss.lehigh.edu

Email: inatl@lehigh.edu

1. TABLE OF CONTENTS

1. Table of Contents	1
2. List of Figures	5
3. Abstract	8
4. Acknowledgements	9
5. Overview	10
6. Background	11
6.1. Precast Bridge Construction	11
6.2. Bulb Tee Sizes	11
6.3. Prestressed Beam Production Methods	13
6.4. Conventional Concrete Materials	15
6.5. Self Consolidating Concrete	15
6.5.1. SCC Method 1: HRWR and FA Modification	16
6.5.2. SCC Method 2: VMA & HRWR Modification	16
6.6. Concerns Regarding SCC in Precast Bridge Construction	16
7. Phase 1 Concrete Material Characteristics	18
7.1. Design Requirements	18
7.2. Current Mix Proportioning Requirements	18
7.2.1. FHWA Survey Comparison	20
7.3. HESC and SCC Mix Designs	20
7.4. Concrete Materials	20
7.4.1. Cementitious Material	21
7.4.2. Aggregate	21
7.4.3. Supplementary Admixtures	22
7.5. Plastic Concrete Characteristics	22
7.5.1. Slump and Spread	23
7.5.2. SCC Dynamic Segregation	24
7.5.3. Initial Set	24
7.6. Mechanical Properties	25
7.6.1. Cylinder Fabrication and Curing	26
7.6.2. Compressive Strength	27
7.6.3. Modulus of Elasticity	28
7.6.4. Tensile Properties	30
7.6.5. Creep and Shrinkage	31

7.7. Phase 1 Conclusions	33
8. Reinforcement and Strand Properties	36
8.1. Conventional Reinforcement	36
8.2. Strand Properties.....	36
8.3. Strand Bond Prequalification.....	37
8.4. Strand Property Discussion and Conclusions	40
9. Beam Design Properties.....	42
9.1. PCEF 45” Deep Bulb Tee.....	42
9.2. Beam Fabrication.....	44
9.3. Design Capacity.....	45
9.3.1. Estimated Prestress Losses.....	45
9.3.2. Transfer Length	45
9.4. Shear and Flexure Capacity	46
9.5. Beam Design Summary	46
10. Phase 2 Non-Destructive Evaluation of Bulb Tee Performance	47
10.1. Initial Camber	47
10.2. Elastic Deformations	47
10.3. Measured Effective Prestress.....	49
10.4. As-built Transfer Lengths.....	50
10.5. Estimated Beam Properties Using Measured Effective Prestress.....	52
10.6. Creep and Shrinkage of In-Situ Beam	52
10.7. Non-Destructive Performance Conclusions	53
11. Fabrication Productivity with SCC	54
11.1. Cost-Benefit of SCC in Precast Production.....	54
11.1.1. Product Quality	55
11.2. Surface and Cost Summary	56
12. Experimental Setup and Instrumentation.....	57
12.1. Testing Methodology.....	57
12.1.1. Load Rate	57
12.2. Test Configuration and Boundary Conditions.....	57
12.2.1. Configuration A.....	57
12.2.2. Configuration B.....	57
12.3. Load Application and Self-Weigh Demands	58
12.4. Instrumentation	59
12.4.1. External Strain, Deformation, and Rotation	60

12.4.2. End Slip.....	60
13. Phase 3 Destructive Evaluation of Bulb Tee Capacity	66
13.1. Elastic Response	66
13.1.1. Method 1 – Initial Stiffness	66
13.1.2. Method 2 Strain Measurements.....	67
13.2. Cracking	68
13.3. Global Behavior.....	69
13.3.1. Global Deformation Response	70
13.3.2. Full Span Response	71
13.3.3. Short Span Response	72
13.3.4. Reduced Section Response.....	73
13.3.5. SCC Full Span Observations (Test 1)	73
13.3.6. SCC Short Span Observations (Test 2).....	75
13.3.7. HESC Full Span Observations (Test 3).....	78
13.3.8. HESC Short Span Observations (Test 4)	79
13.3.9. HESC Full Span Observations (Test 5).....	81
13.3.10. HESC Reduced Section Observations (Test 6)	82
13.3.11. SCC Full Span Observations (Test 7)	84
13.3.12. SCC Reduced Section Observations (Test 8).....	84
13.3.13. Bond Slip.....	85
13.4. Phase 2 Conclusions	87
14. Phase 3 – Strand to Concrete Bond Mechanics	89
14.1. Phase 3 Test Matrix	90
14.2. Phase 3 Test Setup.....	90
14.3. Material Properties	91
14.4. Large Block Pullout Tests	91
14.5. Phase 3 Preliminary Conclusions	92
15. Project Conclusions	93
15.1. Mechanical and Durability of Concrete.....	93
15.2. Prestressing Strand	94
15.3. Nondestructive Assessment of Beam	94
15.4. Economic Viability.....	95
15.5. Ultimate Strength of Bridge Beams.....	95
15.6. Summary Conclusions	96
16. SCC Code Recommendations.....	97

17. Future Work..... 98
18. References..... 99

2. LIST OF FIGURES

Figure 1: Precast bridge construction.....	11
Figure 2: PCEF bulb tee standard sections [SPI 2005].....	12
Figure 3: Inverted slump spread test.....	23
Figure 4: J-ring test.....	24
Figure 5: Columnar segregation.....	25
Figure 6: Initial setting time.....	25
Figure 7: Cylinder and prism fabrication.....	26
Figure 8: Temperature variation during initial cure.....	27
Figure 9: Compressive strength gain.....	28
Figure 10: Compressive tests.....	29
Figure 11: Stress-strain response.....	29
Figure 12: Tensile tests.....	31
Figure 13: In-situ instrumentation.....	31
Figure 14: Shrinkage response of material.....	33
Figure 15: Creep response of material.....	33
Figure 16: Large block pullout setup.....	38
Figure 17: Typical strand surface condition.....	38
Figure 18: Pullout load-deformation response.....	39
Figure 19: Specimen cross-section details [SPI].....	42
Figure 20: Beam geometry.....	42
Figure 21: Conventional reinforcement details [SPI].....	43
Figure 22: Beam elevation [SPI].....	43
Figure 23: Modified cross section showing cut prestress strands for tests 6 & 8.....	44
Figure 24: Modified beam geometry.....	44
Figure 25: Beam placement schematic.....	44
Figure 26: Concrete strain gauges.....	47
Figure 27: Strand strain gauge layout.....	48
Figure 28: Overall internal gauge layout.....	48
Figure 29: Effective prestress in beams.....	50
Figure 30: Transfer stress and strain distribution.....	51
Figure 31: Bond stress distribution near member end.....	51
Figure 32: Measured transfer length.....	52
Figure 33: In-situ creep and shrinkage strain.....	53

Figure 34: Surface conditions	55
Figure 35: Force demands on cracked section	57
Figure 36: Side elevation of beam loading plates	59
Figure 37: Moment and shear distribution for loading configurations	59
Figure 38: Instrumentation.....	60
Figure 39: Global instrumentation Test 1 (SCC Full Span).....	61
Figure 40: Global instrumentation Test 2 (SCC Short Span)	61
Figure 41: Global instrumentation Test 3 (HESC Full Span).....	62
Figure 42: Global instrumentation Test 4 (HESC Short Span).....	62
Figure 43: Global instrumentation Test 5 (HESC Full Span).....	63
Figure 44: Global instrumentation Test 6 (HESC Short Cut Span).....	63
Figure 45: Global instrumentation Test 7 (SCC Full Span).....	64
Figure 46: Global instrumentation Test 8 (SCC Short Cut Span).....	64
Figure 47: Slip instrumentation.....	65
Figure 48: Slip LVDT contact	65
Figure 49: Elastic beam deformation	66
Figure 50: Elastic response and tangent stiffness	67
Figure 51: HESC (Test 3) cracking moment	68
Figure 52: SCC (Test 7) cracking moment	69
Figure 53: Global moment-deformation at point load	70
Figure 54: Global shear-deformation at point load	71
Figure 55: Full span moment – deformation response.....	71
Figure 56: Full span shear – deformation response	72
Figure 57: Short span moment – deformation response.....	72
Figure 58: Short span shear – deformation response	72
Figure 59: Reduced section moment – deformation response	73
Figure 60: Reduced section shear – deformation response	73
Figure 61: Failure progression in test 1 (SCC full span)	75
Figure 62: Failure progression in test 2 (SCC short span).....	78
Figure 63: Failure progression in test 3 (HESC full span).....	79
Figure 64: Failure progression in test 4 (HESC2 short span)	81
Figure 65: Failure progression in test 5 (HESC1 full span).....	82
Figure 66: Failure progression in test 6 (HESC1 reduced section).....	83
Figure 67: Failure progression in test 7 (SCC2 full span)	84
Figure 68: Failure progression in test 8 (SCC2 short span).....	85

Figure 69: Bond Slip HESC full Ld (Test 3)	86
Figure 70: Bond Slip SCC full Ld (Test 1).....	86
Figure 71: Bond Slip HESC full Ld (Test 5)	86
Figure 72: Bond Slip SCC full Ld (Test 7).....	86
Figure 73: Bond Slip HESC 58%Ld (Test 4)	87
Figure 74: Bond Slip SCC 58%Ld (Test 2).....	87
Figure 75: Bond Slip HESC Full Ld reduced section (Test 6)	87
Figure 76: Bond Slip SCC Full Ld reduced section (Test 8).....	87
Figure 77: Test specimens	89
Figure 78: Testing configuration.....	91
Figure 79: Load – slip response	92

3. ABSTRACT

ATLSS Report # 05-03: PITA Project PIT-457-04 - Comparative Performance of High Early Strength and Self Consolidating Concrete for Use in Precast Bridge Beam Construction - Final Report By Clay Naito, Greg Parent, Geoffrey Brunn, and Tyler Tate

This report evaluates the performance of precast prestressed bulb tee bridge beams using self consolidating concrete (SCC) and conventional high early strength concrete (HESC). SCC and HESC were examined and compared through a three phase research program at Lehigh University. The first phase consists of a comparison of material characteristics through a series of plastic and hardened concrete tests. The second phase examines the structural performance of the materials through non-destructive evaluation and destructive load testing of full-scale bulb tee beams. The third phase examines the concrete strand bond characteristics through a series of stressed, unstressed, and single wire pullout tests and small flexural beam tests.

The research shows that SCC and HESC produce acceptable strength gain, modulus of rupture, splitting tension, shrinkage, creep, hardened and plastic air, and chloride permeability. Results indicate that the SCC meets material performance specifications set by many DOTs. Moreover, the SCC beams have a transfer length that outperforms the Precast/Prestressed Concrete Institute's (PCI) recommendations. Finally, cost benefit analysis of fabrication time, material cost, and aesthetics indicate a potential long-term savings for SCC over conventional HESC.

4. ACKNOWLEDGEMENTS

The project was financed by Schuylkill Products Inc. and a grant from the Commonwealth of Pennsylvania, department of Community and Economic Development, through the Pennsylvania Infrastructure Technology Alliance (PITA) and through the support of, the Pennsylvania Department of Transportation, the Precast Association of Pennsylvania, and DeGussa Construction Chemicals.

The researchers would like to thank Mark Hoover, Dennis Fink, Troy Jenkins, Dave Bretzius and the staff at Schuylkill Products Inc. for their valuable contributions to this project. Without their hard work and expertise this project would not have been successful. The authors would also like to thank Heinrich Bonstedt of PCAP for his assistance with pushing the project forward. Also Robert Horwhat, Serge Ter-Arkelov, and Bryan Spangler at the Pennsylvania Department of Transportation for guidance on the achieving project objectives, assistance with detailed material evaluation, and review of the final report.

5. OVERVIEW

Self-consolidating concrete offers both cost and quality improvements over conventional concretes. The high fluidity of the concrete allows for placement in densely reinforced sections or sections with architectural features without vibration. Placement times are decreased and labor requirements are lowered. Consequently, self-consolidating concrete has become a popular alternate for conventional concrete in US precast construction. It has achieved wide-spread use in non-structural applications and is becoming popular for use in structural building precast components. To achieve acceptance for use in bridge precast a research program was conducted at Lehigh University in coordination with Schuylkill Products Inc. and Pennsylvania Department of Transportation.

The following focus areas were identified by the project team to facilitate the use of SCC for prestressed concrete construction. Results for both HESC and SCC were studied to characterize and compare results between the two concrete mixtures.

1. Concrete to strand bond
2. Creep properties
3. Shrinkage properties
4. Compressive & tensile strengths
5. Strength gain
6. Material costs
7. Concrete durability

To address these concerns a three phase experimental research program was developed. The phases are identified as:

1. Assessment of plastic and hardened concrete properties
2. Non-destructive evaluation and ultimate load testing of full-scale bulb tee beams
3. Strand to concrete bond evaluation

Using an appropriate physical model of a conventional bridge beam, modes of failure are evaluated. Inadequacies of the material (or lack thereof) are identified and design recommendations are developed and tested as part of the research program.

6. BACKGROUND

6.1. Precast Bridge Construction

The use of precast concrete elements provides a cost effective means of building bridge systems. The precast operation consists of off-site fabrication of members such as cellular box piers or prefabricated beams in a controlled environment. These members are then typically transported by truck or barge to the construction site for erection. The off-site fabrication allows for control of concrete batching properties, proper curing conditions, and the use of a highly skilled group of workers. As a consequence, precast operations produce a high quality, reliable, and durable product. Under proper conditions the fabrication and erection time can be much shorter than conventional cast-in-place construction methods. Typically fabrication of bridge beams in excess of 165 ft can be accomplished in two days. Erection of the members can be accomplished as the precast elements arrive on site. With its allowance for a short construction schedule, the high quality of the product, and the long term durability, precast concrete has become one of the main construction methods for new bridges in the US (Figure 1).



a) Precast piers b) Precast box segments c) Prestressed bulb beams d) Prestressed superstructure

Figure 1: Precast bridge construction

The construction methods used for conventional precast bridges are fairly standardized. Multiple bridge beams are placed adjacent to one another and are used to span from pier/abutment to pier/abutment. The beams are often considered simply supported; however, they can be made continuous with continuity steel and a cast-in-place diaphragm at the supports. Once the beams are erected a deck is cast-in-place on top of the beams. Horizontal shear ties are used to ensure composite action of the beams with the deck.

6.2. Bulb Tee Sizes

Bulb tee beam sections with constant tendon eccentricity are examined. The bulb tee geometry was developed through work of the Mid-Atlantic States Prestressed Concrete Committee for Economic Fabrication (PCEF). The goal of the group was to develop a standard set of bulb tee sections that could be used cost-effectively throughout the Mid-Atlantic region. The sections were chosen such that one set of forms could be used by manufacturers to construct up to 162 different shapes. The PCEF sections include 9 girder depths, 3 web thicknesses, 3 top flange widths and 2 bottom flange thicknesses. The bulb tee beams are capable of reaching spans of up to 180-ft, for a 95-in. depth section. The geometries of the PCEF bulb tee sections are summarized in Figure 2 and Table 1. Currently the PCEF bulb tee is permitted as a direct substitute for the New England bulb tee in New York State. In Pennsylvania the 8-in. web PCEF bulb tees has been adopted as a PA standard beam size by Pennsylvania DOT. The top flange depth however has been increased by 0.5-inches.

A bulb tee geometry is evaluated as part of the research program (highlighted region Table 1). The bulb tee measures 45-in. deep with a 7-in. web width. The beams fabricated for the research project are part

of the same construction line as beams used in a multi-span mid-Atlantic region bridge. The average span of the bridge is 60-ft.

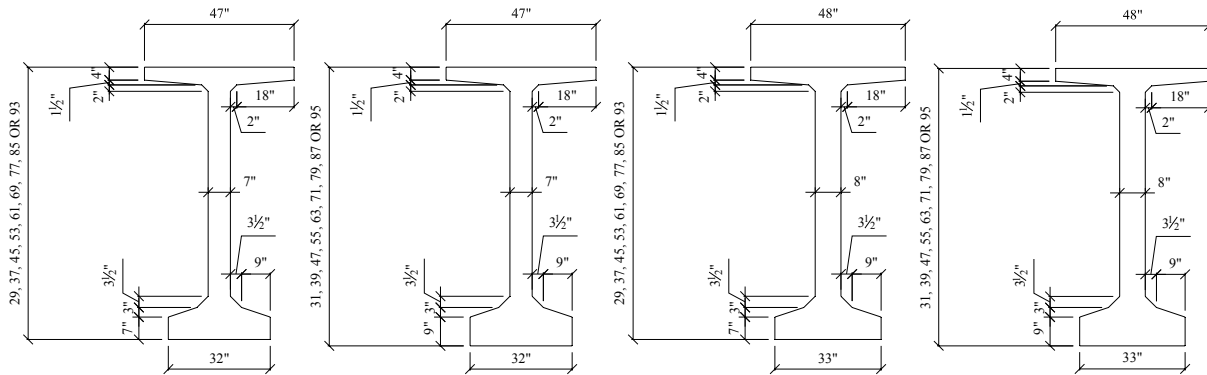
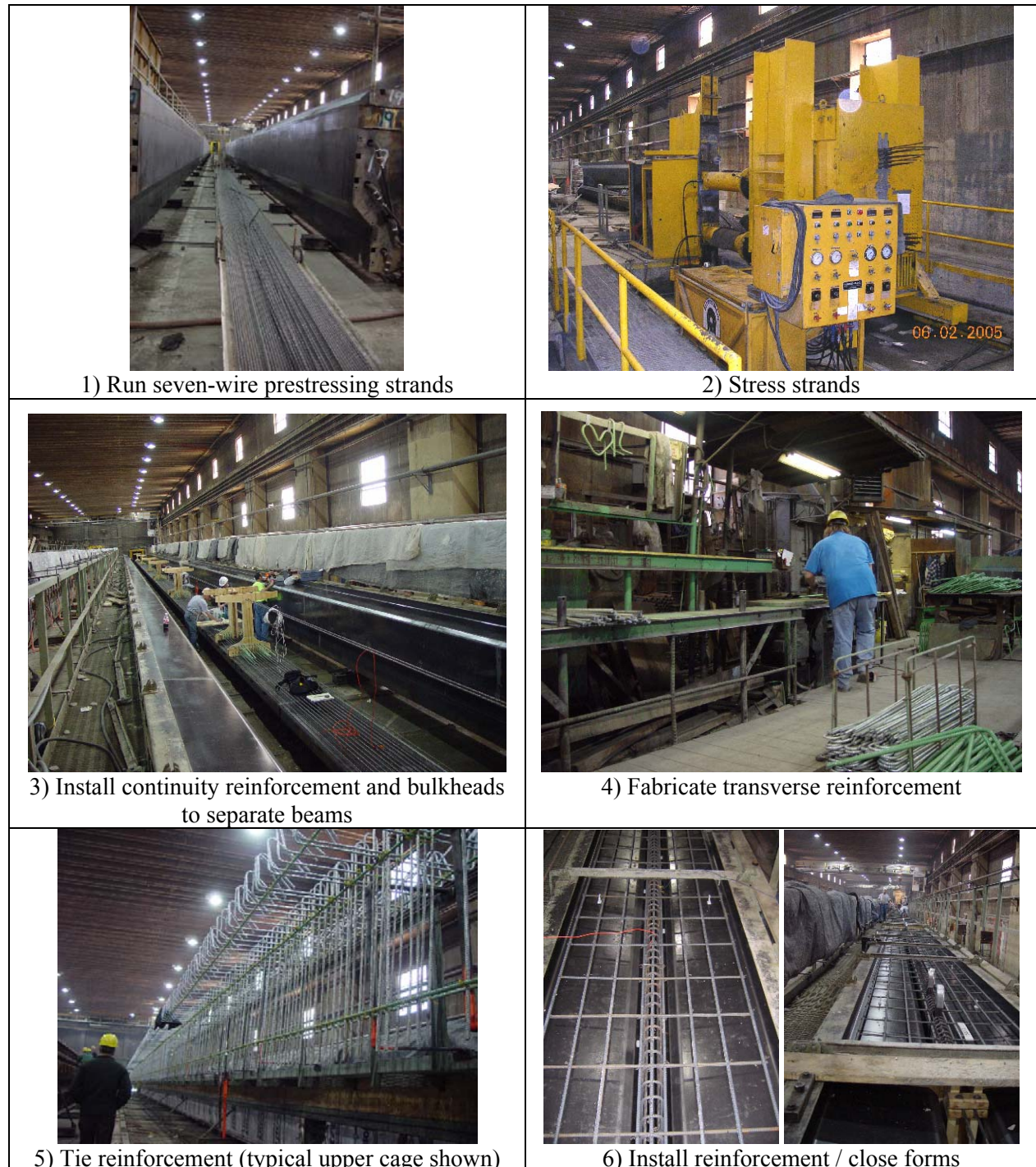


Figure 2: PCEF bulb tee standard sections [SPI 2005]

Designation	Bottom Flange Width [in.]	Web Width [in.]	Bottom Flange Depth [in.]	Beam Depth [in.]	Area [sq.in]	y _b [in]	I [in ⁴]	Weight [kips/ft]	Concrete Volume [cy/ft]
32/29	32	7	7	29	635	14.65	66940	0.662	0.163
32/32	32	7	7	37	691	18.42	126219	0.720	0.178
32/45	32	7	7	45	747	22.22	207554	0.778	0.192
32/53	32	7	7	53	803	26.05	312750	0.837	0.206
32/61	32	7	7	61	859	29.90	443610	0.895	0.221
32/69	32	7	7	69	915	33.77	601933	0.953	0.235
32/77	32	7	7	77	971	37.65	789516	1.012	0.250
32/85	32	7	7	85	1027	41.55	1008156	1.070	0.264
32/93	32	7	7	93	1083	45.46	1259648	1.128	0.278
32/31	32	7	9	31	699	15.22	81199	0.728	0.180
32/39	32	7	9	39	755	18.77	148321	0.787	0.194
32/47	32	7	9	47	811	22.39	239351	0.845	0.208
32/55	32	7	9	55	867	26.05	356133	0.903	0.223
32/63	32	7	9	63	923	29.76	500495	0.962	0.237
32/71	32	7	9	71	979	33.50	674259	1.020	0.252
32/79	32	7	9	79	1035	37.26	879241	1.078	0.266
32/87	32	7	9	87	1091	41.05	1117250	1.137	0.280
32/95	32	7	9	95	1147	44.87	1390094	1.195	0.295
33/29	33	8	7	29	664	14.64	68973	0.692	0.171
33/37	33	8	7	37	728	18.42	130440	0.759	0.187
33/45	33	8	7	45	792	22.23	215151	0.825	0.204
33/53	33	8	7	53	856	26.07	325167	0.892	0.220
33/61	33	8	7	61	920	29.94	462546	0.959	0.236
33/69	33	8	7	69	984	33.82	629343	1.025	0.253
33/77	33	8	7	77	1048	37.71	827611	1.092	0.267
33/85	33	8	7	85	1112	41.62	1059404	1.159	0.286
33/93	33	8	7	93	1176	45.54	1326771	1.225	0.302
33/31	33	8	9	31	730	15.23	83684	0.761	0.188
33/39	33	8	9	39	794	18.81	153284	0.827	0.204
33/47	33	8	9	47	858	22.45	248059	0.894	0.221
33/55	33	8	9	55	922	26.14	370106	0.961	0.237
33/63	33	8	9	63	986	29.87	521512	1.027	0.253
33/71	33	8	9	71	1050	33.63	704351	1.094	0.270
33/79	33	8	9	79	1114	37.42	920695	1.161	0.286
33/87	33	8	9	87	1178	41.23	1172608	1.227	0.303
33/95	33	8	9	95	1242	45.07	1462151	1.294	0.319

6.3. Prestressed Beam Production Methods

Conventional prestressed/precast beam production methods were used. The beams are cast on a 350-ft. long stressing bed located at Schuylkill Products Inc. (a certified PCI plant), in Cressona, Pennsylvania. The casting bed is a multi strand tensioning operation, which allows for simultaneous stressing of all strands in the cross-section. This configuration also allows for slow release of prestress after casting operations are complete, thus minimizing uneven release and unintentional damage to the precast members. The sequence of precast and prestressing operations is illustrated in Table 2. The photos represent the methods used for fabrication of the test specimens and other single web beams.





7) Batch concrete and perform QA/QC checks



8) Place concrete in form via 3cy bucket



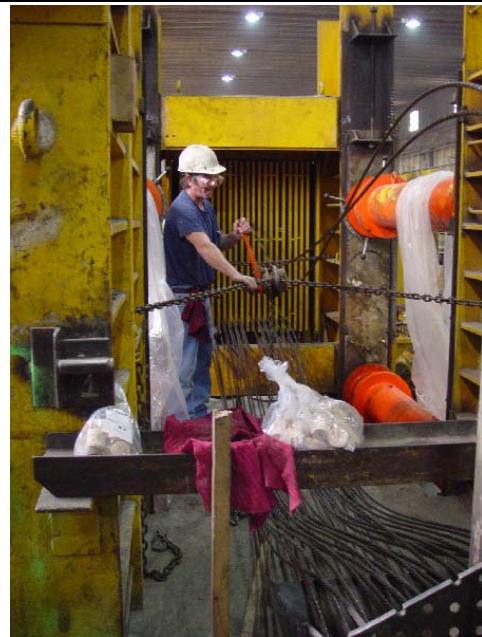
9) Vibrate, screed, and finish (HESC)



10) Fill form w/o vibration (SCC)



11) Cover and heat beams with radiant heat for initial cure period (~24 hours). Open forms on completion of cure



12) Release stress

	
13) Flame cut unstressed strands at bulkheads	14) Re-oil forms for subsequent operations
Table 2: Prestress sequence	

6.4. Conventional Concrete Materials

Successful precast operations are dependent on rapid gain of concrete strength. Conventional concretes used for structural applications typically range from 3000psi to 12000psi. Though the required compressive strength is dependent on the beam design, strengths on the order of 8000 psi are commonplace. Significant principal investments are required to fabricate bridge beam stressing beds. These include the cost for reusable steel forms, heating systems, building space, and stressing frames. To most effectively recoup these initial costs requires producing the maximum amount of product on each bed. This can be achieved by minimizing the cure times.

To achieve short cure times Type III cement is used in combination with elevated curing temperatures. As discussed in section 7.6.2, these methods can be used to achieve compressive strengths greater than 5000 psi in 24 hours. The mix designs typically utilize a high-range water reducer to allow for easy placement without compromising strength, air entraining agents to assist with durability, and conventional coarse and fine aggregates. These methods have been used successfully for many years in the precast industry to create high early strength concrete (HESC).

When properly designed and placed, HESC meets all durability and mechanical requirements. Nevertheless, enhancement of placement operations can significantly decrease precast costs and improve quality. Placement of conventional concretes requires heavy external and internal vibration to ensure consolidation. This requires the use of numerous skilled laborers (Table 2 step 10). Consolidation is often accomplished using hand operated immersion vibrators and large external form vibrators. These devices generate multiple health concerns. Form vibration can generate significant noise levels. Recent measurements taken near a form vibrator reached 110-115 decibels. The occupational health and safety administration requires that a safety plan and monitoring be used when the sound threshold exceeds 85 decibels. For levels exceeding 95 decibels annual audiograms and training programs are required. The use of form vibrators clearly requires additional training and costs for the precast producer. In addition to noise concerns, hand operated vibrators can lead to hand-arm vibration syndrome which can lead to muscle weakness, fatigue and shoulder or arm pain. Eliminating the need to vibrate the plastic concrete reduces labor costs, training and monitoring requirements, and can greatly improve the precast plant working environment. Self consolidating concrete provides an ideal means of achieving these goals.

6.5. Self Consolidating Concrete

Self consolidating concrete (SCC) has the potential of increasing durability and quality, reducing costs of construction, and improving the work environment. The flowability of the product allows for placement in members with high amount of reinforcement congestion. The use of conventional concretes in this situation would require significant mechanical vibration and still leave the risk of honeycomb formation.

The use of SCC allows for reduced labor during construction and a more aesthetically pleasing void free product. SCC also has the potential of lower permeability which could increase the life-cycle cost of precast construction.

To achieve self consolidating properties the concrete must be in a highly flowable state. This requires modification of the slump of the concrete (where slump is measured according to ASTM C143). High slump concrete (6 to 10-in.) can be achieved through addition of high range water reducing (HRWR or superplasticizer) admixtures alone. To achieve self-consolidating characteristics, slump greater than 10-in. must be achieved. At this level of flowability the concrete can be placed as a viscous liquid.

Self consolidating concrete mixtures have been developed by a number of construction chemical producers including WR Grace, Master Builders, and Sika. Two methods are commonly used to achieve self consolidating action. They are: 1) elevated dosages of high range water reducers with significant modification of fine aggregate (FA) quantities and proportions, and 2) viscosity modifying admixtures (VMA) in combination with moderate doses of high range water reducers.

6.5.1. SCC Method 1: HRWR and FA Modification

Method one uses elevated levels of HRWR in combination with modification in fine aggregate gradations. In addition, coarse aggregate quantities are decreased and fine aggregate quantities are increased. This method has been successfully used for non-structural applications and is gaining popularity for structural applications.

Segregation of the aggregate during placement and excessive creep and shrinkage are concerns regarding use of this method. Since the mix is highly fluid there is little resistance to settlement of the aggregate. This can lead to poor mechanical characteristics such as reduced steel to concrete bond, and non uniform strengths and stiffness. Placement should be properly controlled to provide best results. Vibration should be eliminated and concrete drop heights should be minimized or eliminated. Mix proportioning recommendations can be developed in conjunction with the admixture supplier. Furthermore, PENNDOT (and others) believe that these types of mixtures, with high fine aggregate to total aggregate ratios are more susceptible to creep and shrinkage. Unexpected creep and shrinkage can lead to excessive losses and a lower amount of available prestress. In some cases this can result in cracking under service loads and in extreme instances structural failure. Creep and shrinkage characteristics should be validated for this concrete production method until additional research findings are produced.

6.5.2. SCC Method 2: VMA & HRWR Modification

The second method uses elevated levels of HRWR and a Viscosity Modifying Admixture (VMA). To control cohesion and segregation, organic- and inorganic-based VMAs have been developed. The term VMA refers specifically to admixtures capable of maintaining suspension of the aggregate while the concrete is in its liquid state. The combined use of HRWR, air entraining admixtures (AEA), and VMA provides flowability while limiting free water to prevent segregation and strand corrosion. The resistance of this mix to segregation lends itself to placement in deep structural members. VMAs are produced by a number of admixture companies including SIKA Ltd., and Master Builders (Degussa Corp.).

6.6. Concerns Regarding SCC in Precast Bridge Construction

Acceptance of SCC for use in bridge applications will require a number of issues to be addressed. SCC is currently being used by a number of precast producers in the Eastern United States for both architectural panels and structural building components. Acceptance for structural applications in the bridge community, however, requires the approval of local Department of Transportation officials. Current limits by Pennsylvania DOT (PennDOT) are set in the construction specifications – publication 408 [Commonwealth 2003]. Publication 408 precludes the use of: 1) high slump concretes, 2) low coarse aggregate quantities, and 3) gradations other than standard AASHTO grade types. SCC method 1

typically requires that all three of these limits be adjusted. SCC method 2 requires that only the slump limit be adjusted. Consequently, the VMA technique is examined in the research program.

In addition to DOT limitations, concerns exist regarding the mechanical and durability characteristics of SCC. In particular:

- 1) Will segregation occur during placement in deep bulb tee beam sections?
- 2) Will excessive creep or shrinkage occur when used in large structural shapes?
- 3) Is the elasticity of the concrete comparable to conventional concretes? If not, is the elastic response or the camber significantly affected?
- 4) Can the required compressive strengths be achieved in the time needed?
- 5) Is the time needed for initial set of SCC different than that of HESC?
- 6) Are the durability characteristics such as freeze-thaw resistance or chloride permeability of SCC material different from conventional concretes?
- 7) Is prestressing strand-to-concrete bond compromised or enhanced when using SCC?

These questions are addressed in the research program with respect to a single SCC mix design used in bulb tee beam construction. A detailed discussion of the performance is conducted throughout the report and is summarized in the conclusions of section 15. In addition, suggested recommendations for modification of PennDOT Publication 408 are provided in section 16.

7. PHASE 1 CONCRETE MATERIAL CHARACTERISTICS

7.1. Design Requirements

Two mix designs are examined, a conventional HESC design used for over 10 years for production of precast/prestressed members and a SCC design developed to achieve the same strength requirements as the HESC. Both concrete types (SCC and HESC) were designed to achieve compressive strength of 6800psi (46.9MPa) within 24 hours from the time of placement and a compressive strength of 8000psi (55.2MPa) at 28-days. The rapid strength gain allows for early release of prestress forces and a short fabrication schedule. This section provides detailed information on the mix design, plastic, and hardened material properties.

7.2. Current Mix Proportioning Requirements

As a means of controlling the quality of concrete used in bridge construction design limitations are often specified by DOTs. The specifications typically limit the cement content, maximum water to cement ratio, compressive strength, slump, aggregate volumes and gradations. Separate requirements are developed for each concrete application: non-structural, structural, precast, or others. The American Association of State Highway and Transportation Officials (AASHTO) Bridge Design Specification [2003] provides general guidelines on mix design for structural precast/prestressed applications (Table 3). The specification loosely provides limits by specifying a minimum cement content, maximum water-cement content and coarse aggregate sizes. These limits however are low and thus allow for a considerable variation in mix proportions.

Class	Minimum Cement [lb/yd ³ (kg/m ³)]	Maximum Water/Cement Ratio	Minimum Compressive Strength [ksi]	Coarse Aggregate SIZE	Air Content [%]	Max Slump [in]
P	564	0.58	-	1.0" – No.4	-	-

To achieve closer control over concrete quality, each state DOT independently prescribes design requirements. Due to the autonomy of each state DOT the requirements vary considerably from state to state. The limits currently prescribed in a number of Eastern US states are presented in Table 4 to Table 9.

The concrete design examined in the research program is proportioned to meet the PennDOT HES specification [PennDOT 2003]. For quality assurance, bounds are placed on the cement content, water-to-cement ratio, relative volume of coarse aggregate, and the compressive strength (Table 4). Compressive strength and water/cement ratios are easily met by most mix designs. The cement quantity and coarse aggregate volume limits however are very strict. The coarse aggregate content is defined as the aggregate volume per total volume. Since the mix is designed by weight the bulk specific gravity is used to estimate the volume. For quality control during placement a limit of 8-in. slump is prescribed for concrete containing superplasticizers. Due to the high flow properties of the SCC mix, the slump limit is only applied to the HESC mix.

Cement [lb/yd ³ (kg/m ³)]		Max Water/Cement Ratio	Minimum Compressive Strength [ksi(MPa)]		Coarse Aggregate Volume	Maximum Slump [in]
Min	Max		3 days	28 days		
752(446)	846(502)	0.4	3.00(20.7)	3.75(25.9)	34% - 44%	8.0

The Northeastern US transportation groups provide similar requirements to the PennDOT mix design. West Virginia, Maryland, Virginia, Rhode Island, New Jersey, and New York DOT specifications are summarized. In general, most DOTs increase the minimum cement contents and decrease the max w/c ratio from that recommended by AASHTO. RIDOT and NYSDOT also prescribe limits on the ratio of fine or coarse aggregates. These requirements are examined in later sections.

Class	Target Cement Content [lb/yd ³ (kg/m ³)]	Max Water/Cement Ratio	Minimum Compressive Strength [ksi]	Coarse Aggregate SIZE	Air Content [%]	Max Slump [in]
Precast	658	0.44	As-Specified	-	7.0±2.0	8.0

Class	Cement [lb/yd ³ (kg/m ³)] Minimum	Max Water/Cement Ratio	Compressive Strength [ksi]		Coarse Aggregate Allowable Sizes	Air Content [%]	Target Slump [in]
			Design	Verification			
P	PCI	(PCI) 0.40	5500	6000	57, 67, 8	5.0±1.5	2.0±1.0
P - 1	PCI	(PCI) 0.40	6000	6500	57, 67, 8	5.0±1.5	2.0±1.0
P - 2	PCI	(PCI) 0.40	6500	7000	57, 67, 8	5.0±1.5	2.0±1.0

Class	Cement [lb/yd ³] Minimum	Max Water/Cement Ratio	Compressive Strength [ksi]		Sand % Total Aggregate (solid volume)	Air Content [%]	Target Slump [in]
			Release	@ 56-days			
F	716	0.38	-	-	34.6	5.0 to 8.0	2.0±1.0
HPC for P/S beams	>5% Microsilica	< 0.40	>7.1 ksi	> 10 ksi All tests	-	≥ 3%	-

Class	Cement [lb/yd ³ (kg/m ³)]		Max Water/Cement Ratio	Minimum Compressive Strength [ksi]		Coarse Aggregate Volume	Air Content [%]	Max Slump [in]
	Min	Max		3 days	28 days			
-	700	-	0.45	As specified, Typically 5.8	8.0	-	5.5 ± 1.5	6.0

Class	Cement [lb/yd ³ (kg/m ³)]		Max Water/Cement Ratio	Minimum Compressive Strength [ksi]		Coarse Aggregate/Total by weight	Air Content [%]	Max Slump [in]
	Min	Max		3 days	28 days			
HP	705	799	0.35	As specified	5.0 or as specified	55%	-	-

7.2.1. FHWA Survey Comparison

A recent study by Napier [2004] conducted for the Federal Highway Administration (FHWA) examined the current practice of each of the 50 state Departments of Transportation. Each DOT was surveyed on their current construction practice using high performance concretes (HPC). The upper and lower limits of a small portion of the survey are presented in Table 10. The majority PennDOT mix properties lie in the middle of typical US practice. The PennDOT maximum allowable cement requirement, however, lies in the upper portion of US Practice. As a consequence, the SCC mix design discussed in the next section may not meet the requirements of a number of DOT's.

Cement [lb/yd ³]		Max Water/Cement Ratio	Design Compressive Strength [ksi]	Max Slump [in.]	Air content [%]
Min	Max				
400-840	550-893	.315-0.5	5.0-12.0	0-10	0-10

7.3. HESC and SCC Mix Designs

Two mix designs were developed and compared: a standard HESC with normal flow characteristics (target 5.00-in.) slump and a high early strength design with self-consolidating characteristics (target spread 23.0-in.). To resist freeze thaw cycles both mixes were designed to have an air content of 5%. Six 2.75yd³ (2.1m³) batches of SCC and six 2.5yd³(1.9m³) batches of HES concrete were made. The mix proportions of all batches vary from the design by less than 1.0%. The intended design proportions and the average of the actual mix proportions are summarized in Table 11. Variations between the design and the actual properties are shown in bold. All properties are within design specifications with the exception of the cement. Due to an oversight, the HESC is 0.2% below the lower limit of required cement content and the SCC mix is 0.7% above the upper limit of cement content. The cement volumes are adjusted in the third phase as described in Section 13.

Material Type	Average of Batches		Design Proportions	
	HESC	SCC	HESC	SCC
Total Cement [lb/yd ³ (kg/m ³)]	750(445)	849(504)	752(446)	850(504)
Slag Cement [%]	34	25	35	25
Fine Aggregate SSD [lb/yd ³ (kg/m ³)]	1172 (695)	1283(761)	1171(695)	1287(763)
Coarse Aggregate #67 SSD [lb/yd ³ (kg/m ³)]	1383(820)	0	1359(806)	0
Coarse Aggregate #8 SSD [lb/yd ³ (kg/m ³)]	552(327)	1651(979)	582(345)	1650(979)
Water / Cement Ratio	0.34	0.32	0.34	0.32
High Range Water Reducer [oz/yd ³ (ml/m ³)]	60.0(2320)	136.2(5270)	60.0(2320)	136.2(5270)
Retarding Admixture [oz/yd ³ (ml/m ³)]	4.0(154)	0	4.0(154)	0
Air Entrainment Admixture (AEA) [oz/yd ³ (ml/m ³)]	2.4(93)	2.0(76)	2.4(93)	2.0(76)
Viscosity Modifying Admixture [oz/yd ³ (ml/m ³)]	0	16.0(620)	0	16.0(620)
Coarse Aggregate Volume [%]	39	34	39	34
Target Air Content [%]	NA	NA	5.0	5.0
Target Slump / Spread [in. (cm)]	NA	NA	5 ± 1 (12.7 ± 2.5)	23 ± 1 (58.4 ± 2.5)

7.4. Concrete Materials

The two mixes include cement, coarse and fine aggregate, water, and a number of admixtures. Details of each constituent are provided in this section.

7.4.1. Cementitious Material

Cementitious properties are provided by Type III cement and ground granulated blast-furnace (GGBF) slag cement. The type III cement is the primary cement constituent and is used to provide high early strength gain. The slag is added to offset the high costs of type III cement (slag is marginally less than type I cement). In addition, slag leads to improvements in workability [Kosmatka 1988], durability [Geiseler 1995], resistance to chloride permeability, and improved mechanical characteristics [Sivasundaram 1992]. The ASTM C989 Grade 120 slag cement properties are summarized in Table 3.

Blaine fineness [cm^2/g]	5418
Specific gravity	2.88
Tricalcium silicate (C_3S) content [%]	53
Dicalcium silicate (C_2S) content [%]	20
Tricalcium aluminate (C_3A) content [%]	8

Slag cement makes up 25% of the cement content in the SCC mix and 34% in the HESC mix. These levels are on order of mix designs used successfully in previous research and practice [Rols 1999, Chan 2003, Khayat 2000]. Furthermore, the GGBF slag quantities commonly used by state DOT range from 0-75% of the total cement weight [Napier 2004]. The levels used in the research program are well within this range.

7.4.2. Aggregate

A crushed Diabase stone is used for coarse aggregate. Diabase is a very hard material with a Moh's scale of hardness greater than 6 (cannot be scratched with glass) and an abrasion resistance (AASHTO T96 / ASTM C131) less than 20%. At this level of hardness bond capacity will not be compromised by premature failure of the aggregate.

AASHTO [2000] #67 (0.75in. max) and #8 (0.375 in. max) gradations are used for the HESC mix (Table 13). Due to the presence of crushed elongated stone in the #67 material which can limit flow in densely reinforced areas, only the #8 aggregate is used in the SCC. The use of smaller max aggregate size ensures good workability in the SCC. Natural silica sand with Type A gradation is used for the fine aggregate. The fine aggregates have a fineness modulus of 2.76; this is within the allowable limits of 2.30 – 3.15. The bulk specific gravities of the #67, #8, and fine aggregate are 2.963, 2.892, and 2.625, respectively as noted in PennDOT Publication #34 [2004].

Aggregate size	Amounts finer than each laboratory sieve (square openings), percent by weight Nominal size sieve opening [in. (mm)]						
	1 (25)	$\frac{3}{4}$ (19)	$\frac{1}{2}$ (12.5)	$\frac{3}{8}$ (9.5)	No.4 (4.75)	No.8 (2.36)	No.16 (1.18)
#67	100	90 to 100	-	20 to 55	0 to 10	0 to 5	-
#8	-	-	100	85 to 100	10 to 30	0 to 10	0 to 5
Aggregate size	Amounts finer than each laboratory sieve (square openings), percent by weight Nominal size sieve opening [in. (mm)]						
	$\frac{3}{8}$ (9.5)	No.4 (4.75)	No.8 (2.36)	No.16 (1.18)	No.30 (600 μm)	No.50 (300 μm)	No.100 (150 μm)
Type A	100	95 to 100	70 to 100	45 to 85	25 to 65	10 to 30	0 to 10

The coarse aggregate volume meets the required values of PennDOT. The SCC is at the bottom of the allowable levels with 34% coarse aggregate by volume. The HESC mix is at the middle of the limits with 39% coarse aggregate by volume. The bulk specific gravity is used to compute the volume percentage in accordance with Section 704.1(b).1 of the PennDOT material specification.

7.4.3. Supplementary Admixtures

A number of admixtures are used to improve the performance and workability of the mix. Both mixes include an ASTM C494 Type F high range water reducer (HRWR) to improve workability and an ASTM C260 neutralized vinsol resin air entraining admixture (AEA). An ASTM C494 Type B retarder is used in the HESC mix in the summer to slow set time. To limit segregation in the SCC mix, a commercially available VMA is used. All admixtures were produced by Master Builders a subsidiary of Degussa Construction Chemicals. The specific admixtures types are summarized in Table 14. The AEA is a natural product and is widely accepted; consequently it has no PennDOT reference number. All admixtures excluding the VMA are approved by PennDOT. The VMA has provisional approval.

Admixture Type	Product	PennDOT Reference Number
Viscosity Modifying	RHEOMAC® VMA 358	01-211
High Range Water Reducing	GLENIUM® 3030 NS	01-188
Retarding	POZZOLITH® 100 XR	69-013
Air Entraining	MB-VR Standard	-

7.5. Plastic Concrete Characteristics

The materials were qualified using standard ASTM requirements for unit weight, ambient temperature, slump and air content and the PCI SCC Interim guideline requirement for spread [PCI 2003]. The plastic tests were observed by PennDOT, VADOT, NJDOT, NYSDOT, DEDOT, and FHWA officials. The properties of the HESC and SCC are summarized in Table 15 and Table 16.

Batch #	Unit Weight [lb/ft ³]	Ambient Temperature [°F]	Concrete Temperature [°F]	Air Content [%]	Slump [in.]
HES 1	148.8	70	72	5.3	6.25
HES 2	148.8	70	74	5.6	5
HES 3	-	-	-	-	-
HES 4	149.6	71	74	5.5	7.5
HES 5	152.0	71	75	5.1	6.5
HES 6	-	-	-	-	-
Average	149.8	71	74	5.4	6.3

	Unit Weight [lb/ft ³]	Ambient Temperature [°F]	Concrete Temperature [°F]	Air Content [%]	Spread [in]	Spread through J-ring [in]	VSI
SCC1	148.8	74	74	5.4	21	19	0
SCC2	148.0	74	75	5.4	20	19	0
SCC3	148.8	74	75	4.7	22.5	20.5	0
SCC4	149.6	76	76	4.8	21.5	18.5	0.5
SCC5	-	-	-	-	-	-	-
SCC6	148.8	76	75	4.7	21.5	22.5	0.5
Average	148.8	75	75	5.0	21.3	N.A.	0 to 0.5

Both concrete designs met the PennDOT specified plastic design requirements. Air content and unit weights were within design targets (Table 11) for both HESC and SCC mixes. The unit weights of the two mixes were statistically the same. The air content of the SCC was marginally lower. This corresponds with the lower dosage of AEA used. The HESC was batched in the morning and the SCC was batched in the afternoon. This resulted in the elevation of initial temperatures with the SCC material.

7.5.1. Slump and Spread

The flow characteristics of the mixes were marginally outside their targeted values. The hydraulic slump of the HESC was measured according to ASTM C 143. The measured slump was consistently higher than the targeted 5.0 inches but within the PennDOT limit of 8 inches. Based on successful past experience with the mix and the high congestion of reinforcement in the bulb tee beams the decision was made to use it in the program.

The flow of the SCC is also evaluated using a standard slump cone. Due to the high flow of SCC mixes the slump is typically greater than 10-in making the traditional ASTM C143 measurement inappropriate, instead the amount of spread of the mix is measured. Details on the method can be found in the SCC Interim Guidelines [PCI 2004]. The test can be conducted with the slump cone oriented in a traditional manner or inverted. The inverted method was used for ease of operation. With the cone inverted it is easier to fill since the larger opening is oriented up and the stability of the cone allows filling without needing to stand on the sides of the cone. (Figure 3 a and b). This method was used consistently throughout the research program.

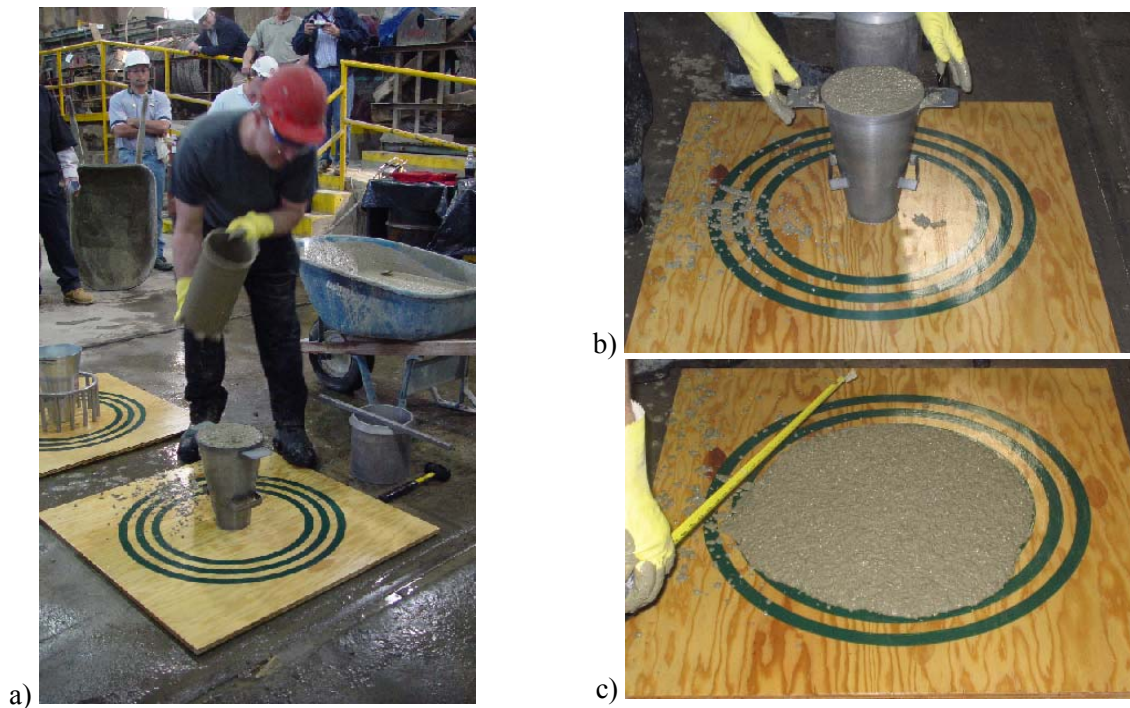


Figure 3: Inverted slump spread test

The spread is computed as the average of two perpendicular measurements. The spread was lower than the targeted 23 \pm 1 in. with an average of 21.4 in. across five batches. This amount of spread is within PCI recommendation of \pm 2-in. of variation [PCI 2003]. The Visual Stability Index (VSI) of the mix however indicated that the quality was acceptable for placement. While the lower spread provides adequate flow for the application, typical SCC mixes range from 22 to 26 inches of spread. With minor adjustments of admixtures these levels can easily be achieved.

A visual stability index (VSI) was determined for each of the inspected SCC batches (Figure 3). The test consists of a visual inspection of the final spread to identify any potential stability problems that could occur during placement. Issues of concern include segregation of the aggregate, excessive bleeding of water, and cohesiveness of the mix. No evidence of aggregate piling, segregation in slump flow, or mortar halo was observed in the batches (VSI = 0). In two of six batches, however, minor bleeding was observed—resulting in a VSI of 0.5. PCI defines VSI ratings less than 2.0 as acceptable [PCI 2003].

7.5.2. SCC Dynamic Segregation

The concrete capability to flow through dense reinforcement was examined with a modified J-ring test. The method consists of an inverted slump cone test conducted in a ring of vertical 0.625 in. diameter bars spaced evenly at 1.2 in. (Figure 4). The passing ability can be quantified by measuring the height of the spread profile. Typically four vertical measurements are taken at the exterior of the ring and five measurements are taken internal to the ring. For the research program a simplified J-ring evaluation was conducted. Instead of the multiple vertical measurements the spread through the J-ring was noted. The reduction in spread from the unrestrained spread was compared. A reduction of more than 15% was deemed unacceptable. The spread decreased from the free spread by a minimal amount (7% on average); no noticeable segregation or piling of aggregate was observed (Figure 4).



Figure 4: J-ring test

To further examine the potential for segregation during placement, a columnar segregation test [Assaad, Khayat, and Daczko 2004] was conducted. This method is currently under review by ASTM. The test consists of measuring the coarse aggregate variation between the top and bottom of a PVC column after 15 minutes of settlement. The column measured 26-in. in height and was divided into 4 equal sections that were kept sealed during the settlement period (Figure 5). An 8-in. diameter PVC pipe was used. The concrete from the top and bottom of the cylinder was separated from the column. The mortar was washed out over a 5mm sieve and the saturated surface dry weight of the remaining aggregate was compared. No difference was measured between the top and bottom sections (0% segregation).

7.5.3. Initial Set

Time of set was measured according to ASTM C403. The method uses a series of weighted needles to determine the resistance to penetration. The setting time refers to the duration needed to resist a surface bearing pressure of 500psi. This duration determines the time needed to wait prior to finishing operations. Shorter set times allow for a faster production schedule. Three samples were examined for each mix design and examined regularly until achievement of set. The samples were taken from the second batches of the SCC and HESC mixes.

The SCC has a longer setting time than the conventional HESC. The SCC reached an initial set in 6.3 hours, while the HESC reached an initial set in 5.2 hours. Both times are within expected durations. Though the setting time is only 50 minutes longer, the added duration will require an adjustment of finishing operations. This can be easily achieved with re-organization of personnel allocation. These methods will be addressed in the cost-benefit analysis Section 10.6.

The initial set follows accepted curing trends [Popovics 1971]. The measured penetration resistance of the samples is plotted versus time in Figure 6. The HESC and SCC follow a power function shown as the dashed and solid lines, respectively. The relationships between time, t [hrs], and penetration resistance, PR [psi], can be estimated by equations 1 and 2.

$$PR_{SCC} = (9.39E - 06) \cdot t^{9.63} \quad (R^2 = 0.98) \quad \text{Eq. 1}$$

$$PR_{HESC} = (2.17E - 03) \cdot t^{7.52} \quad (R^2 = 0.99) \quad \text{Eq. 2}$$



Figure 5: Columnar segregation

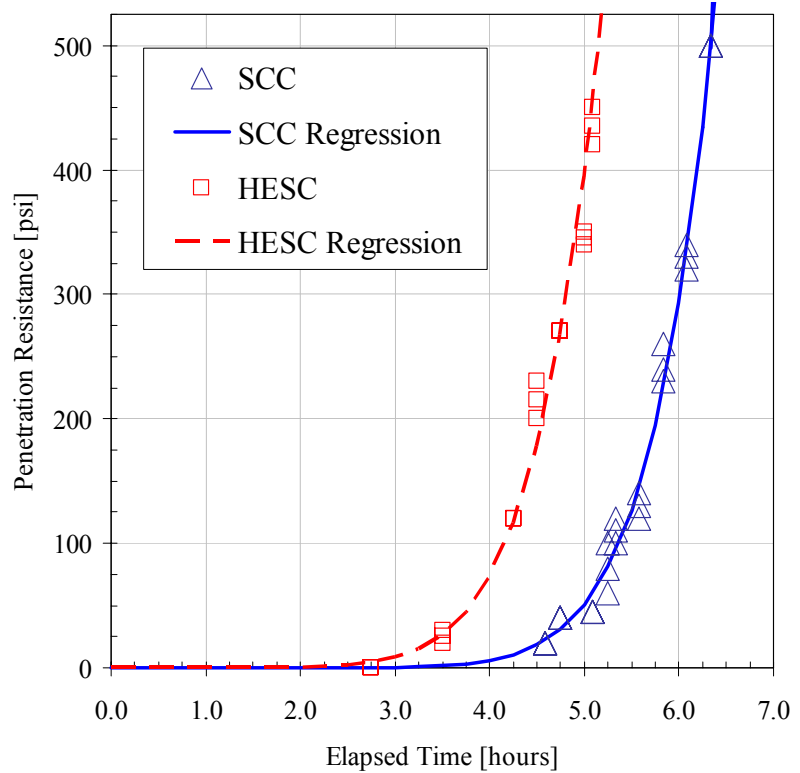


Figure 6: Initial setting time

7.6. Mechanical Properties

The concrete mechanical properties were evaluated in detail through a series of tests on concrete cylinders and prisms taken from the six batches of concrete. Both batches were examined for both mechanical and durability properties. The mechanical properties include the compressive strength, elastic modulus, modulus of rupture, splitting tension strength, creep, and shrinkage properties. Durability was assessed through determination of hardened air, freeze-thaw resistance, and chloride permeability. A summary of the tests performed is presented in Table 17. Details of the mechanical tests and the results are summarized in this section.

Table 17: Hardened concrete material tests	
Durability Tests	Mechanical Tests
Chloride Permeability	Creep/Shrinkage (ASTM C512)
ASTM C1202	Cylinders 6"x12"
Cylinders 4"x8"	Compressive Strength (ASTM C39)
Rapid Freeze Thaw Resistance	Cylinders 4"x8" & 6"x12"
ASTM C666 Method B	Flexural Strength (ASTM C78)
Cylinders 6"x12"	Beams 6"x6"x20"
Hardened Air Void Analysis	Splitting Tensile Strength (ASTM C496)
ASTM C457	Cylinders 6"x12"
PennDOT Test Method 623B	Stress-Strain & Poisson's Ratio (C469)
Cylinders 6"x12"	Cylinders 6"x12"

7.6.1. Cylinder Fabrication and Curing

The material tests were conducted on cylinders and prisms. Three sizes of material test samples are used: 4x8-in and 6x12-in. cylinders and 6x6x20-in. prisms. The samples were prepared according to ASTM C31 (Figure 7). All material test specimens were prepared from the second batch of concrete.



Figure 7: Cylinder and prism fabrication

The material test specimens were cured according to ASTM requirements. The cylinders and prisms were cured under the same conditions as the bulb tee beams examined in the following research phases. Where space was available on the casting bed the test samples were cured alongside the bulb tee beams. The remaining materials were match cured for the initial curing period. The initial cure temperatures for the SCC and the HESC were monitored using a thermocouple within the bulb tee beams and material specimens. The temperature variation for the casting bed and the match cure bed is presented in Figure 8.

Elevated curing temperatures were used to assist in early strength gain. The HESC and SCC beams reached a maximum internal temperature of 147F and 144F, respectively.

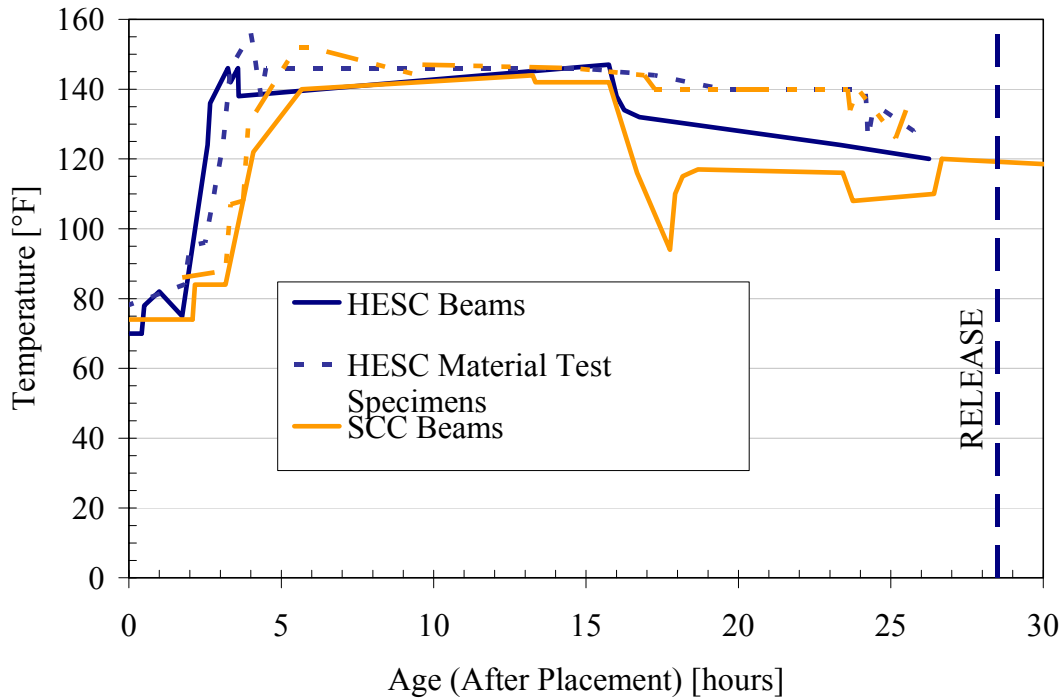


Figure 8: Temperature variation during initial cure

7.6.2. Compressive Strength

Compressive strength gain for the two concrete mixes were comparable and within expected values. The strength was measured using ASTM C 39 procedure (Figure 10a). The tests were conducted starting at 24 hours and repeated regularly until 101 days after placement. Both concrete mixes gained over 90% of their 28-day compressive strength in the first 24 hours. The strength remained relatively stable for the first 56 days and increased at later ages (Figure 9). Release and ultimate design strength requirements were met; however, design strength on the HESC mix was achieved only after 80 days. The long-term strength gain can be improved by modification of the heating temperature and/or duration during the first 24 hours [Freyne 2003]. To ensure statistical integrity, the concrete cylinders taken from the six different batches were randomized. This resulted in apparent strength variations over time as shown in Table 18 and Figure 9. For consistency, the data tabulated represents only the 4x8-in cylinder test results. The strength data from the elastic modulus tests are included in section 0.

Age [days]	SCC [psi]	HESC [psi]
1	8232	6809
3	7809	6802
7	8724	7568
14	7980	7520
28	8276	7366
38	9166	-
56	8634	7155
61	-	7136
79	-	7580
89	9842	-
101	10427	8950

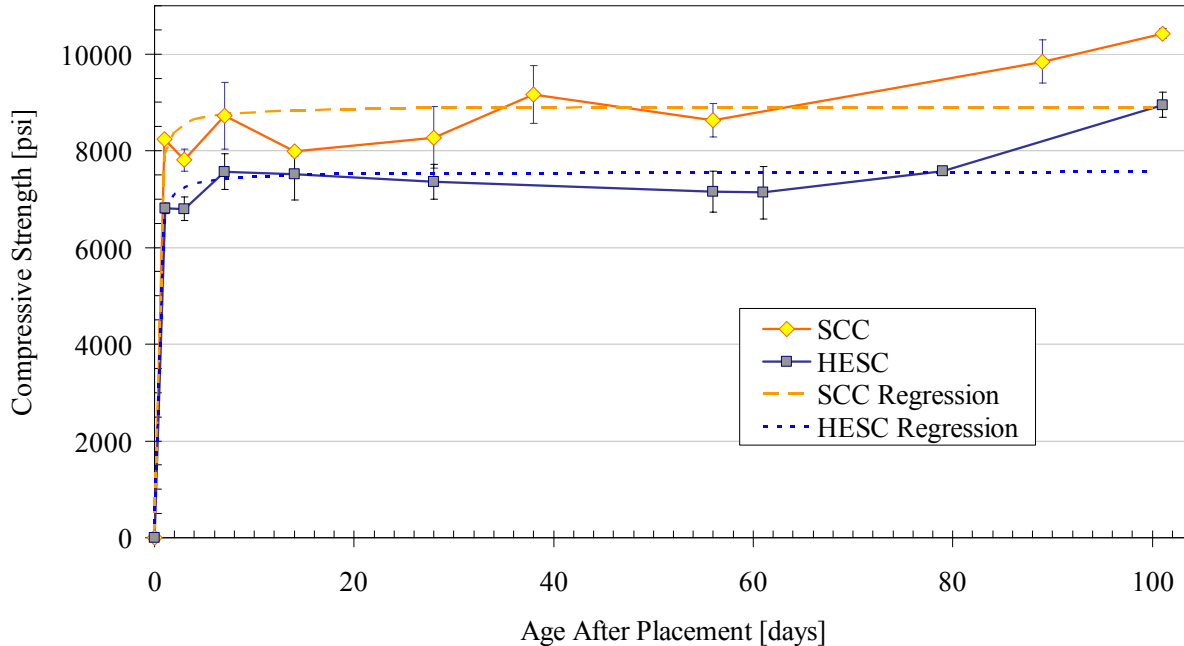


Figure 9: Compressive strength gain

The measured strength gain does not correlate well with ACI 209 [1997] formulations. The compressive strength gain estimates from ACI are of the form shown in equation 3. The constants a and β are estimated by ACI as 0.70 and 0.98 for steam cured concrete using type III cement. A regression analysis of the compressive strength gain results in lower values for the constants. The constants are tabulated in Table 19 and shown graphically in Figure 9; note the goodness of fit is poor. The compressive strength gain formulas are based on conventional cements and concretes without admixtures, consequently the poor fit is can be expected.

Regression	ACI 209-97	SCC	HESC
a	0.70	0.12	0.13
β	0.98	0.93	0.97
R^2	-	0.18	0.29

$$f' c(t) = \frac{t}{a + \beta \cdot t} f' c_{28-Days} \quad \text{Eq. 3}$$

7.6.3. Modulus of Elasticity

The concrete modulus of elasticity was measured in accordance with ASTM C469. The tests were conducted using a ring frame with two Linear Variable Displacement Transducers (LVDTs) mounted on opposing sides of a 6x12-in. concrete cylinder (Figure 10b). The stress-strain response of the two mixes was similar. A sample stress-strain response for SCC (98-day) and HESC (79-day) is shown in Figure 11. The higher elastic modulus and strength is clearly observed on the graph. The unloading branch of the HESC mix was obtained. Due to the abrupt failure of the SCC mix the unloading branch was not measured.



A) Compressive strength



b) Modulus of elasticity

Figure 10: Compressive tests

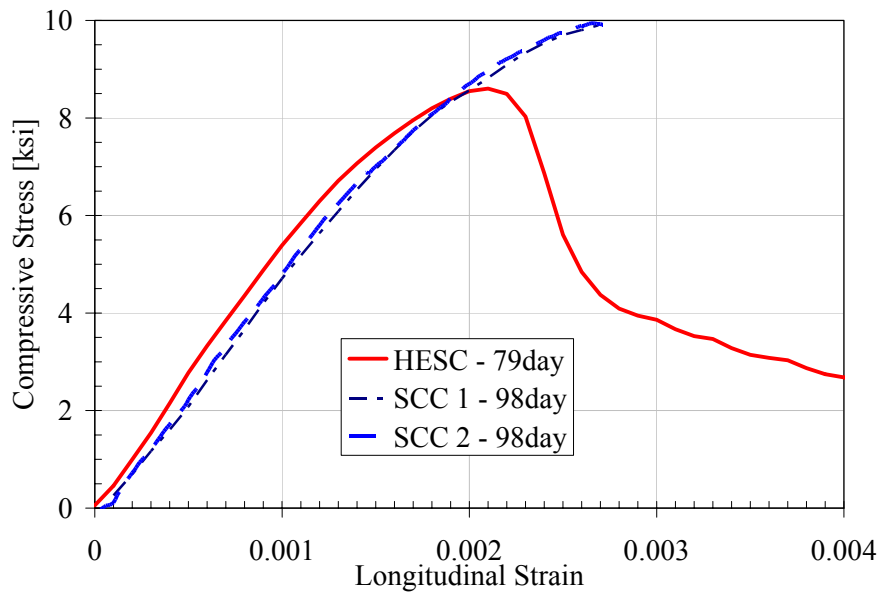


Figure 11: Stress-strain response

The elastic modulus is computed from the stress-strain response using three methods. In method 1, a linear regression of the data up to 40% of the compressive strength is conducted. In method 2, secant stiffness is taken to 40% of the peak compressive strength. In method 3, secant stiffness is taken to the stress-strain curve at a strain of $450\mu\epsilon$. The three methods result in similar estimates of elastic modulus. For the remaining discussions the modulus computed using linear regression is used.

The elastic modulus of the SCC and HESC are comparable (Table 20). The HESC is marginally stiffer at both early (14-days) and later dates. The higher HESC modulus may be attributed to the elevated levels of coarse aggregate in the HESC (39% versus 34%). Since the aggregate is quite hard, the elevated quantity and larger gradation used in the HESC could attribute to the consistently stiffer properties. These accuracy of these properties must be verified with the in-situ beam behavior.

The elastic modulus of the concrete, E_c , was observed at 14 days to be 5627 ksi for HESC and 5043 ksi for SCC. The values measured are compared to ACI and PCI estimates [2004]. Two formulations are commonly used: one is dependent on the compressive strength, f'_c , (Eq. 4) and the other on the unit weight, w_c , and strength (Eq.5) [PCI Eq.2.5.3.1-1]. The ACI formulations marginally over predict the

elastic modulus of the SCC and underestimate the elastic modulus of the HESC (Table 21). The variation is within the expected variability.

Material	Age [days]	Compressive strength, f'_c [psi]	E_c , Linear regression [ksi]	R-squared	E_c @40% f'_c [ksi]	E_c @ 450 $\mu\epsilon$ [ksi]
SCC	14	8170	4940	1.000	4930	4930
SCC	14	8420	5190	1.000	5200	5170
SCC	14	8270	5000	1.000	5010	5000
SCC	38	9740	4755	0.993	4854	4703
SCC	98	9968	4821	0.996	5178	5057
SCC	98	9989	5224	0.996	5036	4928
HESC	14	6520	5610	1.000	5670	5670
HESC	14	7090	5500	0.999	5570	5590
HESC	14	7180	5770	1.000	5790	5840
HESC	79	8901	5623	0.995	5520	5628
AVG SCC	14	8287	5043	-	5047	5033
AVG HESC	14	6930	5627	-	5677	5700
AVG SCC	All	9093	4988	-	5035	4965
AVG HESC	All	7423	5626	-	5638	5682

Formulation	SCC E_c – Computed [ksi]	SCC Error [%]	HESC E_c – Computed [ksi]	HESC Error [%]
$E_c = 57000\sqrt{f'_c}$ (Eq. 4)	5060	+0.3	4940	-12.2
$E_c = 33 \cdot w_c^{1.5}\sqrt{f'_c}$ (Eq. 5)	5320	+5.5	5250	-6.7

7.6.4. Tensile Properties

The tensile properties are quantified through ASTM C496 and C78. ASTM C496 determines the direct tensile strength, f'_t , of concrete through evaluation of the splitting strength of cylinders (Figure 12a). ASTM C78 determines the tensile flexural strength of concrete, f'_r , through third point loading of concrete 6x6x20-inch prisms (Figure 12b). The tensile tests on each material were conducted twice with each date corresponding to the destructive testing of the bulb-tee beams. The resulting strengths are provided in Table 22.

The tensile strengths are higher than commonly accepted values. The modulus of rupture was consistently higher than the accepted value of $7.5\sqrt{f'_c}$, and the splitting tension strength was consistently higher than $6.0\sqrt{f'_c}$. Use of the standard assumptions for design purposes would be conservative for both of the mixes. The splitting tensile strength increases with age and is comparable (relative to compressive strength) between the SCC and HESC. The modulus of rupture is also similar between the mixes. The strength, however, decreased with age. This is attributed to poor curing control on the last test series and not due to actual mechanical properties.



a) Splitting tension test



b) Modulus of rupture

Figure 12: Tensile tests

Table 22: Tensile strength							
Material	Age [days]	f _c [psi]	f _t [psi]	f _t [# of $\sqrt{f'_c}$]	f _r [psi]		
					Average	Standard deviation	# of $\sqrt{f'_c}$
SCC	38	9166	736 ¹	7.7	1066	53.6	11.1
SCC	89	9842	858 ²	8.6	886	49.8	8.9
HESC	61	7136	599 ¹	7.1	926	51.1	11.0
HESC	82	7770 ³	747 ²	8.5	762	38.4	8.6

¹Average of two tests on 6x12 cylinders, ²Single test conducted on 4x8 cylinder,
³Interpolated from test data

7.6.5. Creep and Shrinkage

Creep and shrinkage of the concretes were measured and compared to expected results. The concrete was examined both in-situ and through material testing of cylinders. In-situ evaluation of the beams were studied using embedded vibrating wire strain gages located at the center of the beam span, at the center of the second layer of strand (Figure 13). The instrumentation is discussed in detail in section 10.2 and 12. Material testing was conducted on 6-in.x12-in. cylinders subject to the same initial curing conditions as the prestressed beams. The cylinders were kept moist prior to creep and shrinkage evaluation. Laboratory testing was conducted to ASTM C512 and commenced 14-days after placement. The shrinkage strain and the creep coefficient are measured at the same time, thus the values are plotted versus age of loading (Figure 14 and Figure 15).



Figure 13: In-situ instrumentation

ACI 209 provides recommendations on estimating the shrinkage strain and creep strain of concrete [1992]. The relationships for shrinkage strain, ϵ_{sh} , and creep coefficient, ν_{cr} , over time, t [days], take the form of eq.6 and eq.7. The values for d and f can be estimated using the ACI values of 10 and 35, respectively or with the factors developed by Hou et. al. [2001]. The ultimate shrinkage strain, $\epsilon_{sh-ultimate}$, and the ultimate creep coefficient, $\nu_{ultimate}$, are computed using the adjustment factors detailed in ACI 209. For the SCC mix the slump adjustment factor is taken as 1.0. The ACI predictions are compared in Figure 14 and Figure 15.

$$\epsilon_{sh} = \epsilon_{sh-ultimate} \times \frac{t^\alpha}{t^\alpha + f} \quad \text{Eq. 6}$$

$$\nu_{cr} = \frac{\text{creep strain}}{\text{initial strain}} = \nu_{ultimate} \times \frac{t^\psi}{t^\psi + d} \quad \text{Eq. 7}$$

Least squares fit of the creep and shrinkage material test data is conducted to develop equations for predicting the response of the bulb tees (Eq. 8 – 11). The equations are plotted in Figure 14 and Figure 15.

$$\epsilon_{sh,SCC} = 341 \times 10^{-6} \times \frac{t}{t + 19.1} \quad R^2=0.99 \quad \text{(Eq. 8)} \quad \epsilon_{sh,HESC} = 284 \times 10^{-6} \times \frac{t}{t + 22.8} \quad R^2=0.93 \quad \text{(Eq. 9)}$$

$$\nu_{cr,SCC} = 2.73 \times \frac{t^{0.6}}{t^{0.6} + 6.36} \quad R^2=0.98 \quad \text{(Eq. 10)} \quad \nu_{HES} = 2.06 \times \frac{t^{0.6}}{t^{0.6} + 7.10} \quad R^2=0.99 \quad \text{(Eq. 11)}$$

The standard ACI creep and shrinkage formulations are modified to account for the level of cement content and fine aggregate percentage used in the concretes. The final ACI formulations for creep and shrinkage are summarized in Eq. 12 – 15.

$$\epsilon_{sh,SCC(ACI)} = 698 \times 10^{-6} \times \frac{t}{t + 35} \quad \text{(Eq. 12)} \quad \epsilon_{sh,HESC(ACI)} = 622 \times 10^{-6} \times \frac{t}{t + 35} \quad \text{(Eq. 13)}$$

$$\nu_{cr,SCC(ACI)} = 2.44 \times \frac{t^{0.6}}{t^{0.6} + 10} \quad \text{(Eq. 14)} \quad \nu_{HES(ACI)} = 2.32 \times \frac{t^{0.6}}{t^{0.6} + 10} \quad \text{(Eq. 15)}$$

The SCC and HESC mixes compare well with ACI estimates of shrinkage and creep. Both the SCC and HESC exhibit lower shrinkage strain than predicted by code. The SCC under predicted the ACI estimate of shrinkage by 18% and HESC under predicted the shrinkage by 39%. This may be attributed to the low fine aggregate content of both mixes. The SCC exhibited a 39% higher shrinkage strain than the HESC on average. The creep coefficient of the HESC was 6% higher than the ACI prediction. The creep coefficient of the SCC however was approximately 40% higher than ACI predictions. In summary, as expected from past experience the HESC performed well for both creep and shrinkage. The SCC performed well for shrinkage but performed lower than expected for creep. The combined effects of lowered shrinkage and elevated creep may cancel each other when examined together in a beam.

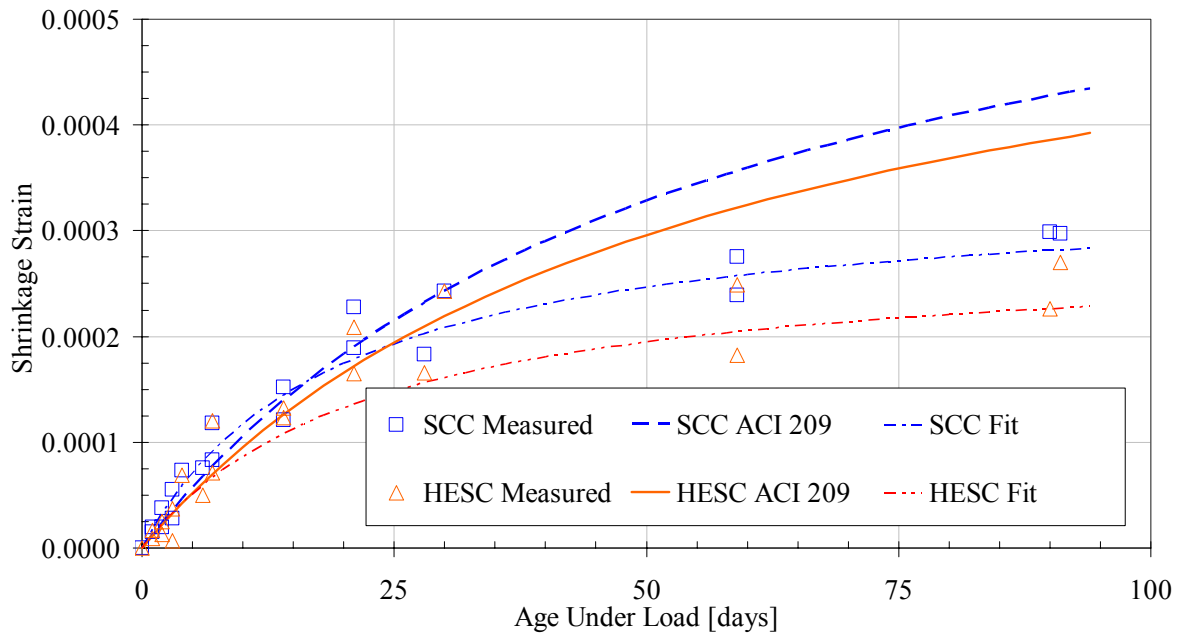


Figure 14: Shrinkage response of material

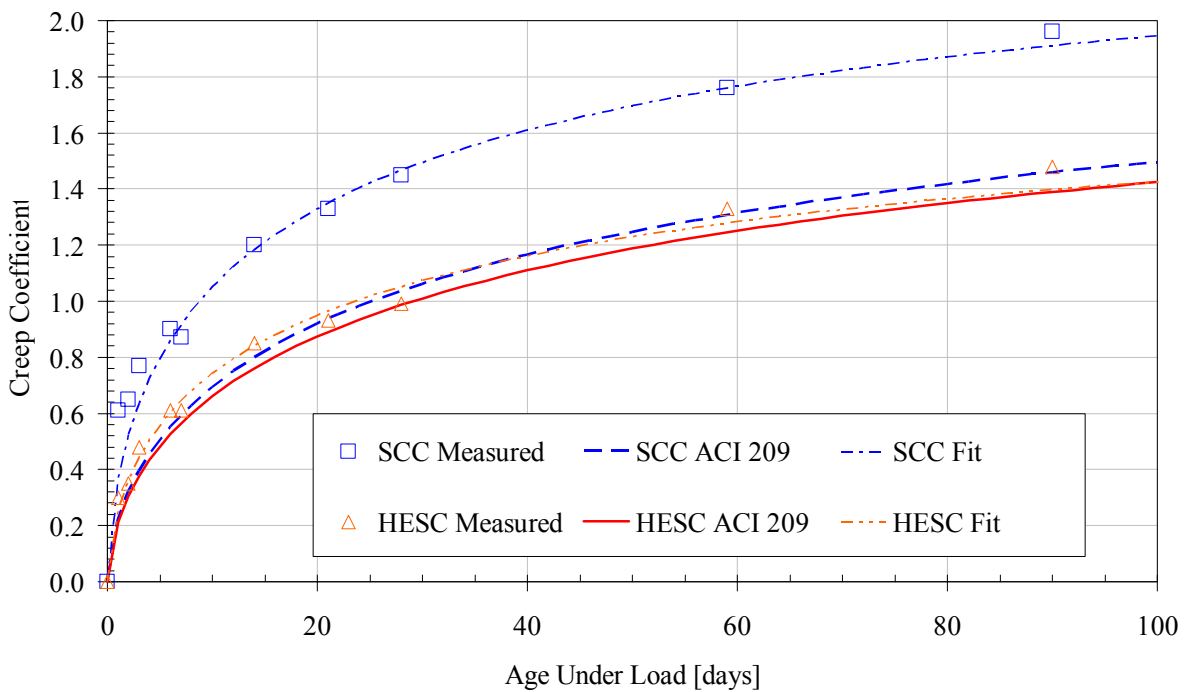


Figure 15: Creep response of material

7.7. Phase 1 Conclusions

The plastic and hardened concrete properties were thoroughly assessed in the first phase of the research. The tests were conducted on the plastic concrete and through material testing of concrete cylinders and prisms. All hardened concrete samples were cured along side the full scale beams or were match cured for the initial curing period. After the initial cure all specimens were cured according to ASTM requirements. The following conclusions can be made from the results of the first research phase:

- The SCC and HESC mix designs are typical of US practice. Specifically the levels of GGBF slag cement and coarse aggregate quantities and gradations are within acceptance levels for PennDOT and most transportation authorities.
- Proportioning of the HESC and SCC mixes was well controlled. The batched weights were within 1% of the design proportions.
- Moderate levels of GGBF slag cement were used along with type III cement to reduce cost and enhance performance. The levels, 35% for HESC and 25% for the SCC were within commonly used proportions.
- A crushed Diabase is used for coarse aggregate in both mixes. The relative hardness of the material should not compromise the structural performance of the concrete.
- The slump of the HESC was higher than the design expectations but was within the PennDOT limit of 8-inches.
- The spread of the SCC was lower than the design target, with a low of 20-in. and a high of 22.5-in. The mix however illustrated good stability and flow through reinforcement. No segregation of the mix was measured.
- The unit weights of the mixes were similar with the HESC having a marginally higher value. This can be attributed to the larger size coarse aggregate used in the mix.
- Batching temperatures were higher for the SCC due to the higher ambient temperature. The temperatures were within allowable levels.
- The time for initial set was 50 minutes longer for the SCC. The 5.2 hour and 6.3 hour setting times are within a reasonable range for precast operations.
- The time of set can be accurately predicted with a power function as detailed in section 7.5.3.
- Elevated curing temperatures on the order of 140°F were used during the initial 24 hours. This resulted in a rapid achievement of compressive strength. In addition, the initial cure resulted in a leveling of the strength up to 56-days followed by a late increase in capacity. The trends observed do not follow conventional ACI models for long-term strength gain.
- The SCC has a higher compressive strength than the HESC. This is most likely attributed to the fact that SCC has a lower w/c ratio and almost 100 lbs/cy more cement than HESC.
- The SCC has a lower elastic modulus than the HESC. This could be attributed to the lower aggregate content or the variation in the larger air void characteristics between mixes. These results should be verified with in-situ evaluation.
- The elastic modulus of the SCC is marginally over-predicted by ACI formulations. Analytical predictions of deflection using ACI formulations could result in a marginally unconservative estimate of deformation.
- The elastic modulus of the HESC is marginally under-predicted by ACI formulations. Analytical predictions of deflection using ACI formulations would result in a conservative estimate of deformation.
- The tension capacities of the concretes are conservatively higher than ACI estimates. The direct tension capacity and modulus of rupture is higher in the SCC than HESC. The strengths are comparable when normalized to the square root of the compressive strength.
- The shrinkage characteristics of the concretes are less than ACI 209 estimates.

- The SCC has 39% higher shrinkage strain than that of the HESC. Both shrinkage responses can be estimated by a standard formulation.
- The creep coefficient of HESC is within code expectations. The SCC has a higher creep coefficient than ACI expectations.

The SCC and HESC meet all mechanical characteristics needed for use in precast prestressed beam production. SCC has a higher creep than expected by code however this is balanced by a lower level of shrinkage. The combination of these effects is examined in the full-scale beam. Both mixes should perform well when evaluated in full scale testing of beams. The long-term durability of the SCC however must be examined to assess the resistance degradation in a freeze-thaw environment. Research on long-term durability is currently underway. A Phase 2 report is expected in Fall 2005.

8. REINFORCEMENT AND STRAND PROPERTIES

Conventional deformed reinforcement and 7-wire prestressing strand were used in the fabrication of the beam sections. The material specifications and bond capacities are detailed in this section.

8.1. Conventional Reinforcement

Grade 60 ASTM A615 conventional reinforcement is used. Conventional reinforcement was used for shear reinforcement and for continuity reinforcement at the end of the beam sections. Details on the bar sizes and use are presented in Section 8. All bars in the concrete were plain, no epoxy coating was used. Reinforcement properties are presented in Table 23.

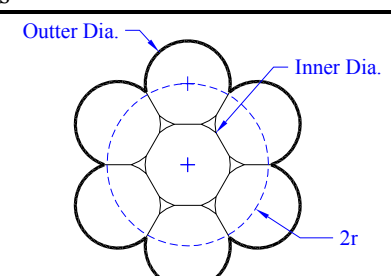
Reinforcement Type	Bar size	Lot	Material	Modulus [ksi]	Area [sq.in.]	Yield [ksi]	Ultimate [psi]
Continuity	#6	T1843	A615-gr60	N.A.	0.44	72.1	111.00
Stirrups	#4	s4-1200	A615-gr60	N.A.	0.20	65.8	104.33
Stirrups	#5	s4-1551	A615-gr60	N.A.	0.31	70.0	101.12

8.2. Strand Properties

The strand used in the project was produced by American Spring Wire Company located in the state of Ohio. The low relaxation 270ksi strand was used in all facets of the project. The production at SPI relies on the use of 1/2-in special strand to lower costs and simplify fabrication operations. Consequently, 1/2-in special is used even when 1/2-in standard is specified. To produce the same amount of prestress in the beams the strand is stressed to a lower level. For example, to achieve the 0.75fpu required of the 1/2" strand an initial prestress of only 0.69fpu is required to accommodate the larger area of the 1/2" special strands. Two lots of strand were used in the project. The mechanical properties are presented in Table 24.

Designation	Lot	Modulus [ksi]	Area [sq.in.]	Yield [ksi]	Yield Strain	Ultimate [ksi]	Fracture Strain	2nd Modulus [ksi]
1/2" Sp. Strand	46017	28970	0.16393	261.0	0.01013	284.51	0.0504	584.8
1/2" Sp. Strand	46179	29010	0.16393	259.22	0.01025	282.07	0.0506	566.2
Average	-	28990	0.16393	260.09	0.01019	283.29	0.0505	575.5

The wire properties were measured from samples taken from the strand reel. The average diameters, surface area, and twist are summarized in Table 25. The inner and outer strand diameters vary by 0.003-inch. ASTM A416 requires a minimum difference between center wire diameter and diameter of any outer wire of 0.003-in. for 0.5-in strand and 0.004-in for 0.6-in strand. The variation of the 1/2" special strand is not directly specified however the variation meets the requirements for 1/2" regular strand.

Strand Size	Inner Wire Diameter [in]	Outer Wire Diameter [in]	Pitch [in]	Exterior surface area [sq.in./ft.]	
1/2" Special	0.176	0.173	7.59	19.82	

The strand surface area is computed for use in bond stress determination. Prestressing strand are in the form of a helix where the six outer wires wrap around the center wire at a constant amount of twist. The pitch is the distance along the strand needed for one wire to complete one revolution around the center wire. Since the wires are in a helix, the unit length of wire per unit length of strand is greater than 1.0. The actual length of wire, L , can be computed by the pitch, p , and radius of the helix, r . The following formula is used: $L = (p^2 + 4\pi^2r^2)^{0.5}$. The resulting surface area is noted in Table 25.

8.3. Strand Bond Prequalification

The strand used for the research study was pre-examined using a large block pullout test [Logan 1997]. The test was conducted using conventional high early strength concrete without AEA or slag to match concrete materials used in previous pullout research. A water reducer was required to provide workability to the mix. Glenium 3030 NS high range water reducer (HRWR) was used; it should be noted that the HRWR has the characteristics of a normal water reducer at the levels used in the mix. Natural sand was used for the fine aggregates and a crushed Diabase stone was used for the coarse aggregate. The crushed stone has a Moh's hardness greater than 6 and an ASTM C131 abrasion resistance less than 20%.

Table 26: Large block concrete mix proportions	
Material Type	Batched
Total Cement [lb/yd ³]	660
Slag Cement [%]	0
Fine Aggregate SSD [lb/yd ³]	1098
Coarse Aggregate #67 SSD [lb/yd ³]	1899
Coarse Aggregate #8 SSD [lb/yd ³]	0
Water / Cement Ratio	0.439
High Range Water Reducer [oz/yd ³]	7.1
Retarding Admixture [oz/yd ³]	0
Air Entrainment Admixture (AEA) [oz/yd ³]	0
Viscosity Modifying Admixture [oz/yd ³]	0
Coarse Aggregate Volume [%]	10.27
Air Content [%]	1.6
Slump [in.]	6.25
Unit Weight [lb/ft ³]	154.4
Ambient/Concrete Temperature [F]	65/70

The bonding capacities of two heats of strand were examined in two pullout blocks. For each heat, samples were taken from three different rolls of strand. A total of six rolls labeled A thru F were studied. Each roll was tested in six pullout tests. As described by Logan [1997] the arrangement of the each of the strands in the block is chosen to provide variability in boundary effects (Figure 16). A total of 35 pullout tests were conducted on the 1/2in. diameter special 270K low relaxation strand. Data was lost for one test and is not included in the discussions.

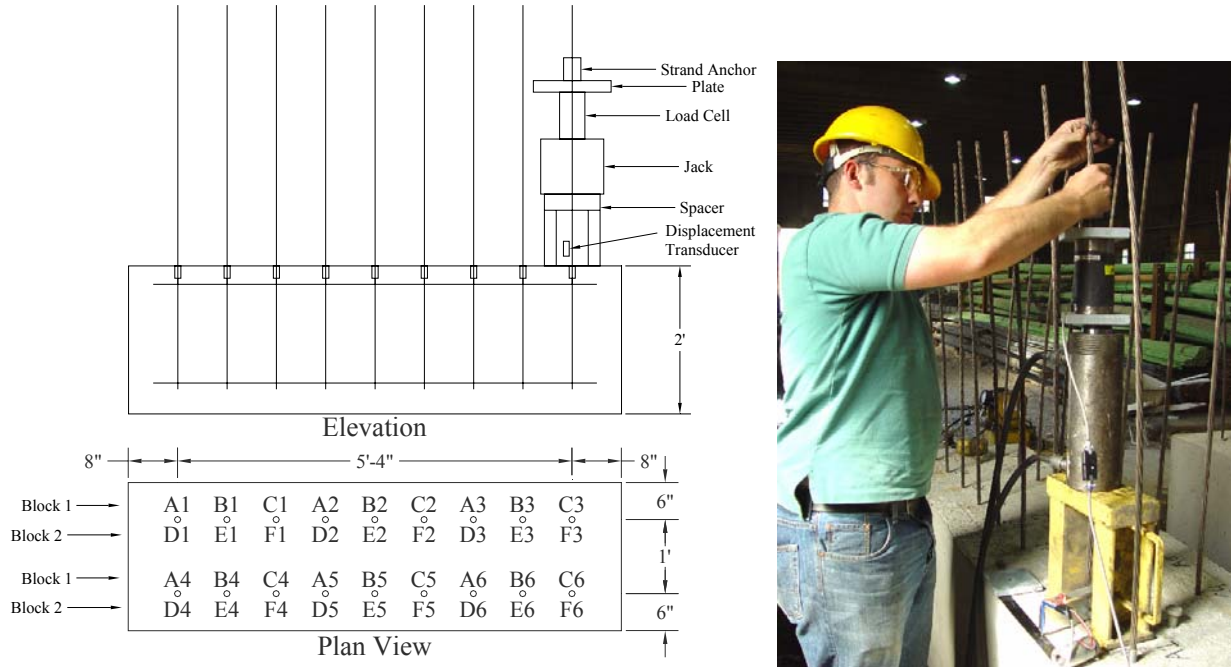


Figure 16: Large block pullout setup

The strand surface conditions were within PennDOT specification 408 requirements (Sec.1107.03.d.1).

“A light coating of surface rust is acceptable if it can be removed completely from the steel by wiping with a cloth.”

The strand surface varied from clean to light surface rust. All strands were wiped with paper towels to remove any excess surface rust (Figure 17). This operation was conducted just prior to placement of the concrete.

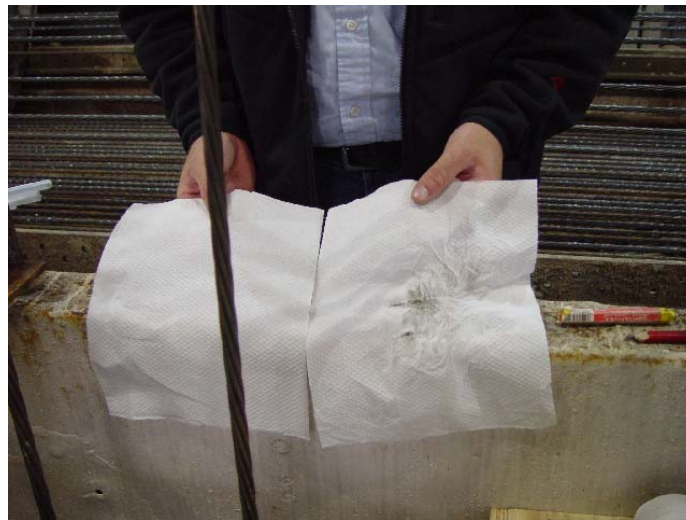


Figure 17: Typical strand surface condition

The pullout tests were conducted 25 hours after concrete placement. The concrete achieved a compressive strength of 3300 psi at 13hours and 3600 psi at 14 hours. The required 4000 psi strength was achieved at the time of the pullout tests. The tests were conducted at a load rate of approximately 20 kips/minute. Load was measured with a load cell in-line with the jack. Displacement of the strand

relative to the top surface of the concrete was measured with a potentiometer connected at the concrete to strand interface (Figure 16).

Strands from heat 1 achieved a marginally higher pullout capacity than heat 2 (Table 27). The coefficient of variation ranged from 9% to 19% for the six rolls of strand examined. Repeatability within a strand group was relatively poor. The pullout behavior followed a general progression. Elastic deformation of the strand initiated with application of load. After approximately 18 kips the pullout stiffness noticeably decreased (Figure 18). This correlates with bond slip of the strand from the concrete. The pullout resistance continued to increase as slip progressed eventually resulting in complete loss of bond capacity. *All* strands failed by pullout. The load – deformation responses of the tested strands are presented in Figure 18. The peak pullout capacity for each strand is indicated with a circle. Deformation of up to 1.4 inches was measured prior to bond loss. The variation between tests can be attributed to field testing conditions. It is envisioned that laboratory testing will be more consistent.

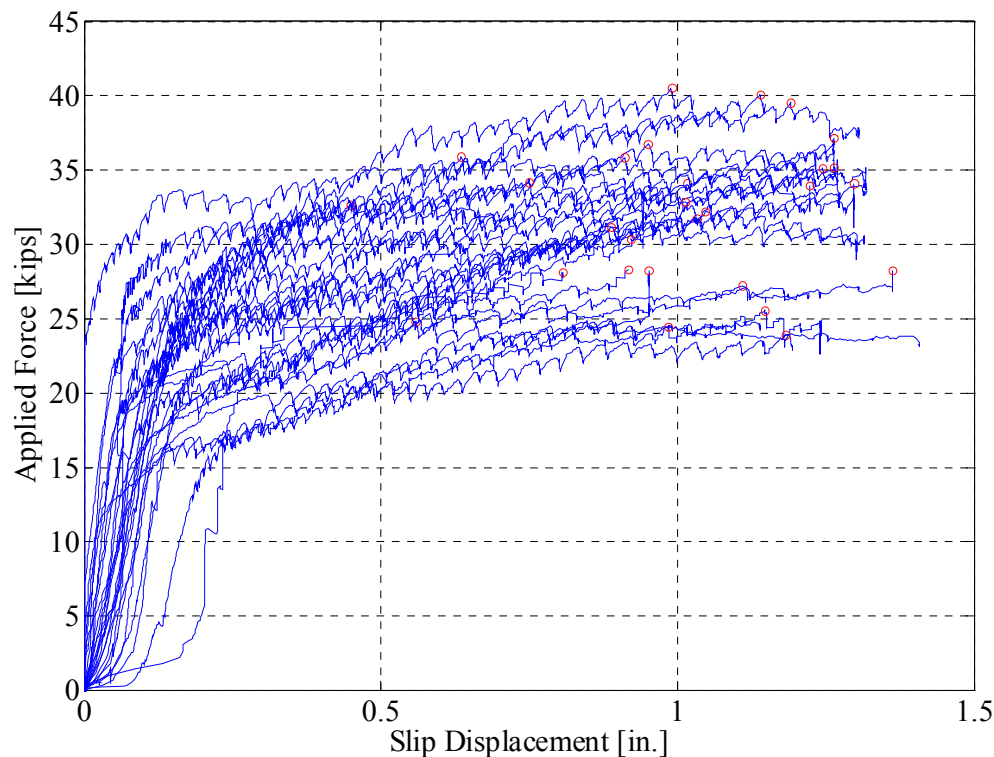


Figure 18: Pullout load-deformation response

The strand pullout strength is below levels recommended by previous researchers. On average the ½” special strand achieved a pullout capacity of 31.5 kips with a coefficient of variation of 15%. Previous research [Logan 1997] recommends an acceptable pullout capacity of 36kips for 1/2in. regular strand. Extrapolation to ½” special based on equivalent surface area (computed from the nominal diameter) results in an acceptance level of 37.4 kips for the ½” special strand. All strand pullout values were below the noted acceptance level.

The measured pullout values indicate that the bond strength is adequate for prestressing applications. This can be demonstrated by evaluating the required embedment length needed for fracture of the strand. Given that the bond test consisted of an 18-in. embedment, the length required for fracture can be computed based on the ratio of the measured bond strength to the fracture strength. The required length is computed for three cases: 1) PCI strand properties with the average bond strength, 2) mill certified strand properties with the average bond strength, and 3) mill certified strand properties with 5th percentile bond strength (assuming a normal distribution $x = x_{\text{mean}} - 1.645\sigma_x$). The results are summarized in Table 28

and Table 29. For both case 1 and 2 the length required to fracture the strand is less than the PCI transfer length of 29-inches. For the 5th percentile level, the required length is higher than the beam transfer length but less than the development length. Considering that only a short embedment length is needed when using the measured bond strength, the strands tested should provide adequate performance in the beams up to their ultimate flexural capacity.

It is important to note that the bond strength does not provide a good indication of slip potential. Slip of the strand during transfer of stress to the concrete could result in lower effective prestress in the beam. Consequently, the effective prestress of the strand in the full-scale beams is closely monitored during the fabrication and curing process. The results are discussed in the next section.

Heat	# of Samples	Group ID	Maximum Pullout Capacity			Pullout Capacity at 0.1"		
			Average	Standard Deviation	COV	Average	Standard Deviation	COV
			[kips]	[kips]	[%]	[kips]	[kips]	[%]
1	6	A	29.09	5.65	19%	19.35	10.64	55%
	6	B	34.33	3.35	10%	15.96	4.61	29%
	6	C	35.29	5.43	15%	20.47	4.23	21%
	18	All	32.90	5.41	16%	18.59	6.98	38%
2	6	A	27.47	2.46	9%	16.03	5.08	32%
	5	B	30.19	3.16	10%	16.30	8.54	52%
	6	C	32.17	4.23	13%	19.50	7.50	38%
	17	All	29.93	3.76	13%	17.33	6.83	39%
1&2	35	All	31.46	4.85	15%	17.95	6.84	38%

Bond Capacity	Strength for 18" embedment	Bond strength
Average	31.46 kip	1058 psi
(Design) 5 th Percentile	23.48 kip	790 psi

Strand Tensile Strength [ksi]	Strand Area [in ²]	Strand Tensile Force [kip]	Assumed Bond Strength [psi]	Required Length [in.]
270	0.167	45.09	1058	25.80
283	0.16393	46.39	1058	26.55
283	0.16393	46.39	790	35.57

8.4. Strand Property Discussion and Conclusions

The following points can be concluded from the discussion provided in this section:

- The prestressing strand examined has an ultimate strength of 283 ksi. While this is higher than the standard 270 ksi assumption it is well within expected design variability.
- Large block pullout tests of the strand resulted in an underperformance of the bond capacity when compared to recommendations available in the literature.

- Large variability was observed in the large block pullout tests. The test should be modified to allow for greater repeatability. This could be achieved through smaller pullout samples which would allow the concrete to cure in a uniform manner.
- The bond capacity of the strand was 31.46 kips or 1.06 kips/in² of surface area.
- A design bond stress was computed from the pullout data. A bond stress capacity of 790 psi is recommended for this group of strand.
- The average bond capacity was less than the accepted value of 37.4 kips.
- The length required for development of the full tensile strength of the strand was less than the transfer length using the average bond strength.
- The length required for development of the full tensile strength of the strand was less than the transfer length using the 5th percentile bond strength.

Based on these results and favorable past experience with the strand by the precast producer, the decision was made to go forward with use of the strand in the full scale bulb tee test program. In-situ measurement of transfer length and slip is performed and reported in the following sections. Combinations of both strand heats were used for fabrication of the beam section.

9. BEAM DESIGN PROPERTIES

The bulb tee sections used for the project model a contemporary elevated highway structure in the Eastern United States. The bridge system consists of approximately 600 precast/prestressed bulb tee beams with 8 separate ramps. A typical span 50 to 60ft with five adjacent bulb tees is used with an 8.5-in. composite slab to support 2 lanes of traffic in the same direction. A standard PCEF bulb tee is used.

9.1. PCEF 45" Deep Bulb Tee

The bulb tee is a 45-in. deep PCEF standard section. A total of 26 strands are used; 24 strands are used in the bulb and 2 in the top flange. All strands are horizontally spaced at a standard distance of 2 inches. The strand locations and bulb tee geometries are presented in Figure 19 and Figure 20. The gross and transformed section properties are given in Table 30.

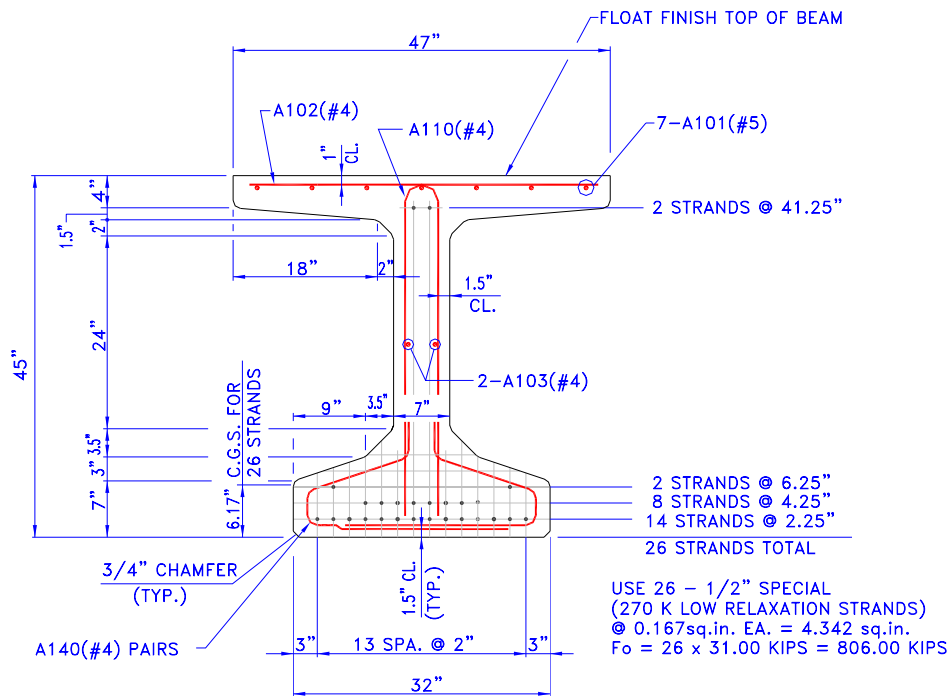


Figure 19: Specimen cross-section details [SPI]

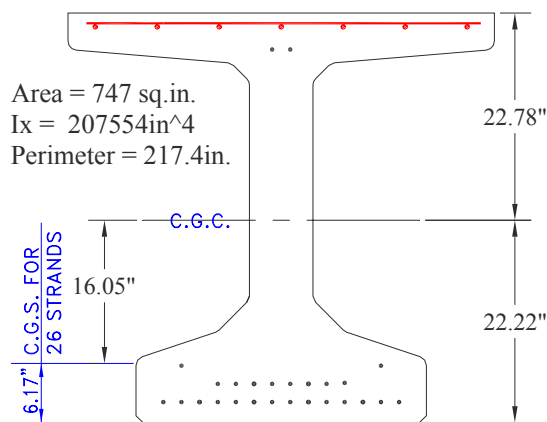


Figure 20: Beam geometry

Table 30: Geometric properties of full section

Gross Area	$A_G = 747 \text{ in}^2$
Gross Moment of Inertia	$I_x = 207,554 \text{ in}^4$
Distance to CGS from top	$d_p = 38.83 \text{ in}$
Distance to CGC from bottom	$y_t = 22.22 \text{ in}$
Eccentricity of strand	$e_p = 16.05 \text{ in}$
Area of one prestressed strand	$a_{ps} = 0.167 \text{ in}^2$
Total prestressed strand area	$A_{ps} = 4.342 \text{ in}^2$
Uncracked transformed inertia	$I_{g-tr} = 228,400 \text{ in}^4$
Cracked transformed inertia	$I_{cr} = 28,900 \text{ in}^4$

The transformed and cracked section properties are computed using the measured material properties. The average of the SCC and HESC elastic moduli are used (Table 20). The strand properties are from mill certification discussed in section 9. An average modular ratio of elasticity, $n_p = E_{strand}/E_{concrete}$, of 5.4 is used. The cracked moment of inertia is based on the PCI approach (PCI Eq.4.8.2) and is presented in Eq. 16. The equation only accounts for the contribution of prestressing steel.

$$I_{cr} = n_p A_{ps} d_p^2 \left(1 - 1.6 \sqrt{n_p \rho_p} \right) \quad (\text{Eq. 16})$$

Shear reinforcement is used throughout the length of the beam. The reinforcement location and details are presented in Figure 21 and Figure 22. Web shear reinforcement is placed at 3-in. on center along the entire length of the beam to allow for variability in loading applications. The beams will be evaluated without the inclusion of the deck slab. Consequently, the horizontal shear reinforcement commonly used in bulb tees is not included.

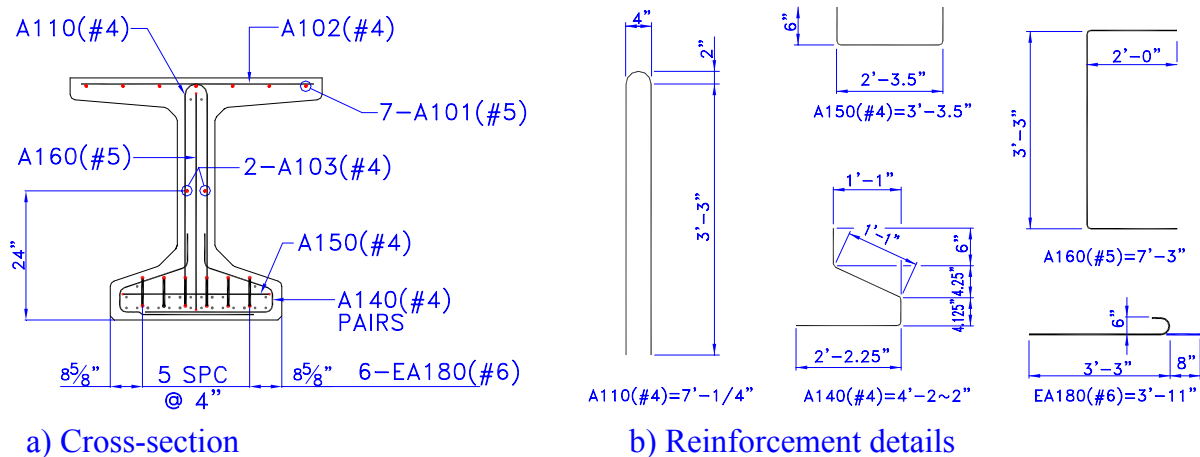


Figure 21: Conventional reinforcement details [SPI]

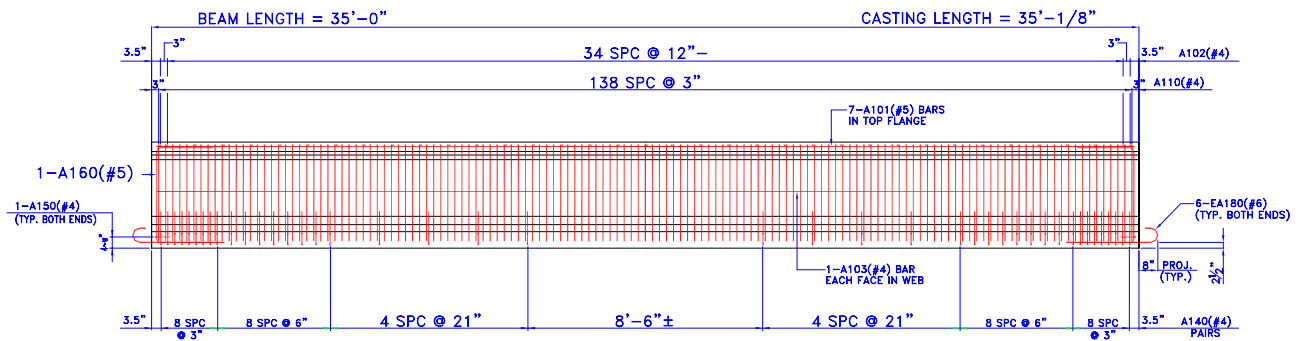


Figure 22: Beam elevation [SPI]

All tests were conducted *without* the addition of the 8.5-in. deck slab. As a consequence the section was predicted to fail due to crushing of the compression flange. To examine the response under a tension failure two beams were modified. The beam section was notched at the load location and the lower 14 strands were severed. With exception to the cutting of the strands at the loading location, all 26 strands were left intact for the rest of the span. The cut section is illustrated in Figure 23. The strand was severed by locally removing the cover concrete around the lower level of strand and flame cutting them. Adequate concrete protection was left above the cut strands to insulate the upper levels from any accidental heat damage. The notched region measured roughly 2 inches wide by 28 inches long by 3 inches deep.



Figure 23: Modified cross section showing cut prestress strands for tests 6 & 8

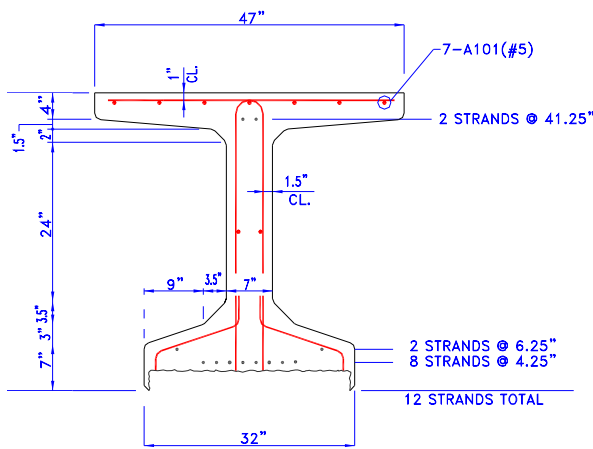


Figure 24: Modified beam geometry

Table 31: Geometric properties of reduced section	
Gross Area	$A_G = 651 \text{ in}^2$
Gross Moment of Inertia	$I_x = 159,300 \text{ in}^4$
Distance to CGS from top	$d_p = 34.25 \text{ in}$
Distance to CGC from bottom	$y_t = 25.29 \text{ in}$
Eccentricity of strand	$e_p = 14.54 \text{ in}$
Area of one prestressed strand	$a_{ps} = 0.167 \text{ in}^2$
Total prestressed strand area	$A_{ps} = 2.00 \text{ in}^2$
Uncracked transformed inertia	$I_{g-tr} = 181,600 \text{ in}^4$
Cracked transformed inertia	$I_{cr} = 11,000 \text{ in}^4$

9.2. Beam Fabrication

The four beams were fabricated from the same run of strand. The concrete was batched on-site and poured from a crane operated bucket. Approximately three batches of concrete were used for each beam. When placing the HESC, the bucket was emptied from one end of the form to the other, moving along the length of the form while filling and finishing, as the schematic in Figure 25 shows. To assist with consolidation, immersion vibrators and external form vibration were used. The SCC beams were fabricated following this process to limit the effects of HESC vibration on the SCC. In contrast with the HESC, the increased flow-ability of the SCC allowed for placement at only two locations along the beam length. First, the bucket was located at one end of the beam and the concrete was allowed to flow to the other end. Then, the process was repeated at the other end to complete placement. Immersion vibration was not used.

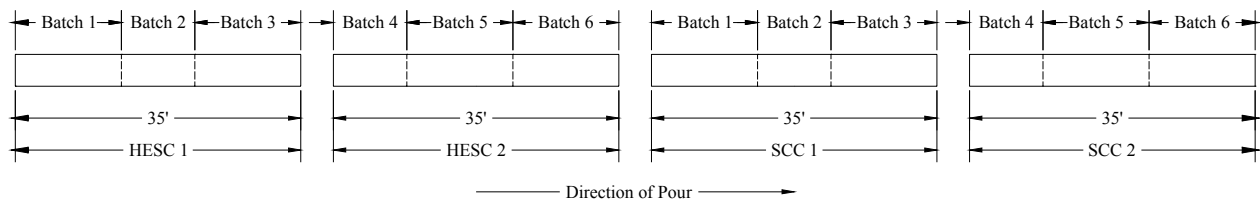


Figure 25: Beam placement schematic

9.3. Design Capacity

The prestressed section is analyzed in accordance with ACI 318 (2004). These procedures are in accordance with the methods of PennDOT, AASHTO, and PCI. The strengths are computed using the actual material properties. This includes the compressive strength, elastic modulus, and modulus of rupture of the concrete, and the effective prestress. Properties are determined for each of the eight beam tests based on the age of the concrete and effective prestress at the day of loading. The conventional and prestressed steel properties are based on the mill certification data detailed in Section 9.

9.3.1. Estimated Prestress Losses

The effective prestress within the beam varies as a function of time. The stress in the strand decreases from the initial jacking stress to the effective prestress due to a number of losses. The decrease in stress can be attributed to the effects of relaxation, creep, shrinkage, and elastic shortening. The strand is initially stressed on the casting bed to an initial jacking stress level, f_j . The jacking stress decreases due to relaxation of the strand in its stressed state. If the duration between initial jacking and release is long (such as 3 to 5 days) the level of relaxation can be large and should be adjusted prior to concrete placement. After the concrete is cast and achieves the required compressive strength for release the strand is at its initial stress level, f_{pi} . During release of the initial prestress the beam shortens due to compatibility with the strand and the concrete. This elastic deformation decreases the length of the strand and thus decreases the applied prestress. Losses also occur over time due to relaxation of the concrete, shrinkage of the concrete and creep of the concrete. Most code approaches lump all the losses together to determine the effective amount of prestress available during the service life of the beam.

The prestress losses are computed according to the equations of the PCI Bridge Design Manual and AASHTO LRFD Bridge Design Specifications. Creep, shrinkage and elastic shortening are identical for both techniques. The creep and shrinkage are independent of concrete type and are the same for both materials. The elastic shortening accounts for the different stiffness of the two concretes.

The loss due to relaxation of the strand is different between the two approaches. PCI uses an adjustment factor of 25% for low relaxation strand and the assumption is made that the intrinsic relaxation prior to transfer is included in the long term calculation. LRFD specification uses an adjustment factor of 30% and the intrinsic relaxation before transfer is added to the long term relaxation when determining losses. Since relaxation contributes only a small percentage of the total loss the impact of the variation between the two methods is minimal. The estimated losses are summarized in Table 32.

	Elastic Shortening	Shrinkage	Creep	Initial Relaxation	Secondary Relaxation	Total Losses	
AASHTO Eq.	5.9.5.2.3a-1	5.9.5.4.2-1	5.9.5.4.3-1	5.9.5.4.4b-2	30% (5.9.5.4.4c-1)		
PCI Eq.				8.6.5.3-1	25% (8.6.10.3-1)		
AASHTO	HESC	10.5	6.5	24.5	1.4	2.9	45.8
	SCC	11.7	6.5	24.5	1.4	2.7	46.8
PCI	HESC	10.5	6.5	24.5	1.2	2.4	43.9
	SCC	11.7	6.5	24.5	1.2	2.3	45.0

The precast producer adjusts the initial jacking force to accommodate the intrinsic relaxation that occurs prior to release. Since all the beams were cast on the same strand the initial prestress is the same for all beams. An initial load of 31.0 kips per strand was applied. This is equivalent to an initial load of 806 kips on the 26 strands or an initial prestress of 185.6 ksi at the time of transfer.

9.3.2. Transfer Length

The length required to transfer the initial prestress into the beam is termed the transfer length. The transfer length, L_t [in.], can be estimated by equation 17 where d_b [in.] is the nominal strand diameter and

f_{pe} [ksi] is the effective prestress. The transfer length for the ½” special strand used is interpolated from data available on smaller strands. A diameter of 0.52-in. is assumed for ½Sp strand and is used in the calculations. The transfer length for the different concrete beams based on the estimated PCI and AASHTO losses presented in Table 33. A transfer length between 24-in. and 25-in. is required.

$$L_t = f_{pe} \frac{d_b}{3} \quad \text{Eq. 17}$$

Table 33: Estimated transfer length			
		Effective Prestress [ksi]	Transfer Length [in.]
AASHTO	HESC	139.8	24.2
	SCC	138.8	24.1
PCI	HESC	141.7	24.6
	SCC	140.6	24.4

9.4. Shear and Flexure Capacity

The design capacity of the beam is computed using the detailed concrete and steel dimensions and eccentricities. The flexure and shear capacities are based on the design compressive strength and AASHTO based losses. The actual material properties and losses are measured and used in Section 10 to determine the strength of the beam more accurately. The design basis capacities are presented in Table 34. At failure the full section is at 98.6% of the ultimate strand stress, therefore the section should fail due to crushing of the compression flange. The reduced beam section will fail due to fracture of the strand.

Loading distances are based on the development length of the section. The development length is based on the nominal capacities of the beam. A failure strand stress of 270 ksi and an effective prestress of 139 ksi are assumed. A resulting development length of 92.2-inches is expected and is used for location of the load application points as discussed in Section 11.

Table 34: AASHTO capacity w/ standard material properties			
Initial stress	185.6 ksi	Prestress at transfer	175.08 ksi
Effective prestress	139.98 ksi	Transfer length	24.26 in.
Compressive strength	8000 psi	Rupture strength	670 psi
Full Section		Reduced Section	
Cracking moment	13,800 kip-in	Cracking moment	7550 kip-in
Fps	266.3 ksi	fps	278.8 ksi
Nominal flexural capacity	43,000 kip-in	Nominal flexural capacity	18,630 kip-in
Nominal shear capacity	456 kip	Nominal shear capacity	421 kip

9.5. Beam Design Summary

The design based strengths are computed according to standard procedures of AASHTO and ACI. The bulb tee beam section is modified to create two possible failure modes. In the full section, compression failure of the flange will be achieved. In the reduced section, tensile failure of the strand will occur. A development length of 92.2 inches is computed based on nominal properties and will be used as the basis of the test setup.

10. PHASE 2 NON-DESTRUCTIVE EVALUATION OF BULB TEE PERFORMANCE

The bulb tee beams were first evaluated in a non-destructive manner to examine the initial camber, creep, shrinkage, elastic response, and transfer length. The methods used and results of this evaluation are presented in detail in this section.

10.1. Initial Camber

The initial camber was measured at the center of each beam after release of prestress to assess the relative stiffness of the two beams. The measurements were taken with a standard tape measure with an accuracy of 1/16 inch. The HESC beams exhibited a camber of 3/8-in. and the SCC beams exhibited a camber of 1/4-inch.

The lower initial camber of the SCC is indicative of higher elastic modulus in the SCC beam over that of the HESC beam. The elastic modulus of the in-situ concrete can be approximated from the camber measurements. The following assumptions are made: 1) the curvature after release of prestress is constant, 2) the beam is supported at the ends, 3) the beam is subjected to the full initial prestress of 806 kips at an eccentricity of 15.73-in from the center of gravity of the concrete, and 4) the self-weight resists the camber deflection. The computed elastic moduli are presented in Table 35. Due to the resolution of the camber measurements the accuracy of the modulus values computed is limited. The elastic properties of the two beams are comparable when taking this error into account.

Member	Camber [in.]	Ec Computed [ksi]
HESC 1	3/8±1/16	3900 ± 700
HESC 2	3/8±1/16	3900 ± 700
SCC 1	1/4±1/16	5900 ± 1600
SCC 2	1/4±1/16	5900 ± 1600

10.2. Elastic Deformations

Concrete strains were measured internally during release of prestress. Resistance and vibration based strain gauge devices were installed prior to concrete placement. Resistance based Texas Measurements PML-60 strain gauges were installed past the computed transfer length at a distance of 152-in. from the beam end and monitored during release. Slope Indicator Vibrating Wire Embedment strain gauges were also used and placed at the center of the beam span. The vibrating wire gauges were measured before and after release and regularly up to the day of test. Both gages were placed between adjacent prestressing strands. The vibrating wire gauges were placed between the center two wires of the second level of strand at a vertical distance of 4.25-in. from the bottom flange face (Figure 26b). The resistance gages were placed between the second and third strand from the side face of the flange at a vertical distance of 2.25-in. from the bottom flange face (Figure 26a). Resistance strain gages were placed in all beams with a majority of instrumentation concentrated in two of the beams. The layout of strain gages used in each beam is presented in Figure 27 and Figure 28.



a) Resistance based gauge



b) Vibrating wire gauge

Figure 26: Concrete strain gauges

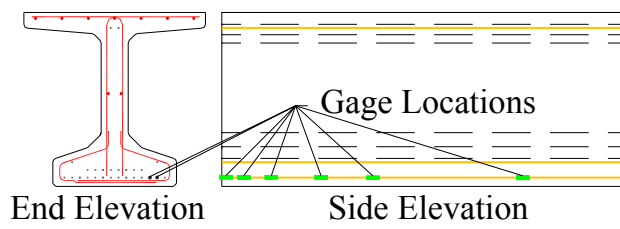


Figure 27: Strand strain gauge layout

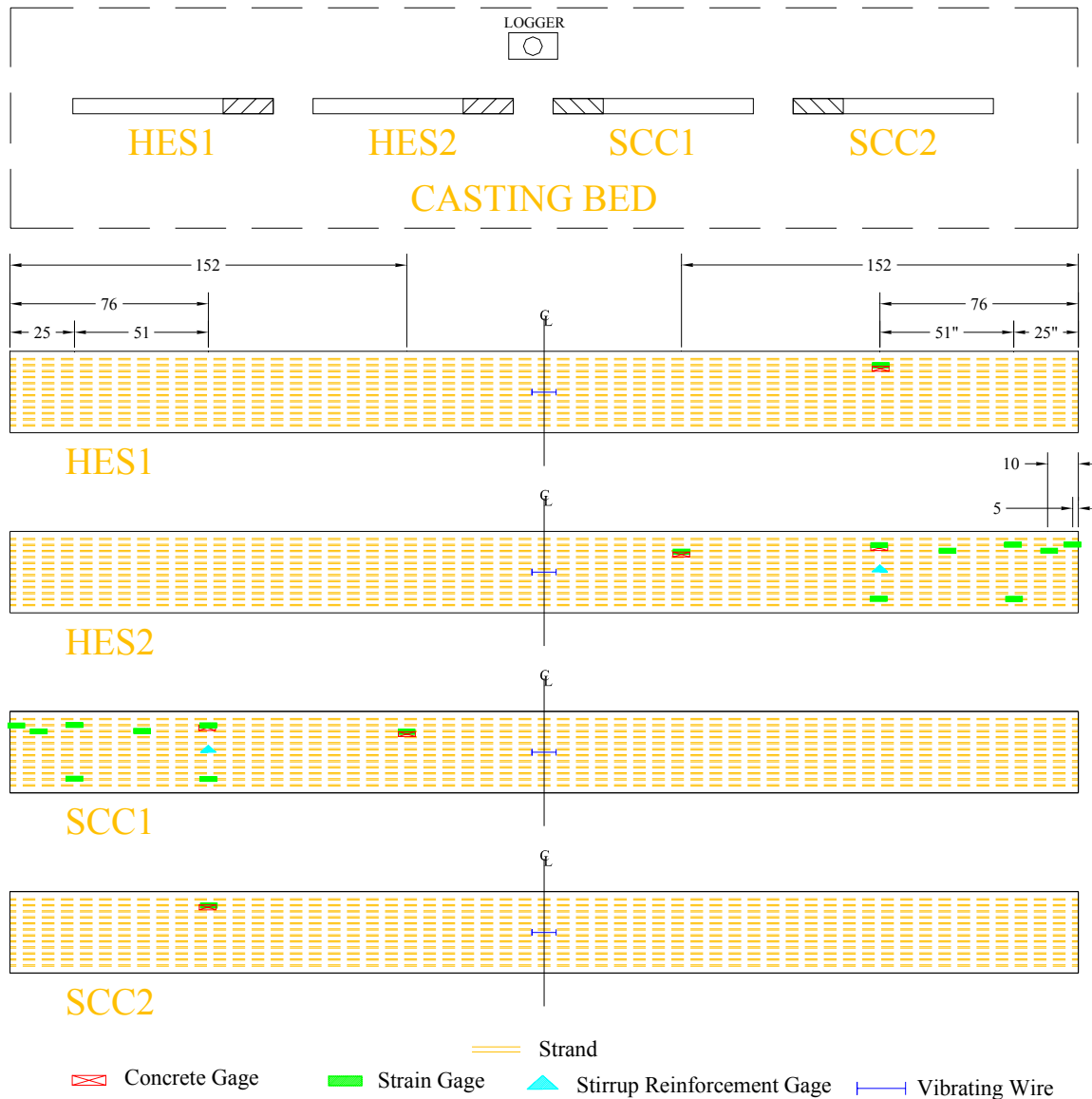


Figure 28: Overall internal gauge layout

The concrete strains generated during release of the initial prestress were measured and are compared to the expected response. The measured strain values are presented in Table 36. One vibrating wire gage was located in each of the four beams. The resistance strain gage was located in SCC beam 1 and HESC beam 2. From these measurements the apparent elastic modulus of the concrete and the effective prestress can be computed.

To compute the apparent elastic modulus an assumption of the initial prestress must be made. Assuming that the initial force at transfer, P_i , is 806 kips (see section 9) the apparent elastic modulus can be determined according to the standard equilibrium and constitutive relations (equation 18). The computation is dependent on the location of the strain gauge from the neutral axis, x , and the measured strain at release, $\epsilon_{measured}$.

$$E_c = \frac{1}{\epsilon_{measured}} \left(\frac{P_i}{A_g} + \frac{P_i \cdot e \cdot x}{I_g} \right) = \frac{1}{\epsilon_{measured}} \left(\frac{806kip}{747in^2} + \frac{806kip \cdot 16.05in \cdot x}{207554in^4} \right) \quad \text{Eq. 18}$$

To compute the apparent amount of initial prestress an assumption of the elastic modulus at release must be made. The measured 14-day elastic modulus is used for the computations. The initial prestress is computed using both the gross section properties and the transformed gross section properties. The results are presented in Table 36.

Beam	Strain gage type	Measured strain at release	Computed Elastic Modulus [ksi]	Computed initial prestress using gross properties [ksi]	Computed initial prestress using gross transformed properties [ksi]
SCC1	Vibrating	0.000400	5497	184.5	170.5
SCC2	Vibrating	0.000426	5162	196.5	181.5
SCC1	Resistance	0.000425	5467	171.2	185.6
HESC1	Vibrating	0.000470	4679	241.0	224.9
HESC2	Vibrating	0.000451	4876	231.5	216.1
HESC2	Resistance	0.000457	5084	207.1	222.2

The elastic strain indicates that the effective elastic modulus of the SCC is higher than that of the HESC. This is contrary to the cylinder test data which indicated that the SCC had a lower modulus than the HESC. The higher stiffness is inline with the initial camber measured. It is important to note that both the camber and the elastic shortening were measured at a concrete age of 1-day while the cylinder tests were conducted after 14-days. The higher stiffness at transfer could be attributed to a rapid initial gain in modulus for the SCC concrete over that of the HESC. The long term modulus is examined again during the load –deflection study.

Using an assumed elastic modulus to compute the initial prestress provides poor correlation with the actual initial prestress applied. The method, however, provides a rough estimation of the level of initial prestress present in the beams. The gauges are consistent and can be used to determine the level of prestress loss in the beams.

10.3. Measured Effective Prestress

The effective prestress is approximated using the embedded vibrating wire strain data. Since the gauge is located in the center of the beam span the assumption is made that no slip occurs between the strand and the concrete. Consequently, the strain in the concrete is equal to the strain in the steel. Using the mill certified elastic modulus of the strand the change in stress in the strand can be determined. This stress change represents the reduction in prestress due to creep, shrinkage and elastic shortening. Since relaxation of the strand occurs without a change in length the relaxation must be added to determine the total loss. The AASHTO estimate of relaxation is used. The resulting effective prestress for the two concretes are presented versus time in Figure 29 a and b. The initial point refers to the time of placement. The decrease at day one refers to the elastic shortening that occurs during release of initial prestress.

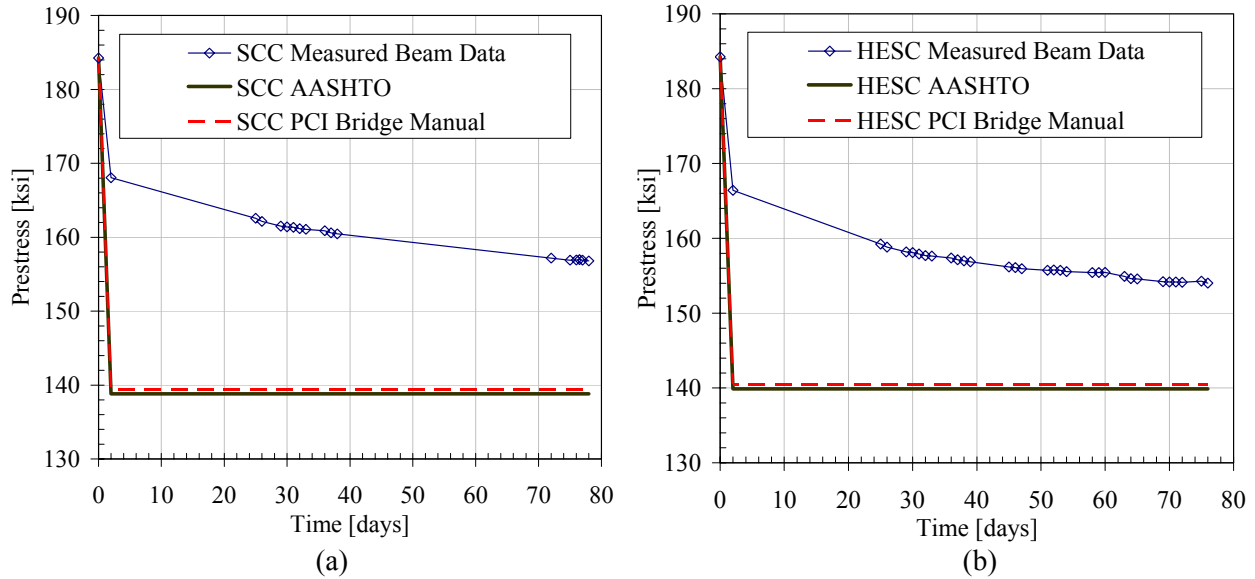


Figure 29: Effective prestress in beams

The measurements indicate that the effective prestress is considerably higher than AASHTO and PCI predictions. This indicates that both the HESC and SCC provide enhanced prestress transfer than standard assumptions. In addition the SCC exhibits less loss than the HESC (compare Figure 29 a and b). This indicates that the SCC provides enhanced resistance to creep and shrinkage than existing conventional HES concretes. Based on the trend of the measured response it appears that the losses are leveling out. From this response it can be expected that the long term losses will not approach the expected levels.

10.4. As-built Transfer Lengths

The transfer length is recomputed based on the effective prestress measured in the preceding section. Transfer length is defined as the length necessary to transfer the initial prestress from the strand into the structural section. This length is dependent on the strand to concrete bond available at initial release of stress into the section. As the stress in the strand is transferred the strand attempts to engage with the surrounding hardened concrete. If strand to concrete bond resistance is assumed to be uniform along the strand the stress and strain distribution in the concrete can be idealized as a linear distribution and take the form shown in Figure 30. As the stress is released in the strand it may tend to dilate thus improving the bond properties. If the concrete is of poor quality near the end of the beam the transfer may be compromised. If either of these conditions exists the strain in the strand may not be uniform as assumed and instead approach an alternate distribution such as those shown in Figure 31.

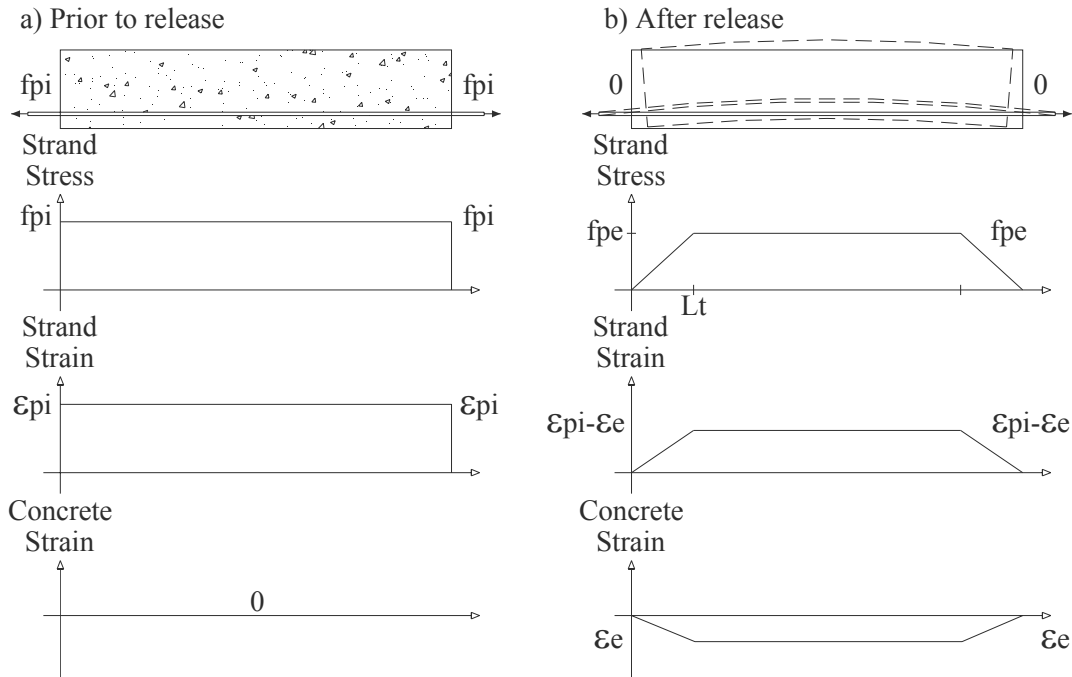


Figure 30: Transfer stress and strain distribution

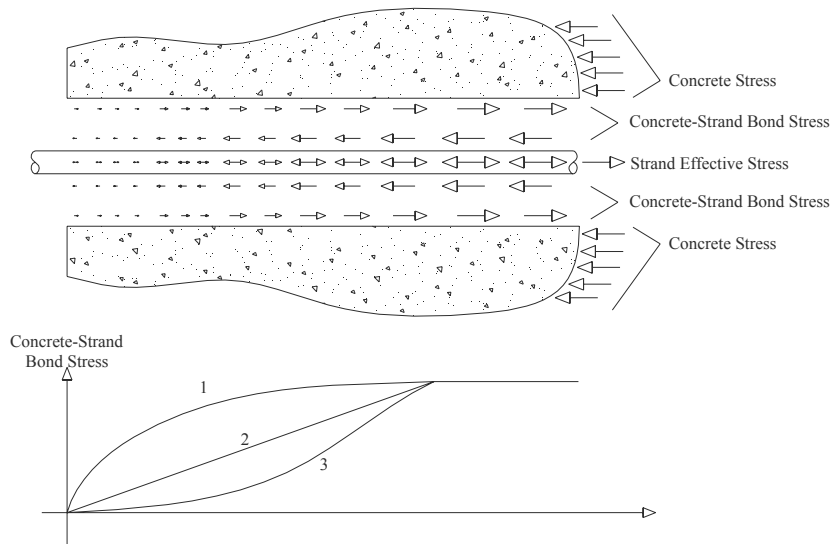


Figure 31: Bond stress distribution near member end

The strain was measured in the beam along the strand during release of prestress as discussed in section 10.2. The strain was monitored during the entire release period. The de-tensioning operation consisted of a simultaneous release of all the strands over a period of a few minutes. Measurements were taken continuously.

The change in strain of each gauge before and after release is used for calculation of transfer length. The strain is corrected to account for the existing strain in the strand and the vertical location where the strains were measured. The strain distribution after release of prestress is presented in Figure 32. Both the SCC and HESC have comparable transfer properties. The distribution is compared with the transfer length required using AASHTO estimated losses (Table 34). The AASHTO transfer length estimate is conservative when compared with the measured response in the SCC and HESC beams.

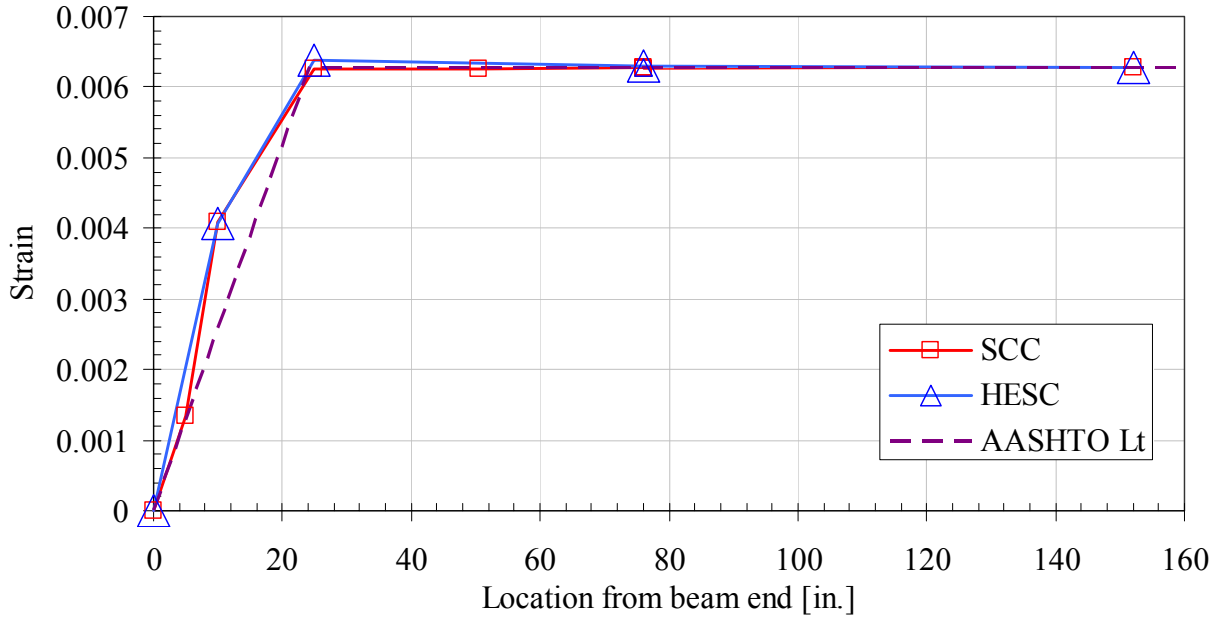


Figure 32: Measured transfer length

10.5. Estimated Beam Properties Using Measured Effective Prestress

The flexural and shear strengths are more accurately predicted using the measured concrete material properties and in-situ effective prestress. The concrete material properties were measured regularly through the research program and are presented in detail in section 7. The concrete elastic moduli, compressive strength, and effective prestress for each beam test are summarized in Table 37. The nominal shear and flexural strengths are higher than previously noted design capacities (Table 44) due to the elevated strength of the in-situ concrete. These values are compared to the measured capacities in later sections.

Test#	Concrete Type	Age [days]	f'_c [ksi]	E_c [ksi]	f_{pe} [ksi]	f_{ps} [ksi]	f_{ps} [% f_{pu}]	Mn [kip-in]	Vn [kip]
1	SCC	38	9166	4988	160.7	268.3	99.4%	43583	472.2
2	SCC	46	8930	4988	159.9	268.3	99.4%	43480	470.6
3	HESC	60	8780	5626	155.2	268.0	99.2%	43400	467.6
4	HESC	71	9183	5626	154.1	268.6	99.5%	43568	469.2
5	HESC	85	9696	5626	156.0	269.5	99.8%	43785	472.5
6	HESC	93	10037	5626	155.2	283.3	104.9%	19051	434.2
7	SCC	99	10330	4988	151.5	270.5	100.2%	44020	473.4
8	SCC	107	10720	4988	150.8	283.3	104.9%	19168	436.4

10.6. Creep and Shrinkage of In-Situ Beam

The creep and shrinkage strains in the bulb tee beam sections were lower than ACI 209 predictions. The strains were measured using vibrating wire strain gages as previously discussed in section 10.2. The strain measured reflects the combination of elastic shortening, creep and shrinkage strain. The ACI 209 predictions discussed in section 7.6.5 were applied to the section using an ACI multiplier to account for size variations between the 6x12-in. cylinders and the bulb tee section. A creep adjustment factor of 0.87 and a shrinkage adjustment factor of 0.47 were used. The beam experienced less creep and shrinkage than ACI predictions (Figure 33). Furthermore the SCC beam experienced less creep and shrinkage than

the HESC beam. From these observations one can conclude that the SCC provides greater resistance than HESC to the combined effects of creep and shrinkage when used in bulb tee beams.

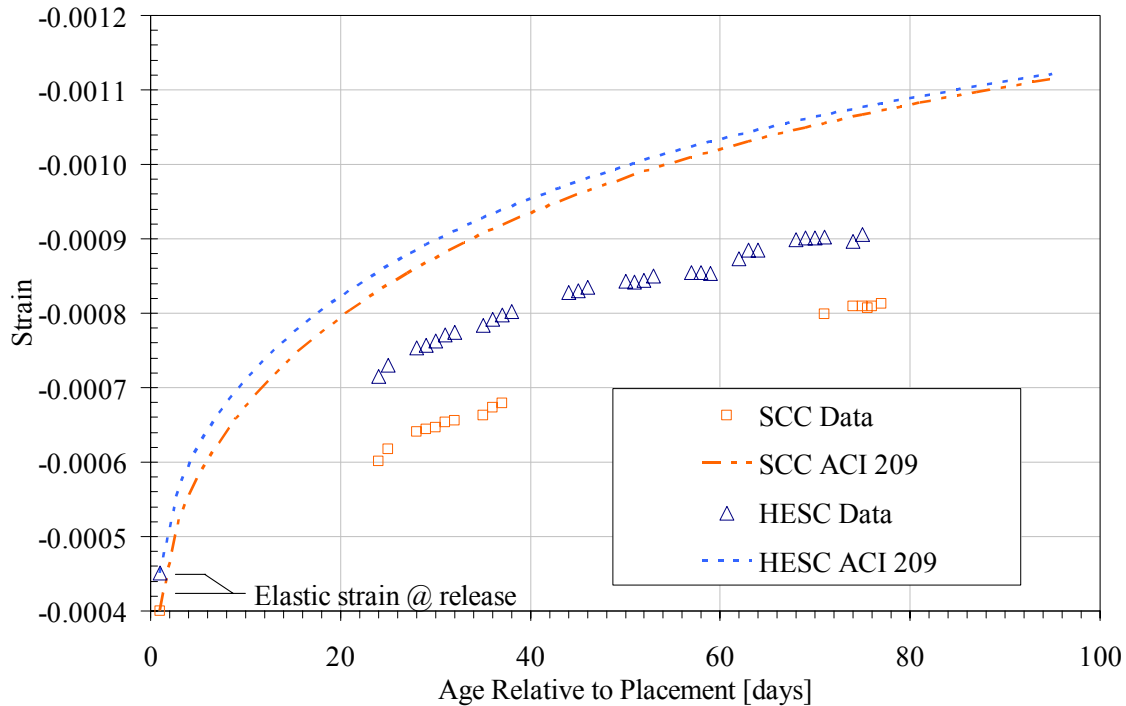


Figure 33: In-situ creep and shrinkage strain

10.7. Non-Destructive Performance Conclusions

Nondestructive evaluation of the beam indicates that the in-situ properties of the beam may be contrary to material test data. Conclusions made from non-destructive evaluation of the beam are summarized in the following bullets:

- The measured camber and elastic shortening of the beams indicate that the SCC is stiffer than the HESC. This contradicts the laboratory tests conducted on cylinders which indicated that the SCC was more flexible.
- The length required for transfer of initial prestress is shorter than that expected from standard PCI formulations. This indicates that the concrete to strand bond properties are within code expectations. Long term monitoring of this trend should be conducted through additional research.
- The transfer length required for both the HESC and the SCC compare well with each other. This indicates that the SCC could be expected to provide strand to concrete bond properties similar to HESC.
- The losses measured in the beam sections are less than code estimations. Furthermore, the SCC exhibits less loss than the HESC. Consequently, use of codified losses will provide a conservative estimate of the beam response.
- The expected shear and flexural capacities increase as a result of the as-built concrete strengths and effective prestress.
- SCC provides greater resistance than HESC to the combined effects of creep and shrinkage when used in bulb tee beams. This is counter to cylinder test data therefore further study should be conducted to evaluate the discrepancy in performance.

11. FABRICATION PRODUCTIVITY WITH SCC

Self consolidating concrete offers physical and economical improvements over conventional concretes due to shortened placement times and enhanced concrete quality. These benefits, however, come at the cost of higher material prices. The benefits and associated costs are examined in this section.

11.1. Cost-Benefit of SCC in Precast Production

In the Eastern US, precast production peaks from March to October. This period allows for the placement of members and cast in place decks prior to the cold winter months. SCC offers a means of achieving increased production over the busy months through reduced fabrication times over conventional mix designs. To assess the financial benefits of the improved productivity a study of the fabrication labor hours of the prototype beams was conducted. It is important to note that the study is conducted on a material which the fabricator has no previous production experience. Therefore the benefits achieved represent a lower bound on the expected gains.

During the fabrication of the SCC and HESC bulb tee beams the labor activities were identified and timed. The HESC and SCC placement tasks are tabulated (Table 38). The HESC consists of six different tasks while the SCC required only four. The use of SCC eliminated the need to advance the bucket during placement, vibrate the plastic concrete, and level the surface. With additional experience the SCC construction tasks could be further reduced to two tasks: placement followed by surface finishing.

Table 38: Fabrication tasks	
<p><u>HESC</u></p> <ol style="list-style-type: none"> 1. Place concrete from bucket/truck, 2. Advance wedge of concrete 3. Externally vibrate 4. Internally vibrate 5. Shovel concrete to approximate level 6. Screed 7. Finish top surface 	<p><u>SCC</u></p> <ol style="list-style-type: none"> 1. Place concrete from bucket/truck, place from end of forms 2. Externally vibrate (if needed) 3. Screed (if needed) 4. Finish top surface

The labor allocation required for fabrication of the bulb tee beams consisted of a 10 person crew for the HESC and a 6 person crew for the SCC (Table 39). Timed cumulative labor effort by the crew for placement, vibration, and screeding was tracked for fabrication of one beam. The working time of each crew member was noted. The HESC beam required a total of 1 hr 44 minutes of labor hours. The SCC beam required only 44 minutes of labor time; providing a labor savings of 1 hour per beam. Since the crew size was larger for the HESC beam, the overall construction time between beams was similar. The clock time needed for placement through screed operations was 39 and 33 minutes for the HESC and SCC respectively. The crew used for placement of the SCC had never worked with the material before. It is expected that placement time and labor savings gained with SCC will increase with greater experience.

Table 39: Fabrication crew		
	<p><u>HESC</u></p> <ol style="list-style-type: none"> (1) Crane Operator (1) Bucket Operator (2) Placement Crew (2) Internal Vibration (2) External Vibration (2) Finishing 	<p><u>SCC</u></p> <ol style="list-style-type: none"> (1) Crane Operator (1) Bucket Operator (1) Placement Crew (1) External Vibration (2) Finishing

Cost – benefit analysis of the two materials indicates that SCC may provide long-term financial benefits. Initially proper placement of SCC will require experienced laborers and additional training for quality control. This may result in higher near term labor costs. The material costs of SCC (as of May 2005) were \$73.08 per yd³ versus \$64.16 per yd³ for HESC due to the additional admixture types and quantities needed.

For a production of 50 bulb tee beams similar to the specimens fabricated, use of SCC equates to an **additional** cost of approximately 5%. This is due to the high quantity of concrete material placed per labor hour. While this indicates a negative impact on cost, it is expected that with complex beam sections where labor requirements are more intensive the savings will be more apparent. In addition, with greater use and experience placement time and labor costs are expected to decrease providing an equal or lowered cost to the manufacturer.

11.1.1. Product Quality

In general, surface quality improves with higher slump flows. SCC concrete mixtures typically provide improved surface finish characteristics over traditional concrete mixtures. The surface conditions were evaluated to quantify quality of the finish and the cost required to repair the girder prior to delivery. PennDOT states that any surface void measuring larger than 10mm×10mm must be filled and covered with mortar [PENNDOT 2004]. Surface condition photos were taken along the face of the beams (Figure 34). The number of voids requiring filling were found to be statistically identical between the two materials.

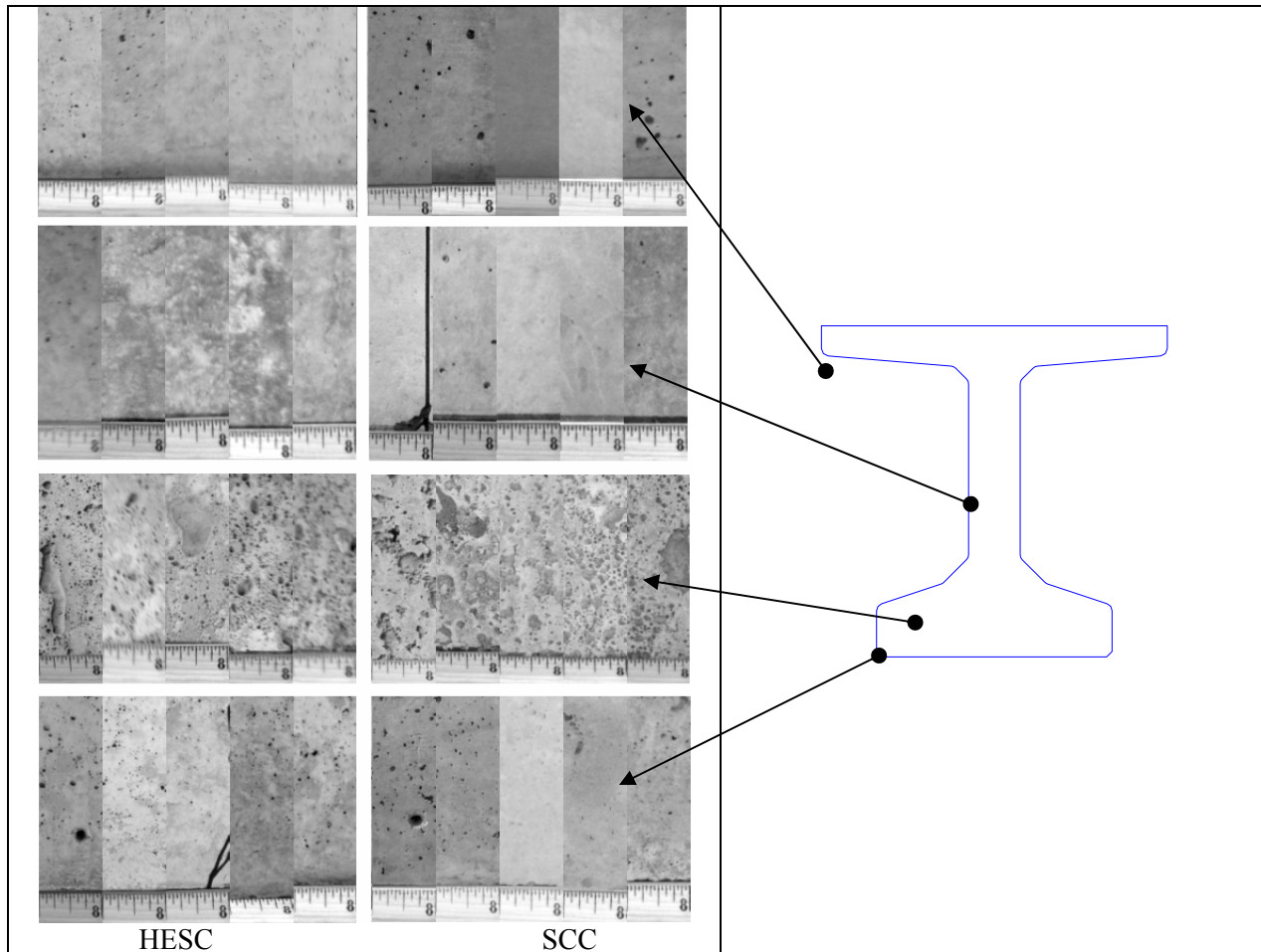


Figure 34: Surface conditions

Although the number of voids requiring filling were found to be statistically identical between the two concrete mixtures, minor adjustments to the SCC mixture and placement techniques may reduce the number of voids and improve the surface finish of the beams. This can be developed in conjunction with greater use.

The majority of voids form on the top of the bottom bulb flange due to the entrapment of bleed water on the shallow slope of the form. This occurs to a similar extent on both the HESC and the SCC beams. The SCC exhibited very good consolidation across the entire section. The presence of surface voids commonly referred to as “bug holes” on the face of the web was minimal.

11.2. Surface and Cost Summary

Based on the production times measured the use of SCC results in a marginal increase in production costs for large scale bulb-tee construction. These costs are based on the times measured for an inexperienced labor crew using SCC for the first time. It is highly likely that training would progress at a rapid rate with repeated use and in turn provide significant cost benefits. In addition the material provides comparable surface finishes to standard HESC mixes without vibration. Full adoption of SCC in the precast plant would significantly reduce the daily operation noise levels thus enhancing the work environment. Furthermore, additional costs would be recouped by eliminating the need to purchase, maintain, and use vibratory equipment. On a larger scope, the flowability of the SCC mix would also allow architectural finishes to be incorporated directly into the structural member, allowing for greater opportunities for structural precast in the bridge market.

The limited cost-benefit study indicates that SCC has good promise in achieving savings in precast production. It is recommended that further research be conducted to comprehensively assess the savings. If the opportunity arises a long term study should be conducted in line with a plant transitioning from HESC to SCC.

12. EXPERIMENTAL SETUP AND INSTRUMENTATION

Four 35-ft. long bulb tee beams were loaded to failure to assess the structural performance of SCC and HESC. Each beam was tested twice resulting in eight destructive tests. A total of three different loading conditions were used. This section describes the experimental setup and instrumentation used.

12.1. Testing Methodology

The beams were tested in the 5 million pound capacity press in the Fritz Laboratory of Lehigh University. The tests were performed by applying a point load at a chosen distance from the supports. An initial elastic cycle was applied to quantify the gross section behavior. Following the elastic cycle the beam was loaded past the cracking load and unloaded. Additional instrumentation was applied and the beam was cycled past the cracking load to assess the effective prestress. The beam was then loaded to failure. Failure was defined as a decrease in the load capacity to 80% of the peak load resisted.

12.1.1. Load Rate

The load tests were conducted in a quasi-static manner. Demands were initially applied under force control at a rate of 10kip/min. For the most flexible beam this equates to a displacement rate of approximately 0.01in./min. This rate was maintained until cracking. After cracking demands were applied under displacement control at a rate of 0.02 to 0.05 inches/min until failure.

12.2. Test Configuration and Boundary Conditions

The beams were tested in two different simply supported configurations. In all cases the load was located closer to the roller support. Each beam was first tested in configuration A until failure. The majority of the damaged section was then cantilevered off of the loaded span and the beam was retested in configuration B.

12.2.1. Configuration A

In configuration A, the full beam span was used. The supports were centered at 8-in. from the face of the beam. The load was applied at a distance of one development length plus the flexural depth of the beam, d_p . This distance was chosen to examine the performance of the beams at the design development length, L_d . A development length of 92.2 inches was used, the formulation is discussed in section 9.4. The assumption was made that the flexural cracks would form at 45-degrees from the load application point. With this damage the strand reaches its ultimate stress at a distance d_p away from the load (Figure 35). In this configuration the flexural strength was less than the shear strength and the development length was adequate. The configuration should force a compressive flexural failure in the beams.

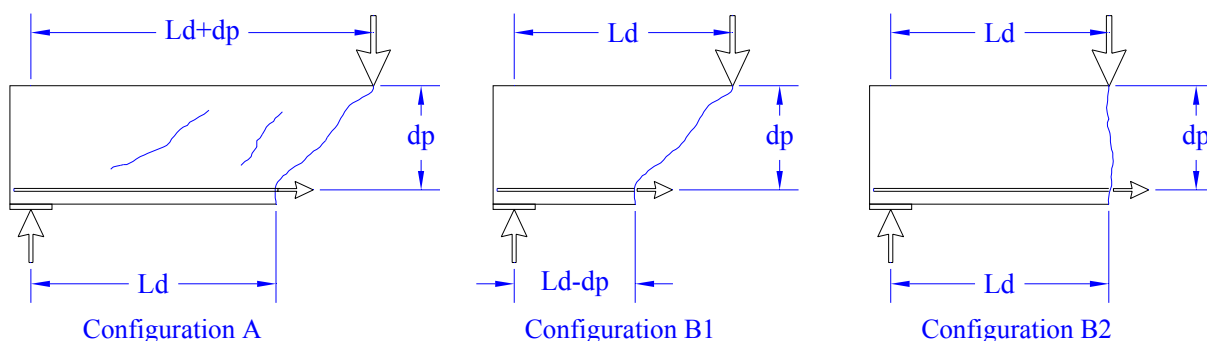


Figure 35: Force demands on cracked section

12.2.2. Configuration B

Configuration B is used after test A has been completed. A shorter span is chosen to minimize the effect of the damage incurred in the configuration A test on the results of test B. It is important to note that since the full span is used in configuration A, the entire beam section will crack to some extent.

Consequently, configuration B may have a lower initial stiffness than the configuration A test. Nevertheless, the ultimate response will not be significantly altered.

In configuration B, the load is applied at the development length from the end of the beam. The beam is altered in two of the tests to create a different failure condition. In the first condition B1, the full section is used. Since the load is applied at a distance closer to the support than A, the ratio of shear to flexure is higher. Consequently the shear strength controls. Furthermore, since cracking will radiate from the load point, the strands will have less than their full development length. This may result in slip of the strand during load application.

In the second condition B2, the lower strands are severed and the beam cross-section is notched. This notch creates a crack initiator which precludes the formation of diagonal cracking and allows for full development of the remaining strand. The reduced cross-section results in a flexural tensile failure mode, thus forcing the strands to a greater bond demand.

In summary, three failure conditions are examined for each concrete material. Configuration A produces a compression flexural failure, configuration B1 produces a shear failure with reduced bond length, and configuration B2 produces a tensile flexural failure. The test matrix for the four beams is summarized in Table 40. The first test on the SCC was loaded incorrectly thus only one full span (configuration A) test result is presented and discussed.

Load Case	A	B1	B2
Failure Mode	Flexure (Compression)	Combined Shear and Flexure	Flexure (Tension)
SCC [# of tests]	1	1	1
HESC [# of tests]	2	1	1
Number of Strands	26	26	12
Span [in.]	404	232	232
Load Location from Support [in.]	130.5	92.2	92.2
Strand Development Length	Ld	58%Ld	Ld

12.3. Load Application and Self-Weigh Demands

The loading conditions are statically determinate. The internal moment and shear is computed as a function of the concrete unit weight of 150lb/ft³. The shear and moment is presented separately for the self-weight and as a function of the applied load, P, Figure 37. In configuration A, the beam is under significant initial positive flexure due to the self-weight. The flexural demand due to self weight is approximately 5% of the cracking strength. In configuration B, however, the cantilevered portion of the span works to counterbalance the positive span resulting in a very low initial flexure in the section.

The additional weight of the loading plates and pin (Figure 36) is not accounted for in the shear and moment diagrams presented in Figure 37. Three different configurations are used. In test 1 the loading plates weigh 1.32 kips. In test 2 through 4 the plates weigh 1.03 kips, and in test 5 through 8 the plates weigh 1.09 kips. These forces are accounted for in the moment and shear capacities presented in the next section.

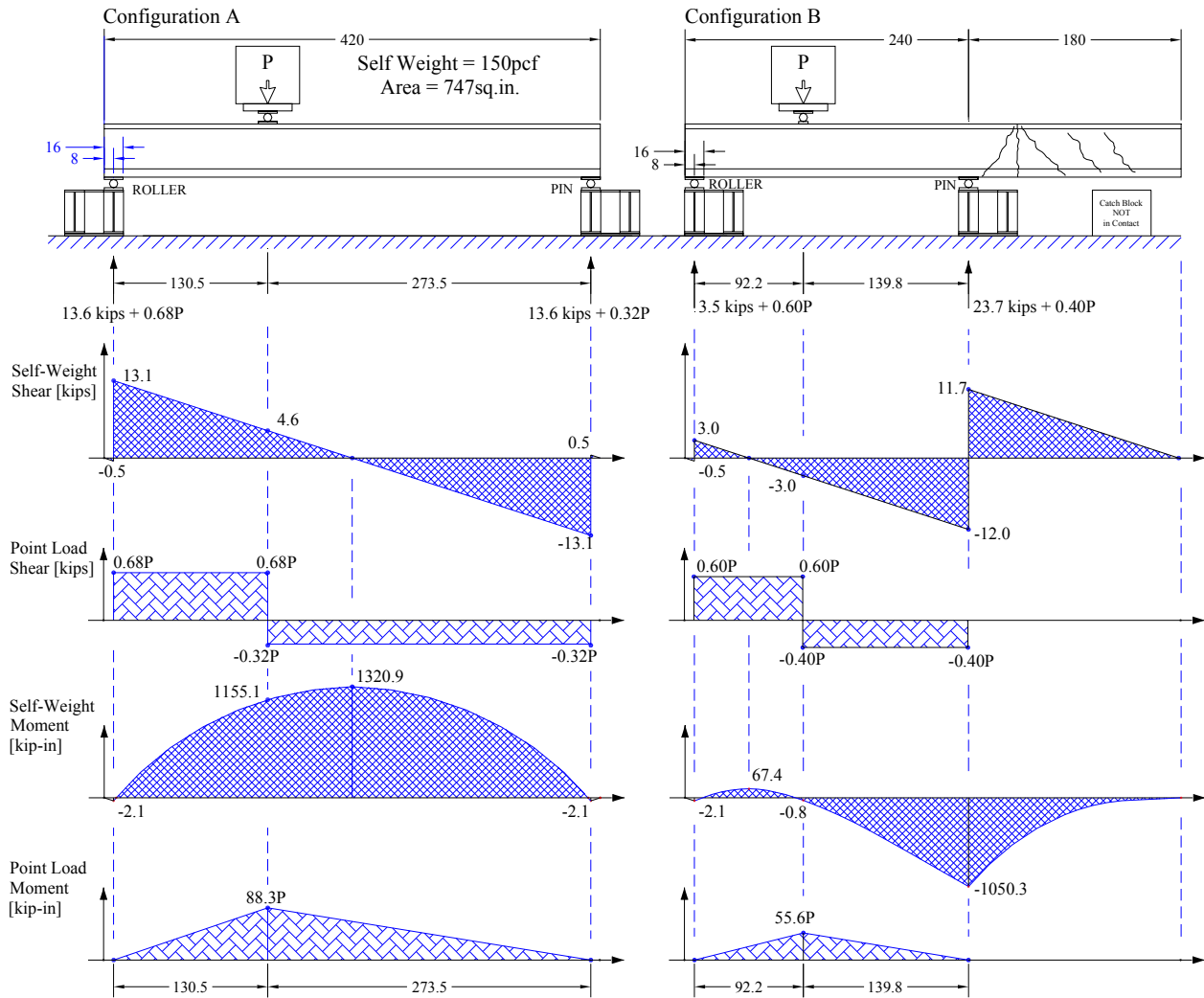
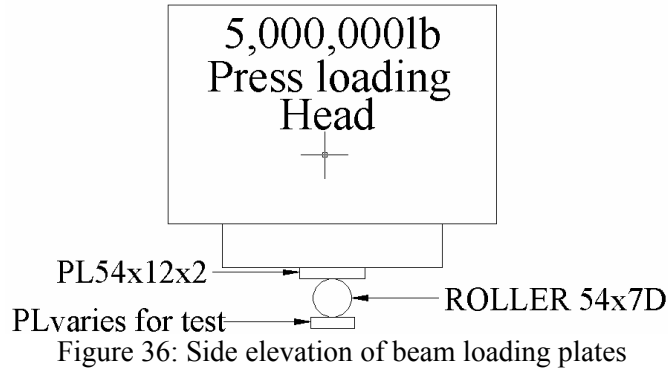


Figure 37: Moment and shear distribution for loading configurations

12.4. Instrumentation

The beams were instrumented to measure global response and local effects using a variety of resistance strain gages, inclinometers, and displacement transducers. The Macro Sensor Linear Variable Differential Transformers (LVDT) are used to measure small single axis displacements. These include slip of the strand and local deformation of the beam face. For deformations greater than 1-inch a wire potentiometer is used. These potentiometers were used to measure the vertical deflection of the beam.

Rotation of the supports was measured using inclinometers. Resistance strain gages were used on the concrete surface, within the concrete, and on the prestressing strand. The strand gages were bonded directly to the individual wires after the strand was stressed and prior to placement of the concrete. Internal strain gage configuration was previously presented (Figure 27 and Figure 28). The surface gages were attached using epoxy. The surface laitance was removed with a grinder prior to epoxy application. The general configuration of the instrumentation used is pictorially illustrated in Figure 38.

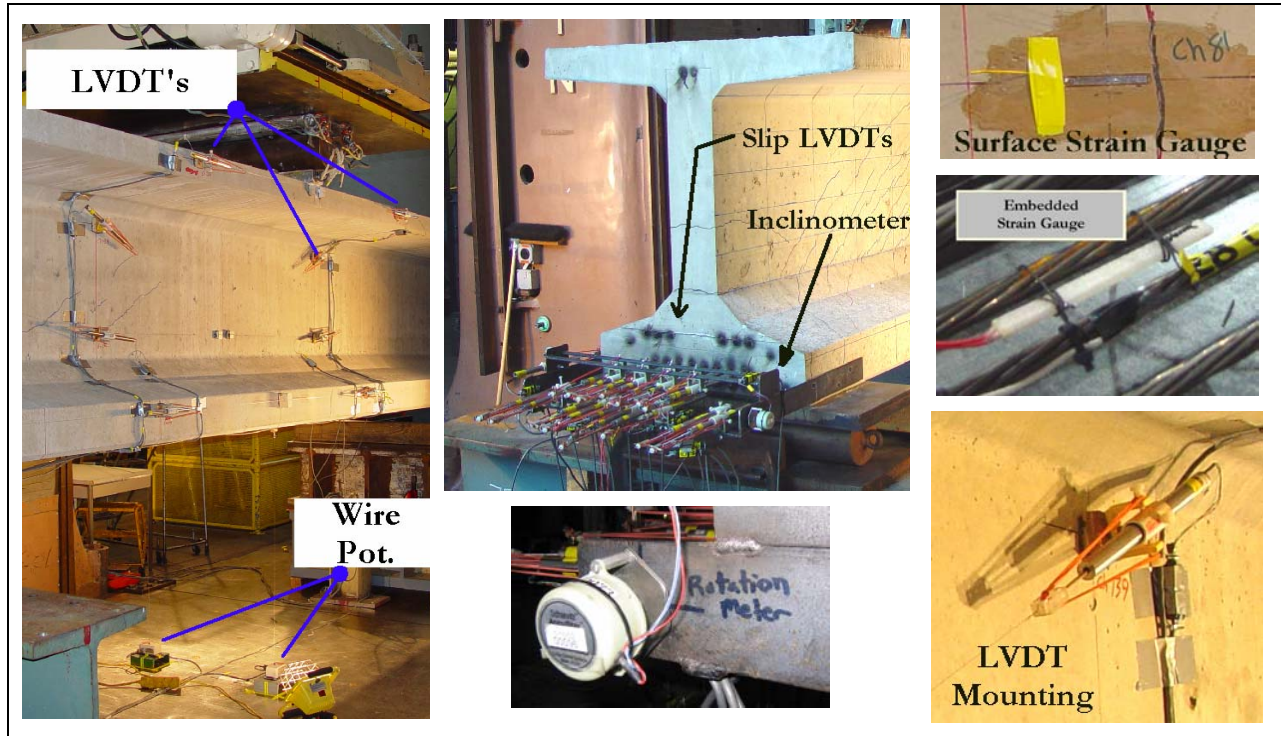


Figure 38: Instrumentation

12.4.1. External Strain, Deformation, and Rotation

The external instrumentation used on each of the tests is detailed in Figure 39 through Figure 46. Additional strain gages and LVDTs were added to the beams as the project progressed to improve understanding of the response.

12.4.2. End Slip

Slip of the strand was measured for each test. To measure slip a steel bracket was mounted directly to the beam end. Slips were measured on both the loaded end and the far end for configuration A. For configuration B the far side of the beam was damaged, therefore slip was measured only on the near end. Spring loaded LVDT's were placed in contact with the bottom two levels of strand. To accommodate instrument contact the strands were cut flush prior to testing. In the first two tests the LVDT's were placed in contact with the strand end without special attention to which of the seven strands the LVDT contacted. Initial observations indicated that the center strand often slipped during large deformations without an accompanying slip of the external six wires. To ensure that true strand-concrete slip was being measured on the last six tests the LVDT was placed in contact with the outer six wires of the strand. The strands instrumentation pattern is illustrated in Figure 47.

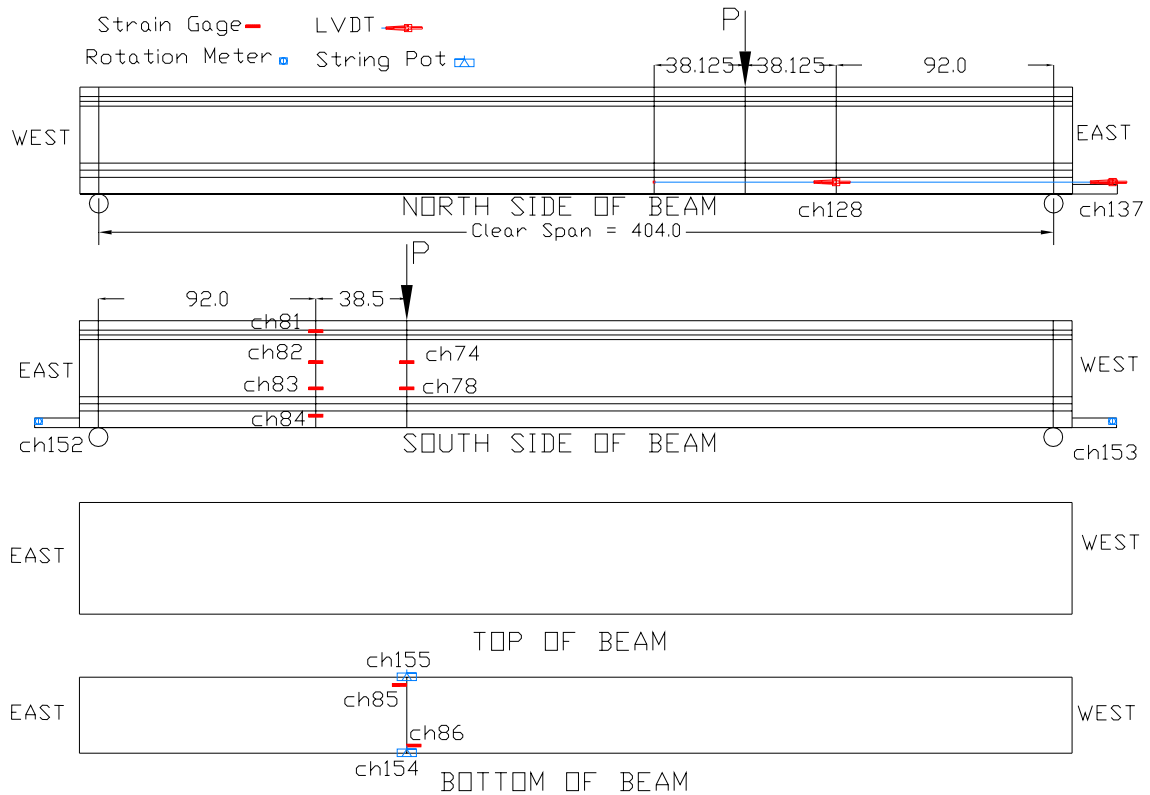


Figure 39: Global instrumentation Test 1 (SCC Full Span)

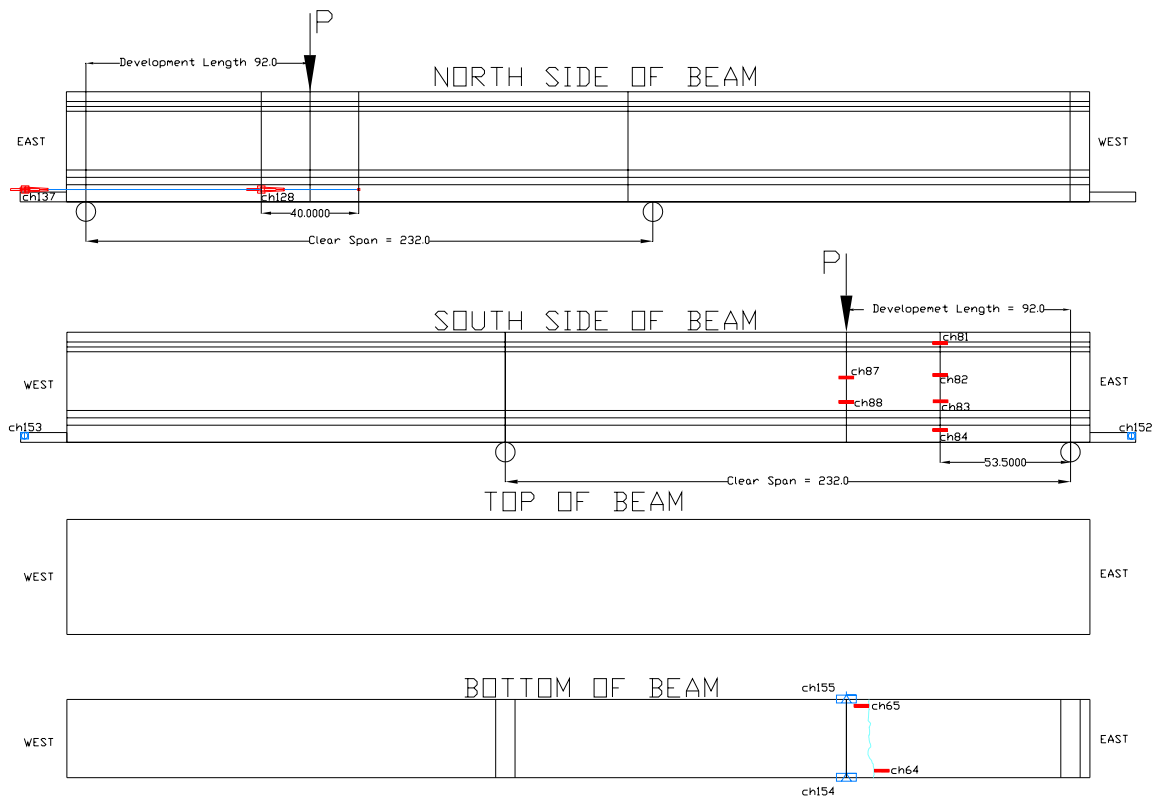


Figure 40: Global instrumentation Test 2 (SCC Short Span)

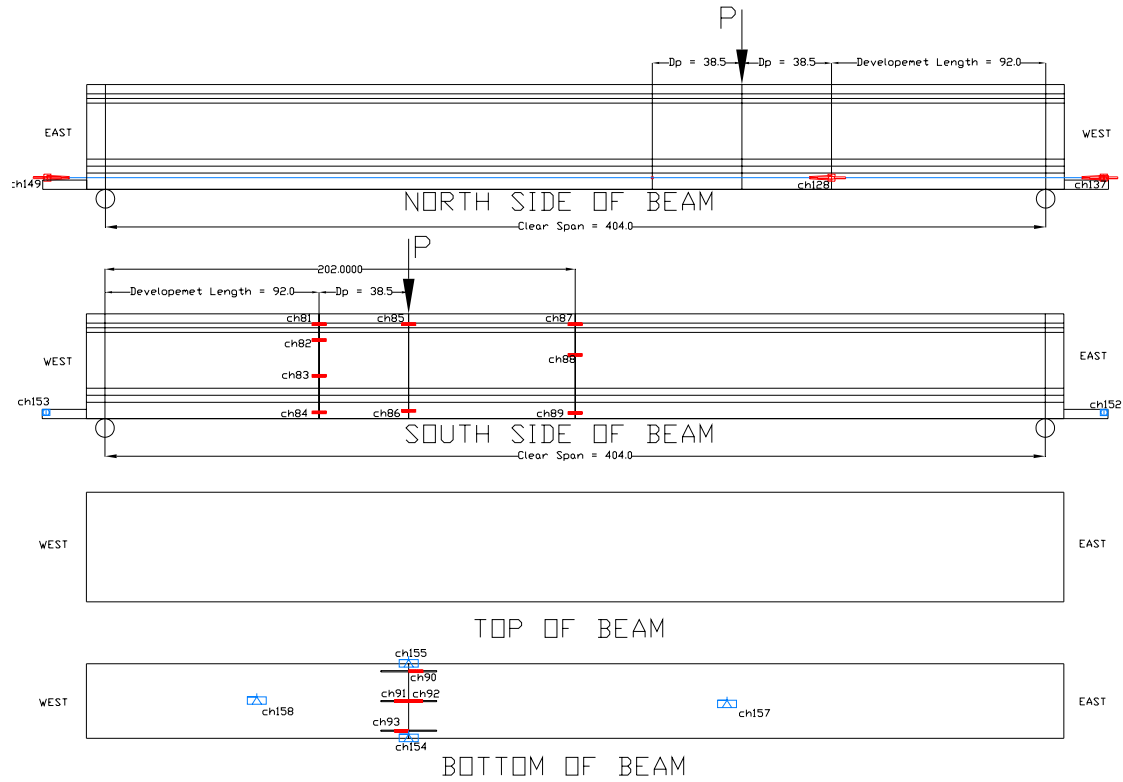


Figure 41: Global instrumentation Test 3 (HESC Full Span)

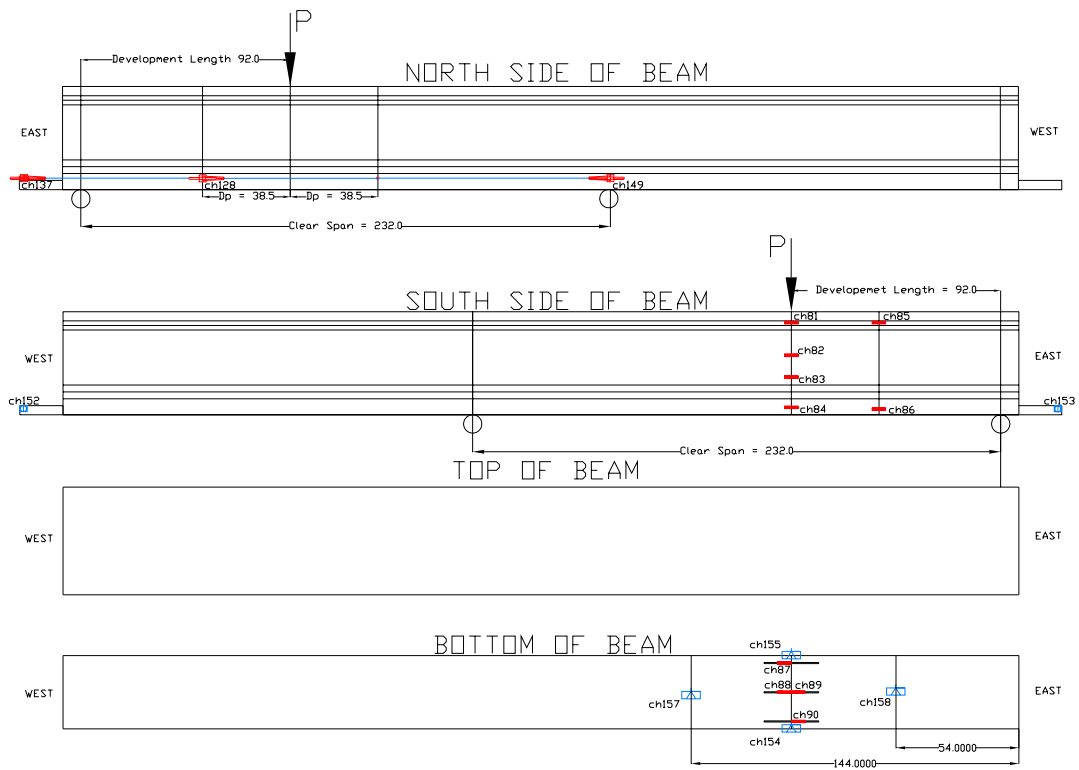


Figure 42: Global instrumentation Test 4 (HESC Short Span)

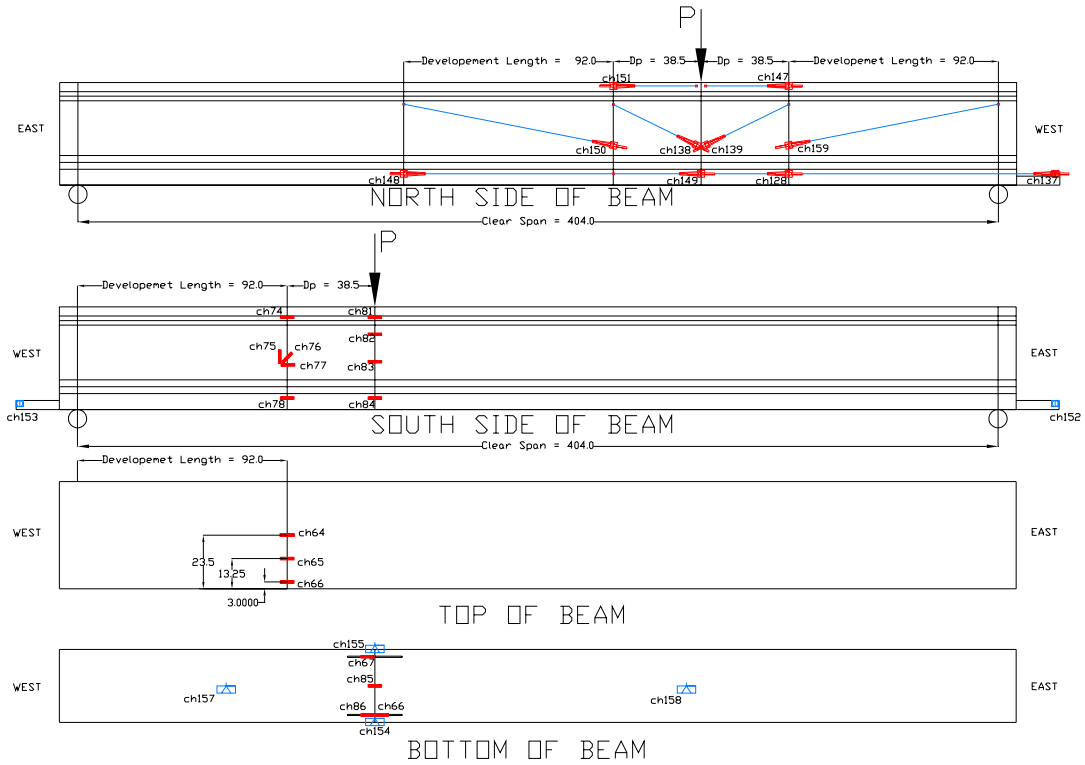


Figure 43: Global instrumentation Test 5 (HESC Full Span)

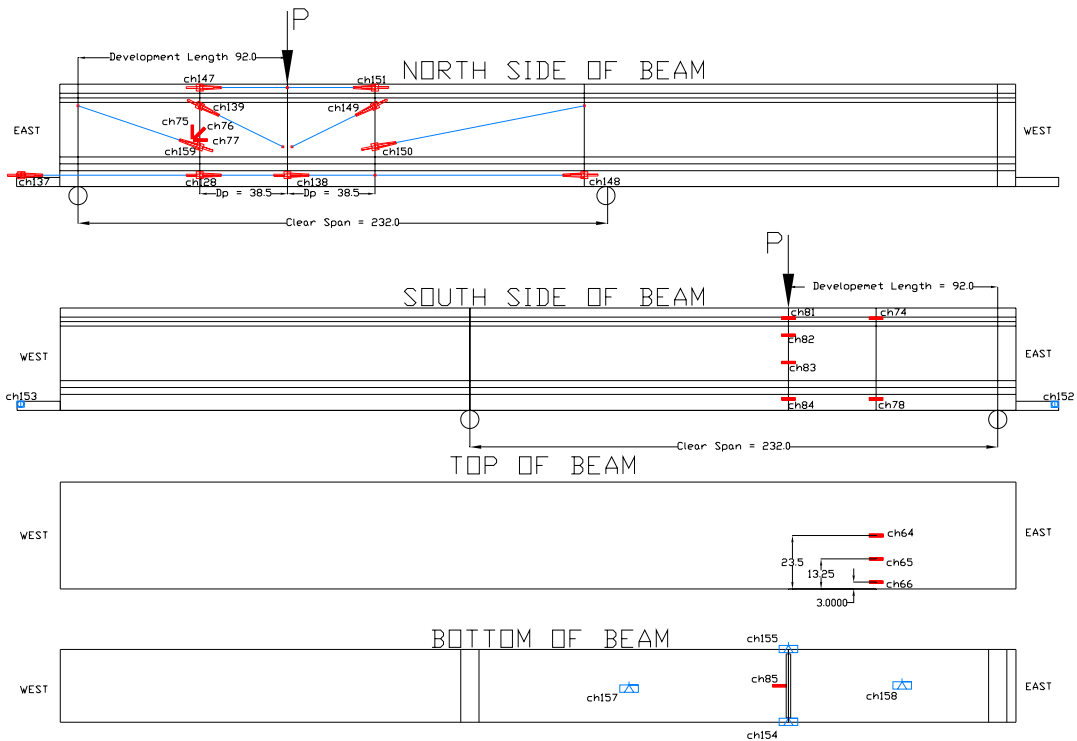


Figure 44: Global instrumentation Test 6 (HESC Short Cut Span)

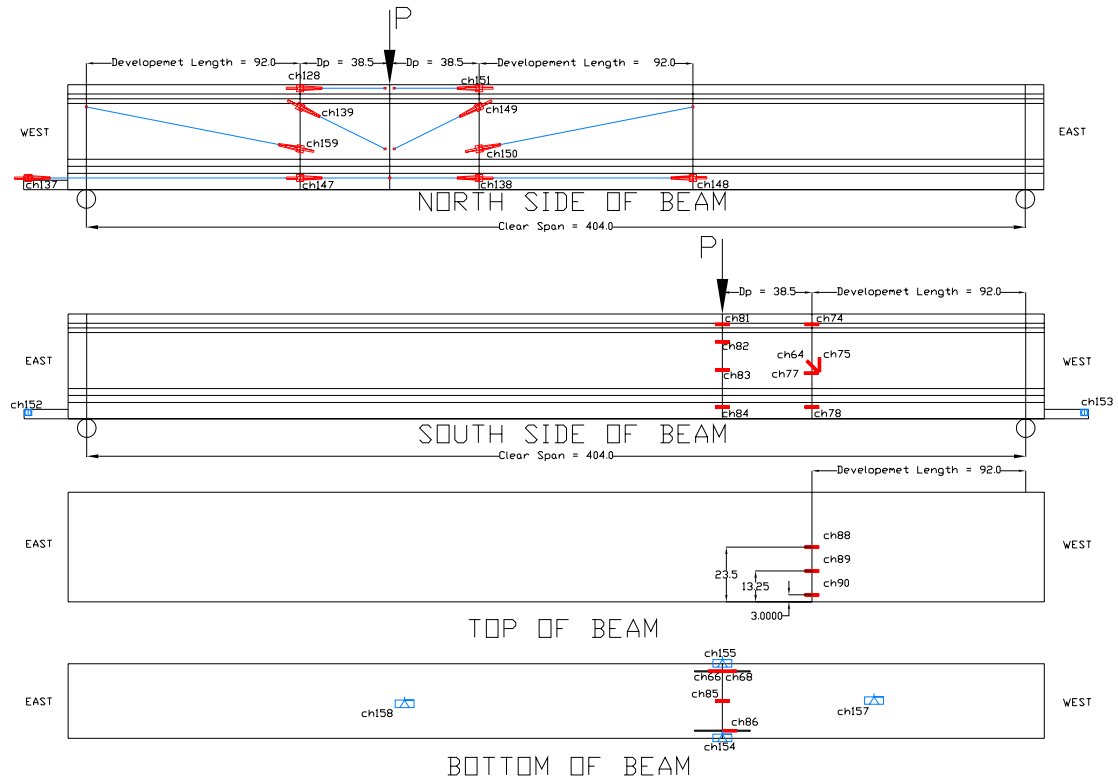


Figure 45: Global instrumentation Test 7 (SCC Full Span)

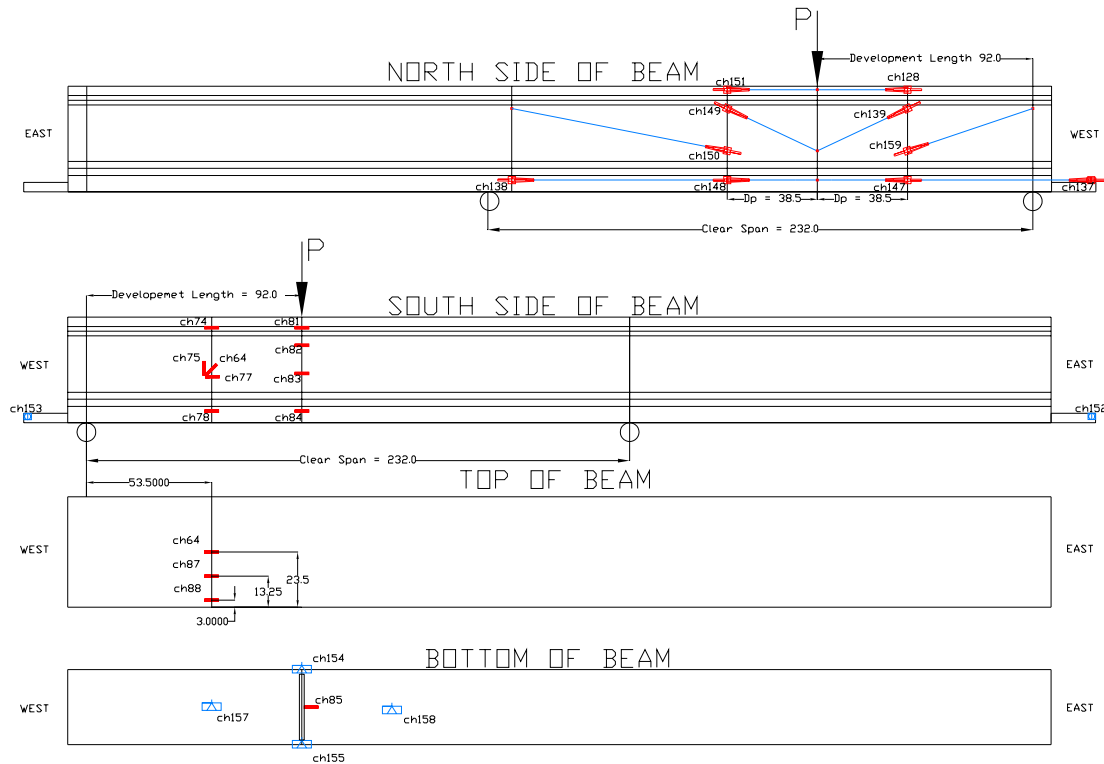


Figure 46: Global instrumentation Test 8 (SCC Short Cut Span)

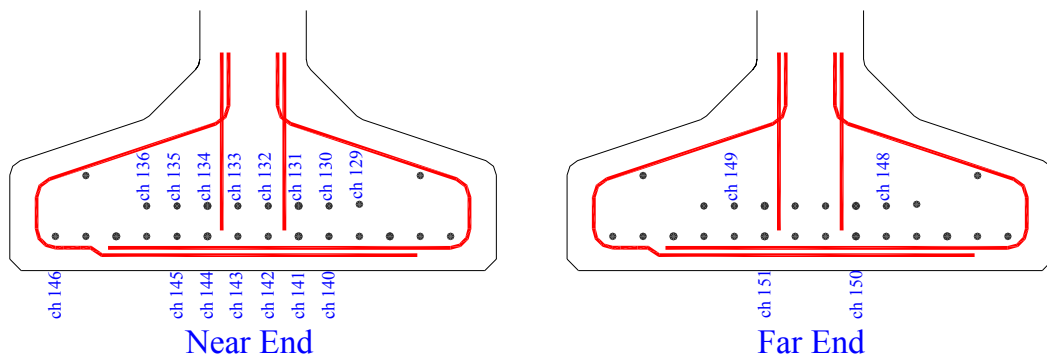


Figure 47: Slip instrumentation



Figure 48: Slip LVDT contact

13. PHASE 3 DESTRUCTIVE EVALUATION OF BULB TEE CAPACITY

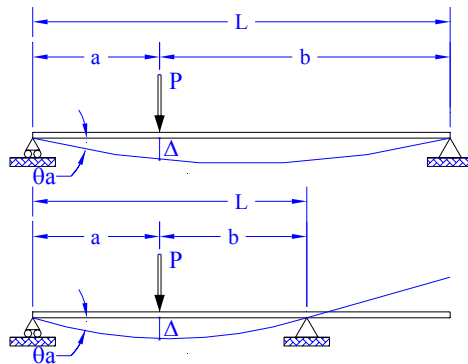
The elastic, cracked and ultimate response of the beams were evaluated. The measured and observed results are presented in detail in this section.

13.1. Elastic Response

The initial elastic response is once again evaluated for the two materials. The elasticity is directly measured from the response to small loads. Two methods are used. The first method estimates the in-situ elastic modulus from the pre-cracking force deformation response measured at the point load. The second method uses the measured surface strain and applied stress at a section.

13.1.1. Method 1 – Initial Stiffness

Each destructive test is initiated with the application of a low level elastic deformation. The force is kept below the cracking moment for the load cycle. Using elastic beam theory the relationship between elastic modulus, E , and the measured load-deformation stiffness K , can be found. The relationship is detailed in equation 19 and Figure 49 where I is the gross moment of inertia of the beam.



$$K = \frac{P}{\Delta} = \frac{3EI}{a^2b^2} \text{ (Eq. 19)}$$

Figure 49: Elastic beam deformation

The elastic stiffness of the beam is measured using a linear regression of the load deformation response. The computed initial stiffness and corresponding measured load-deformation response is presented in Figure 50 and tabulated in Table 41. The full span results are highlighted in grey. The SCC beams have consistent moduli between the two tests. The HESC beam on average exhibited a higher elastic stiffness however the variability was large. The second test conducted on each beam resulted in a considerably lower stiffness. During the full span test, damage was concentrated around the loaded region however partial cracking of the specimen likely spread over the length of the beam. Consequently during the second test the loaded section was partially cracked resulting in a lower initial stiffness.

Table 41: Elastic stiffness from load - deformation								
Concrete Material	Age [days]	Test #	Stiffness [kip/in]	Span [in]	a [in]	b [in]	Uncracked Inertia [in ⁴]	Elastic Modulus [ksi]
SCC	37	1	810.7	404	130.5	273.5	207554	4105.2
SCC	99	7	819.6	404	130.5	273.5	207554	4150.3
HESC	60	3	1048.5	404	130.5	273.5	207554	5309.6
HESC	85	5	791.4	404	130.5	273.5	207554	4152.3
SCC	45	2	2077.6	232	92.2	139.8	207554	2389.4
SCC	111	8	2003.0	232	92.2	139.8	171030	2795.6
HESC	71	4	2593.6	232	92.2	139.8	207554	2982.9
HESC	93	6	1756.7	232	92.2	139.8	171030	2451.8d

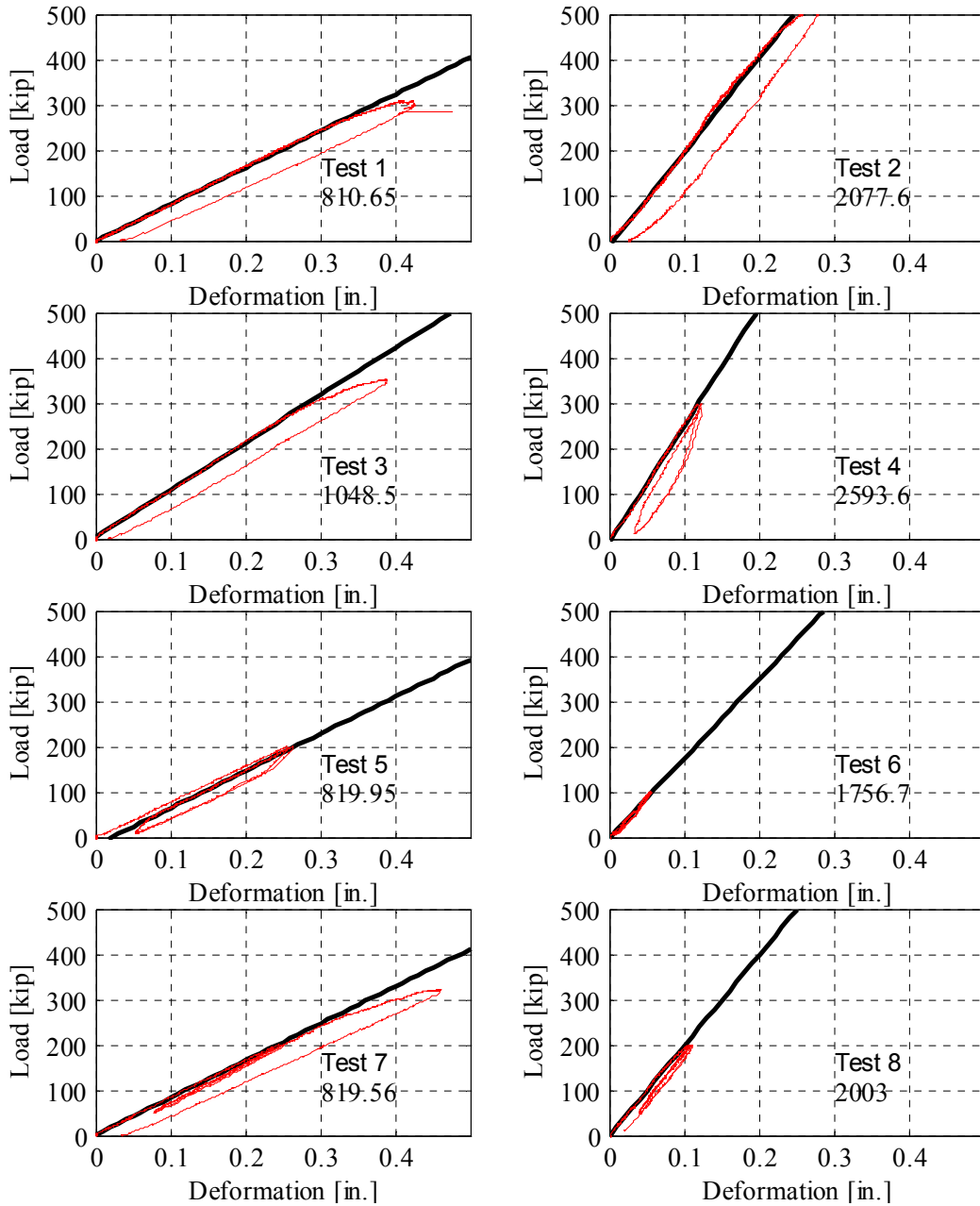


Figure 50: Elastic response and tangent stiffness

13.1.2. Method 2 Strain Measurements

To accurately assess the in-situ modulus of the concrete, the applied stress and measured strain is used. Prior to load application, surface strain gages were applied to the concrete section. Gages were installed on the top or on the underside of the top flange near the load application (see section 12.4). The strain was measured directly from the strain gage. The corresponding stress was computed based on the measured applied load and location of the gage. The assumption was made that the section was uncracked. Each modulus represents the combined response of 1 to 3 strain gauges. The results are summarized in Table 42.

The in-situ stiffness using the strain method results in a higher value for the SCC than that of the HESC. These results along with the camber and elastic shortening results support the fact that the SCC provides a

higher stiffness than the HESC baseline. Early cylinder test results were contrary to the measured in-situ properties. The variation between the cylinder and beam test results could be attributed to dissimilar curing. The cylinders were cured alongside the beams for the initial 24 hours and were then kept moist at a controlled temperature as required by ASTM. The beam section, however, was subjected to environmental temperature and humidity variations. Consequently the beam and the cylinders were subject to different hydration conditions. For future assessment of concrete elastic properties using cylinders these differences should be addressed.

Test	Configuration	Material	Ec [ksi]	Average [ksi]
2	B1	SCC	5680.7	5660
7	A	SCC	5868.6	
8	B2	SCC	5430.0	
3	A	HESC	5555.2	5190
4	B1	HESC	5493.1	
5	A	HESC	5476.3	
6	B2	HESC	4233.0	

13.2. Cracking

The cracking moment, M_{cr} , was approximated using the global load deformation response of the beam. The cracking level was defined as the point where the stiffness of the beam changes from the initial stiffness. To compute the cracking point two lines were fit to the cracking load – deformation curve. In most cases the cracking point was not pronounced. Using this procedure the cracking moment is comparable between the HESC and SCC beams. In both cases the measured cracking moment is much higher than the calculated. The values are presented in Figure 51, Figure 52 and Table 43.

Test #	M_{cr} Measured	M_{cr} Calculated.
HESC (3)	22790	13800
SCC (7)	23030	13800

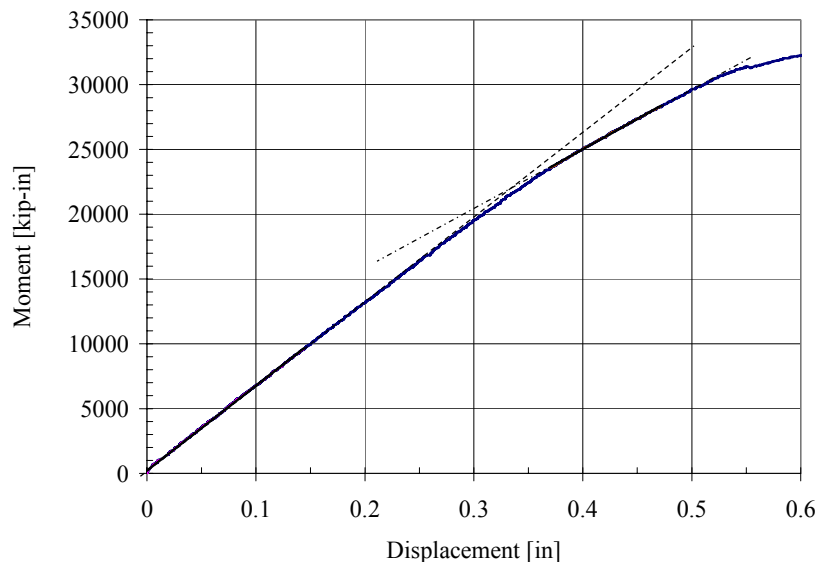


Figure 51: HESC (Test 3) cracking moment

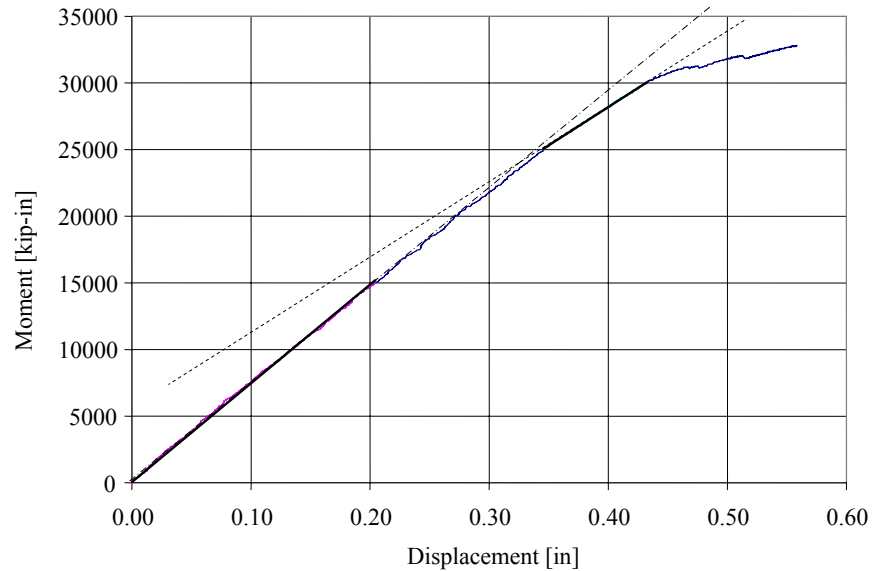


Figure 52: SCC (Test 7) cracking moment

13.3. Global Behavior

Tests 1, 3, 5, & 7 examined the performance of the HESC and SCC beams subjected to a point load applied to the full span. In all cases the beams were estimated to fail in a flexural mode with ultimate response controlled by crushing of the flange. In tests 3, 5 and 7, this failure mode was achieved with the measured load capacity exceeding the design strength by 3 to 4%. In test 1, premature failure of the top flange occurred resulting in a lower capacity. This is attributed to inappropriate loading conditions and is discussed later in this section. The measured flexure and shear demands are compared to the nominal capacities in Table 44.

Tests 2 (SCC) & 4 (HESC) were designed to fail due to shear failure of the beams. Both beams failed abruptly at a level in excess of the nominal shear and moment capacities. The beam exhibited damage associated with shear failure; however the failure may have been initiated by compression failure of the flange. The flexural demand was 103% and 104% of the nominal moment capacity for the SCC and HESC, respectively. The shear demand was 106% and 107% of the nominal shear capacity for the SCC and HESC, respectively.

In tests 6 and 8, fourteen of the strands were cut to force a tensile flexural failure of the section. Both beams failed due to fracture of the strands. The tensile flexural failure mode provided a greater factor of safety over nominal design capacity than the compressive failure modes. The overstrength for each beam is presented in Table 44.

Table 44: Measured beam resistance								
ID	Mater.	Maximum Applied Moment, Mmax [kip-in]	Maximum Applied Shear, Vmax [kip]	Mn (design)	Vn (design)	Mn (as-built)	Vn (as-built)	Failure mode
1	SCC	39497	306.9	92%	67%	91%	67%	Premature top flange failure
2	SCC	44314	483.7	103%	106%	102%	106%	Web Shear
3	HESC	44670	346.6	104%	76%	103%	76%	Compressive flexural failure
4	HESC	44792	488.8	104%	107%	103%	107%	Web Shear
5	HESC	44316	343.9	103%	75%	101%	75%	Compressive flexural failure
6	HESC	19812	217.9	106%	52%	104%	52%	Tensile flexural failure
7	SCC	44463	345.0	103%	76%	101%	76%	Compressive flexural failure
8	SCC	19452	214.0	104%	51%	101%	51%	Tensile flexural failure

13.3.1. Global Deformation Response

The global load deformation response of each beam is presented in Figure 53 and Figure 54. The vertical beam deformation at the location of the applied load is plotted with respect to the moment and shear at the section. All eight load histories are compared on each graph. With the exception of Test 1, the moment resistance measured for the unmodified beam sections are consistent between the tests and between materials. The SCC has a consistently higher deformation capacity than that of the HESC. The limited ductility exhibited by tests 2 and 4, in comparison to tests 5 and 7, is due to the higher shear demands resisted (Figure 54). The lower moment capacity of tests 6 and 8 are due to the reduced cross-section. The characteristics of each beam are described in greater detail in the following subsections.

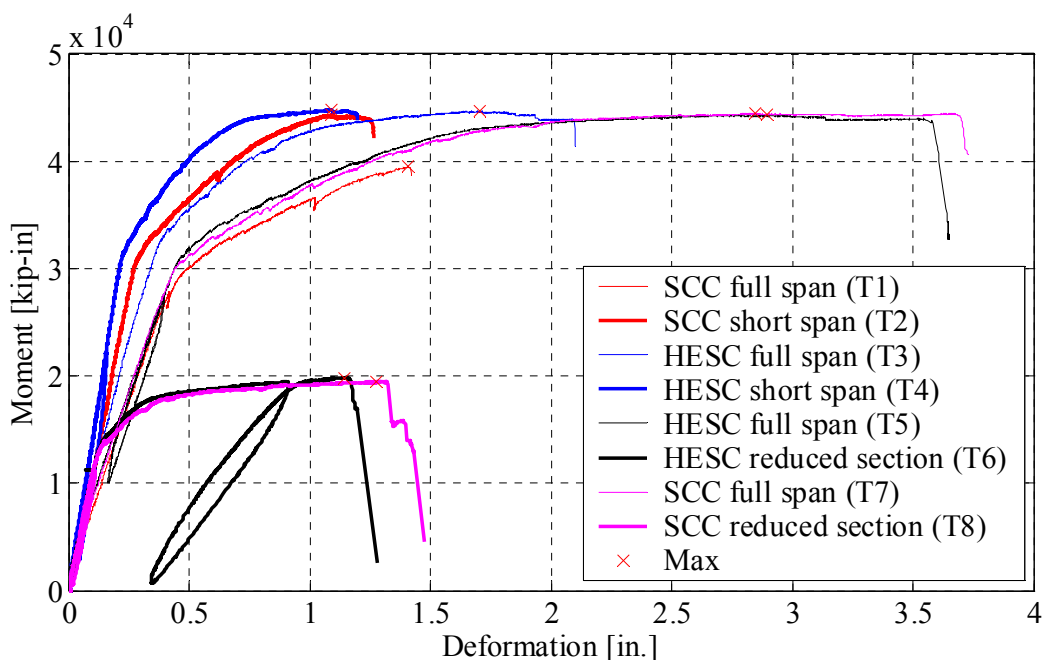


Figure 53: Global moment-deformation at point load

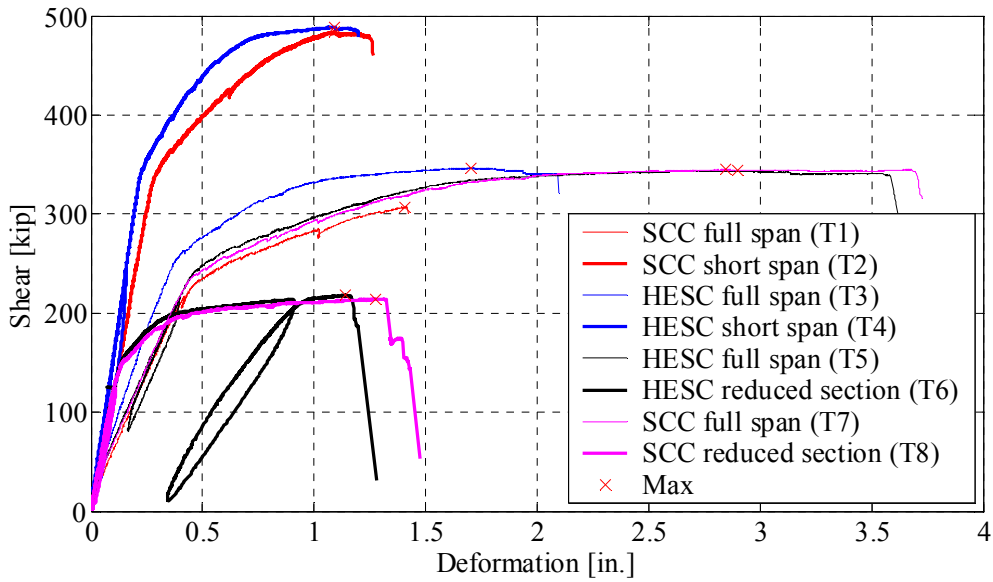


Figure 54: Global shear-deformation at point load

13.3.2. Full Span Response

Four full span tests were conducted: two SCC beams and two HESC beams. The first test on the SCC and HESC beams resulted in a lower deformability than the final two tests. This difference is due to a variation in the loading. The earlier tests were conducted with load applied primarily over the center portion of the top flange while in the following tests load was applied over the full width of the top flange. The first test on the SCC beam, load was applied with a neoprene bearing pad over the top flange width. The use of a deformable pad resulted in flow of the pad. This caused the free edge of the flange to deform more than the center resulting in premature failure of the top flange. The first test on the HESC beam was conducted with a point load applied over the web width. This resulted in a stiffer initial response and an earlier flange failure due to the elevated compression forces. The final two tests conducted on the HESC and SCC beams were tested in an identical manner with a uniform deformation applied to the full width of the top flange. Comparing these two responses it can be seen that the HESC and SCC beams provide comparable resistance to compression flexural failure. Both beams exceed the design strength. The SCC beam is capable of resisting a marginally greater deformation than the HESC (Figure 55 and Figure 56).

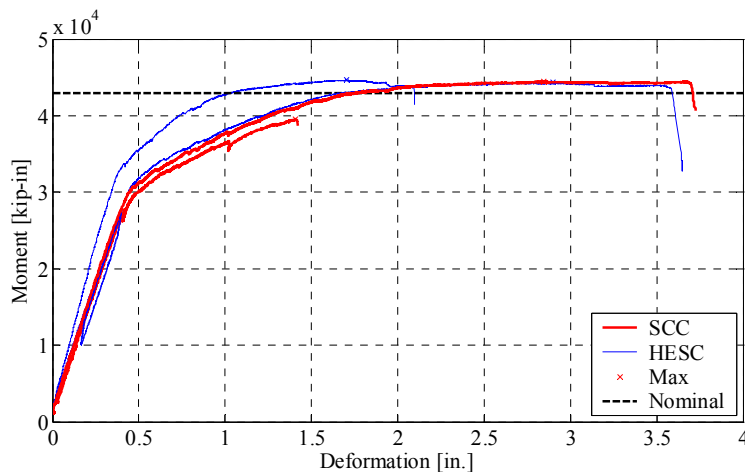


Figure 55: Full span moment – deformation response

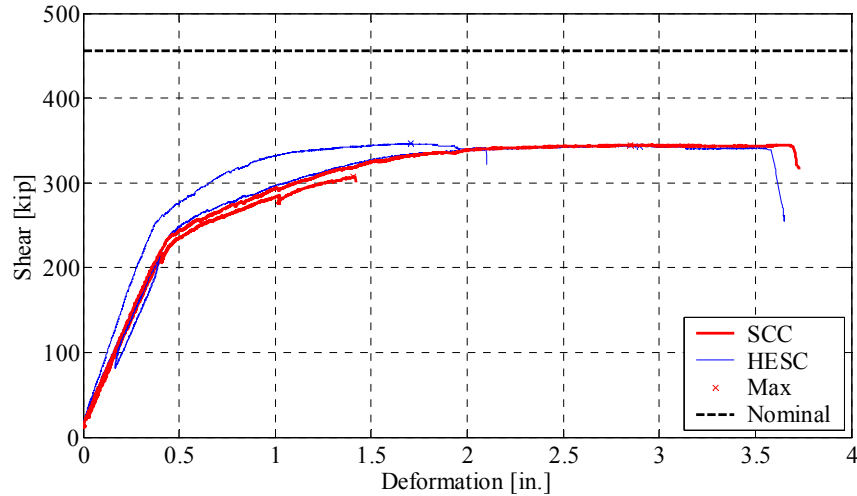


Figure 56: Full span shear – deformation response

13.3.3. Short Span Response

Short span tests were conducted on both the SCC and HESC beams. The shear and moment resistance is presented in Figure 57 and Figure 58. Both beams exceeded their nominal shear and flexural capacities. The SCC beam exhibited a lower initial stiffness and greater deformability than the HESC.

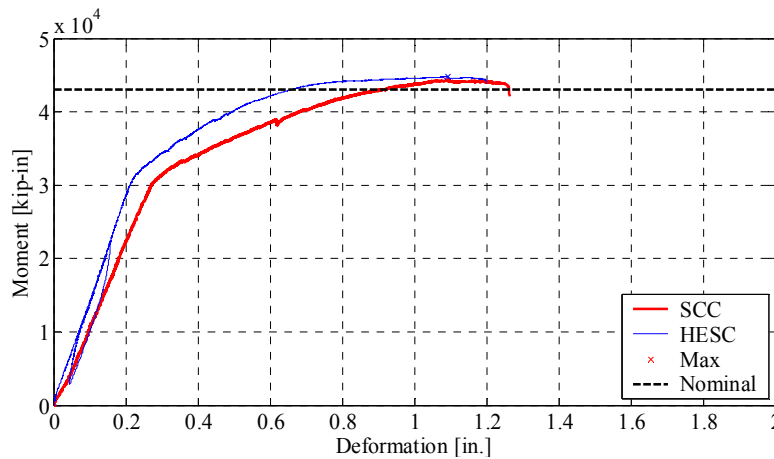


Figure 57: Short span moment – deformation response

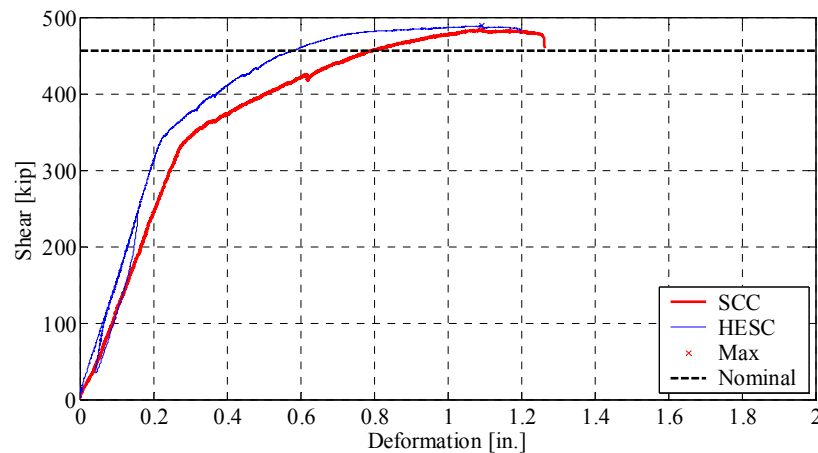


Figure 58: Short span shear – deformation response

13.3.4. Reduced Section Response

The SCC and HESC beams exhibited similar elastic response. Both beams exceeded the design flexural strength (Figure 59). The shear demand was much lower than the design level (Figure 60). The SCC exhibited lower ultimate capacity but was capable of supporting greater ductility.

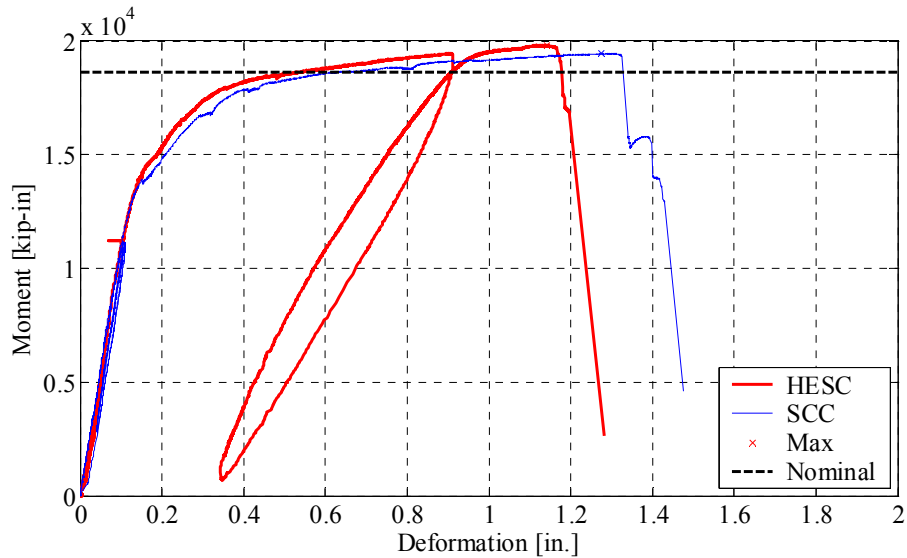


Figure 59: Reduced section moment – deformation response

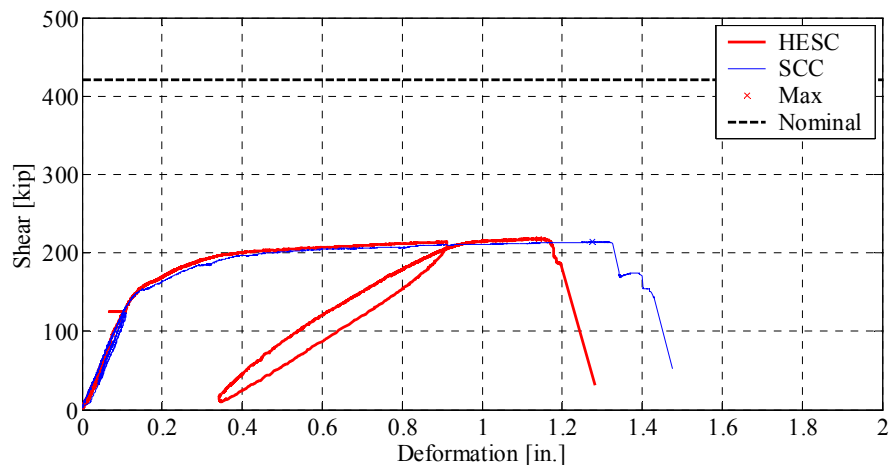


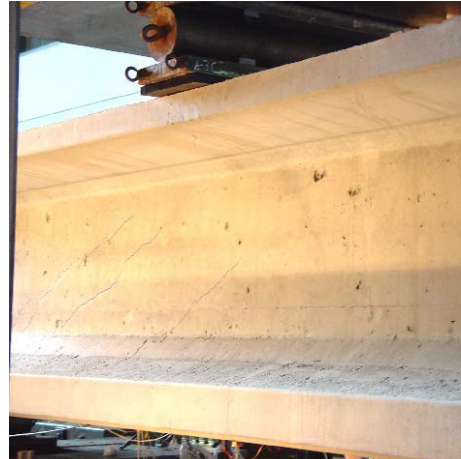
Figure 60: Reduced section shear – deformation response

13.3.5. SCC Full Span Observations (Test 1)

The first test was conducted on the full span of the SCC beam 1. The progression of failure is presented pictorially in Figure 61. Prior to testing hairline horizontal end cracks were observed and marked on the beam ends (a). Damage to the beam initiated with local flexural cracking of the top flange under the load point. This was attributed to the use of a neoprene pad under the loading plate. Since the neoprene is compressible a uniform *pressure* is applied to the top flange. The uniform pressure resulted in a greater deformation at the thin face of the flange leading to premature cracking. High strength grout was used in place of neoprene for subsequent tests. Shear cracking in the web and flexural cracking of the bottom flange followed next. Flexure cracks lengthened and a greater number of shear cracks formed. At the peak measured load an abrupt compressive failure of the top flange occurred due to the local bending near the loading plate. Following flange failure crushing progressed through the web.



a) Initial configuration: horizontal end cracks



b) Flexural top flange & shear cracking of web



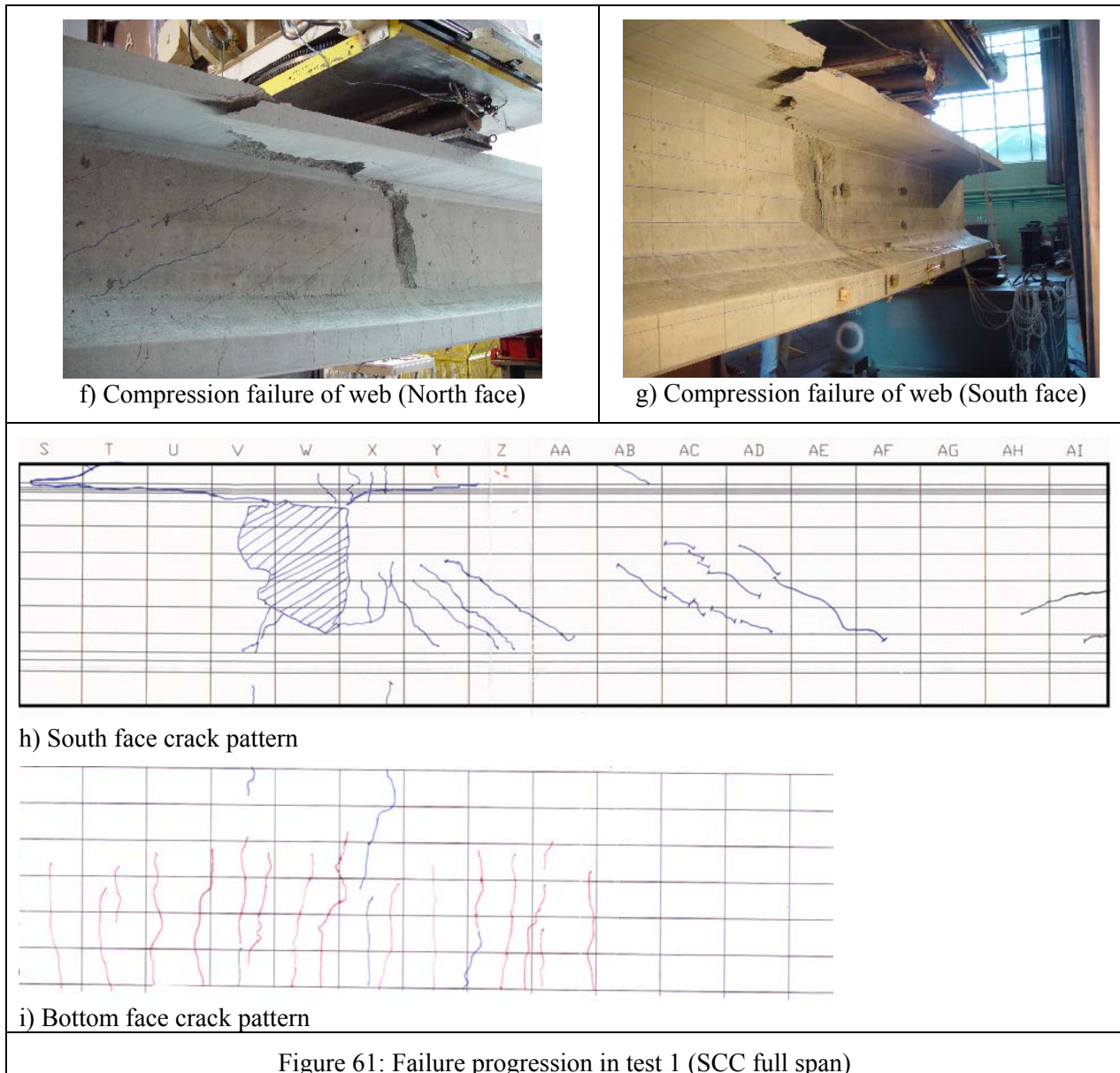
c) Flexure and shear cracking



d) Local failure of top flange

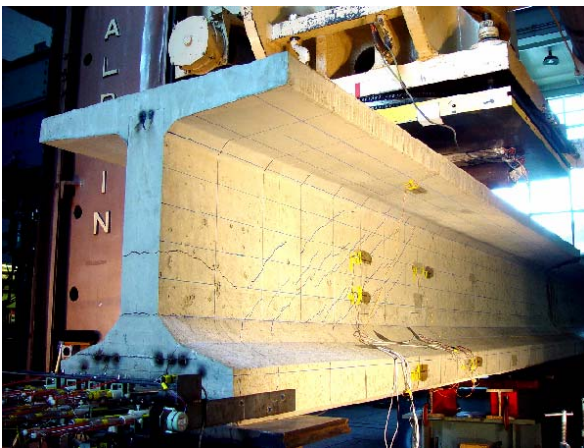


e) Local failure of flange



13.3.6. SCC Short Span Observations (Test 2)

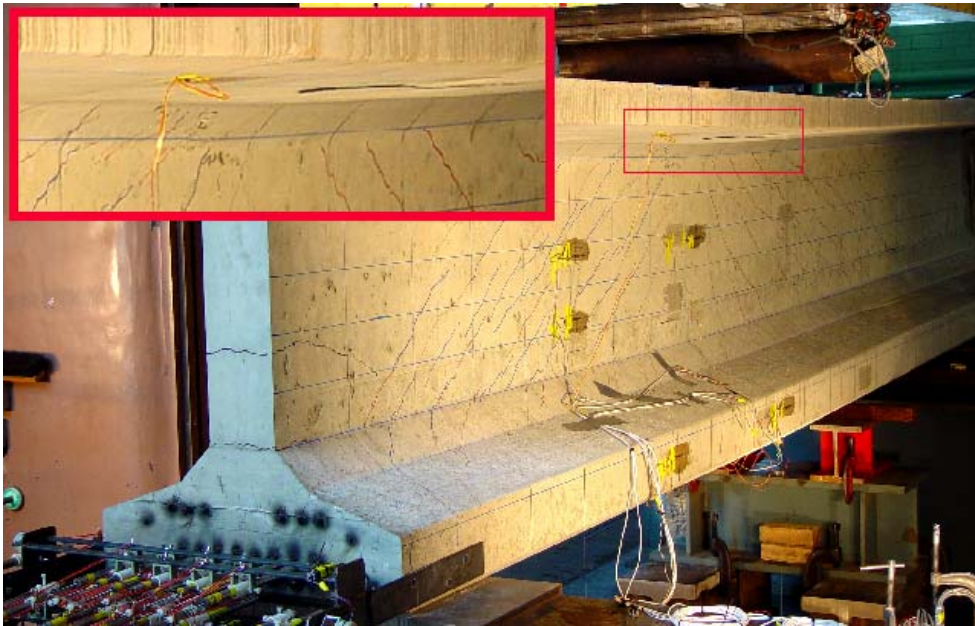
The second test was conducted on the undamaged portion of the SCC beam. The progression of failure is illustrated in Figure 62. Small flexural cracks formed in combination with shear cracking of the web. With increased load flexural cracks lengthened and significant shear cracking of the web was observed. A greater number of shear cracks formed toward the near support. Just prior to achieving the peak load, local crushing of the top flange was observed at the web to flange junction (c). The test ended with an abrupt shear failure of the beam progressing from the compression flange toward the tension flange. Slip of a number of strands was observed at the end face of the beam (h) after completion of the test.



a) Flexure and shear cracking (South face)



b) Flexure and shear cracking (North face)



c) Crushing of compression flange



d) Shear failure (North face)



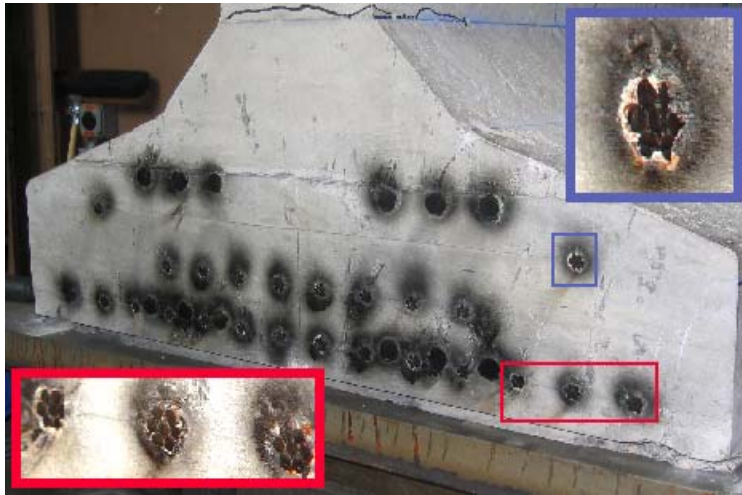
e) Shear failure (South face)



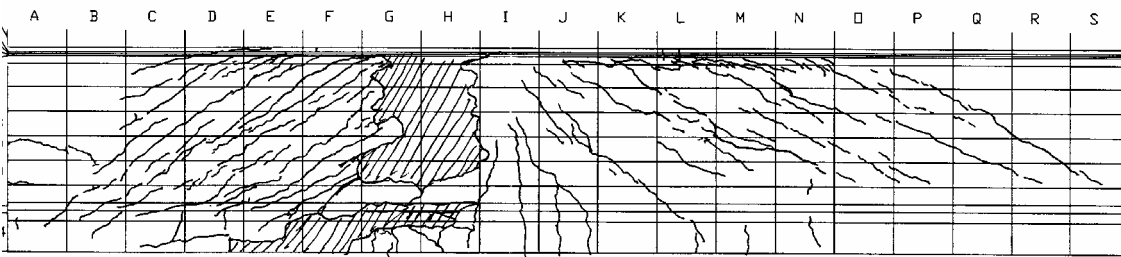
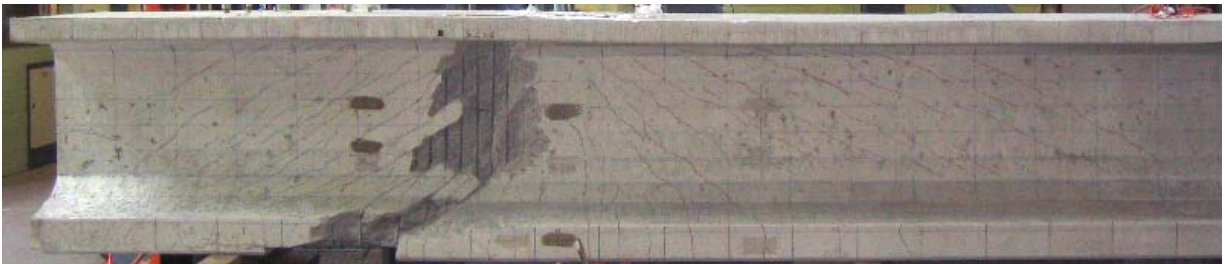
f) Damage to bottom flange



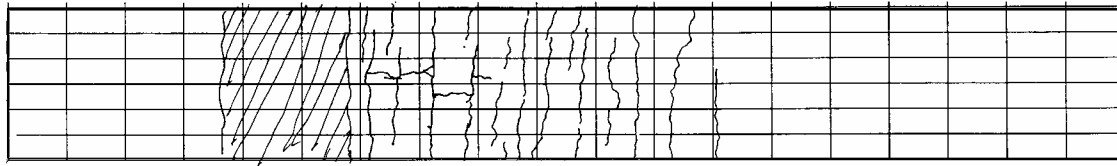
g) Close-up of bottom right strands



h) Slip of end strands



i) South face crack pattern

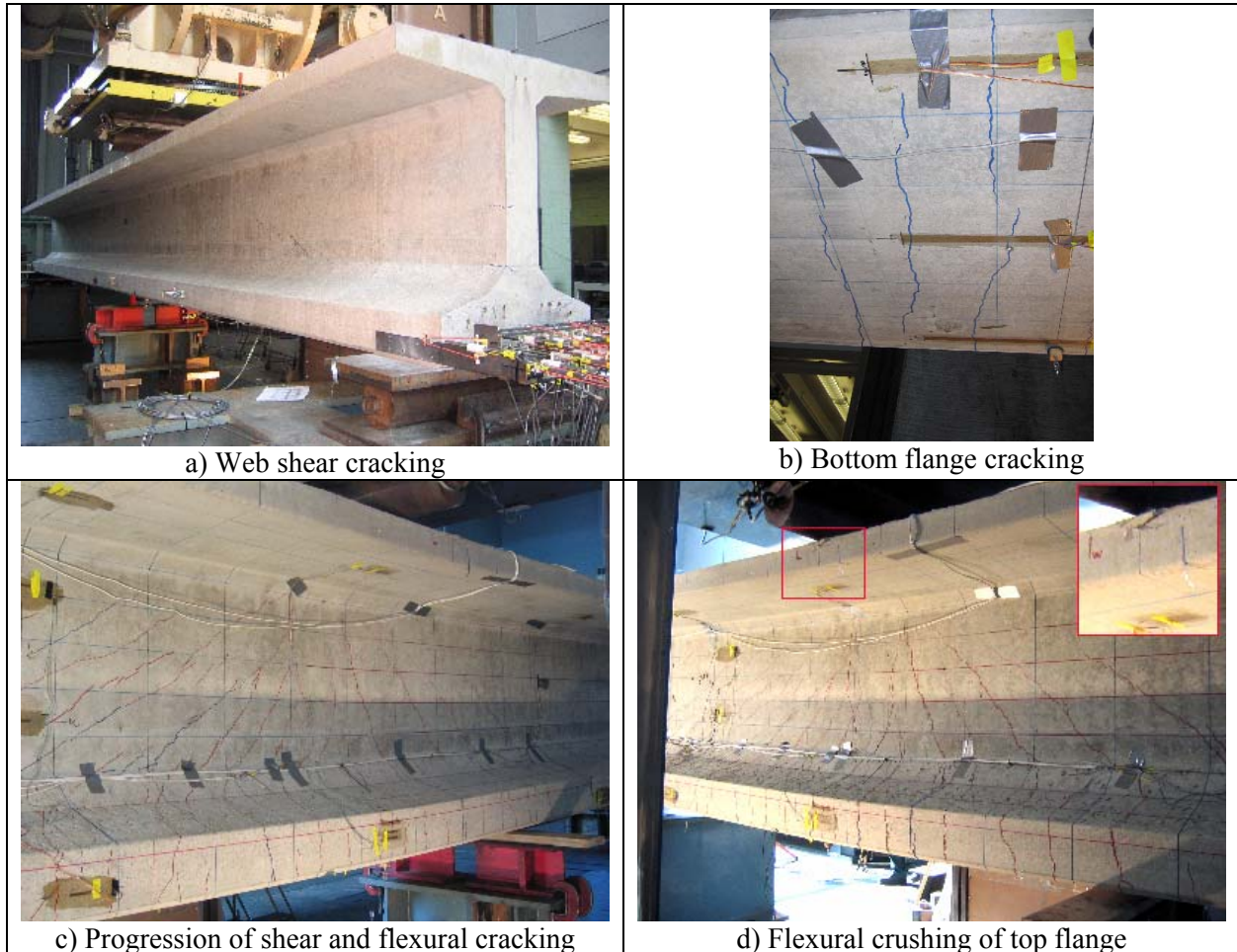


j) Bottom face crack pattern

Figure 62: Failure progression in test 2 (SCC short span)

13.3.7. HESC Full Span Observations (Test 3)

The third test was conducted on the full span of the HESC beam. The progression of failure is illustrated in Figure 63. Horizontal end cracking was observed and marked prior to loading. Flexural cracking at the load point and shear cracking toward the near support initiated first. This was followed by a spread of shear and flexure cracking. The ultimate strength was controlled by an abrupt compression failure initiating from the top flange and progressing into the web.



a) Web shear cracking

b) Bottom flange cracking

c) Progression of shear and flexural cracking

d) Flexural crushing of top flange

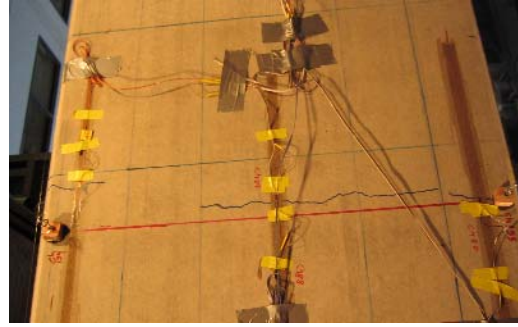


13.3.8. HESC Short Span Observations (Test 4)

The fourth test was conducted on the previously tested HESC beam. The damaged portion was cantilevered off of the far support. The progression of failure is illustrated in Figure 64. Flexural cracking initiated first followed by shear cracking. Shear cracking was concentrated to a greater extent toward the near support. End splitting cracks were observed for the first time at the end of the beam. No visible slip was associated with this cracking. The beam failed by due to an abrupt shear damage to the web.



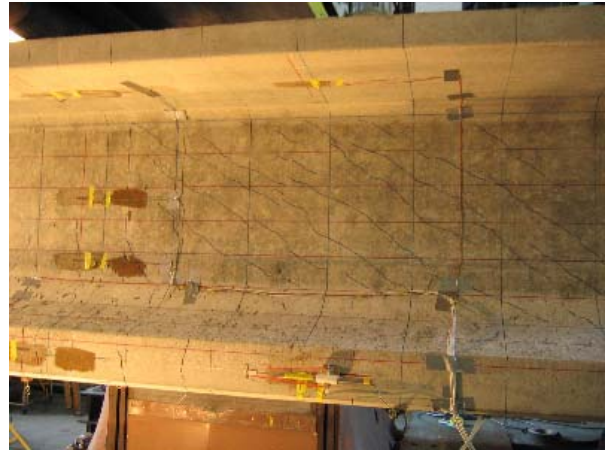
a) Flexural cracking of bottom flange



b) View of underside of bottom flange



c) Shear cracking of web



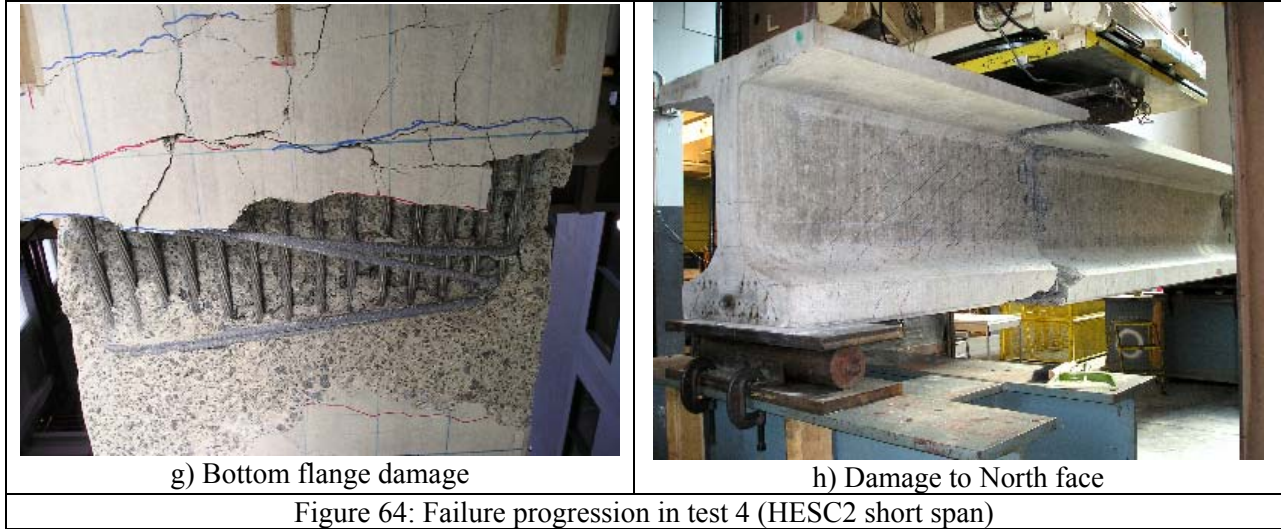
d) Shear cracking of web



e) End splitting cracks

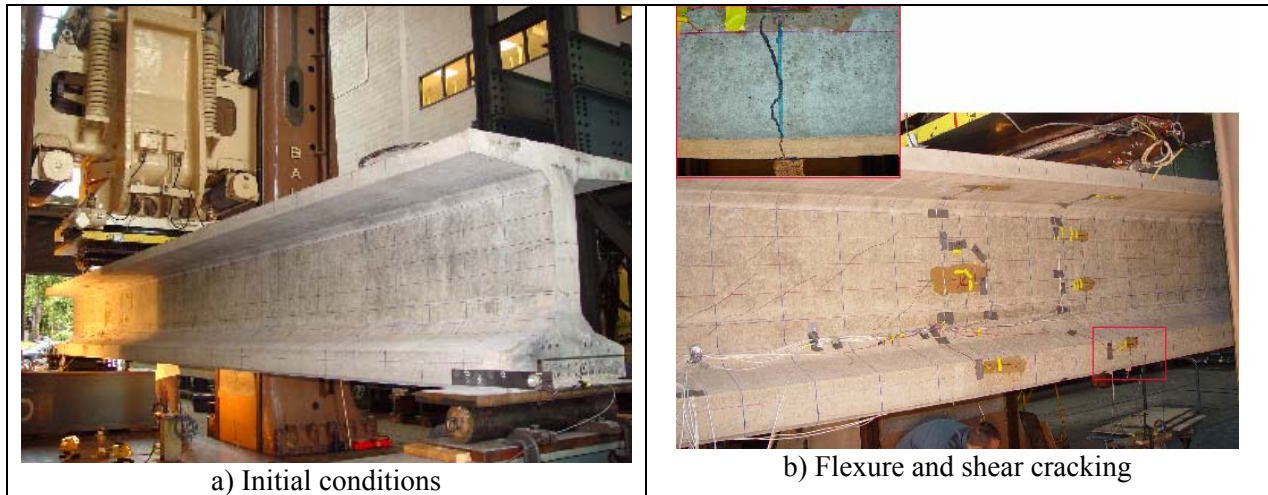


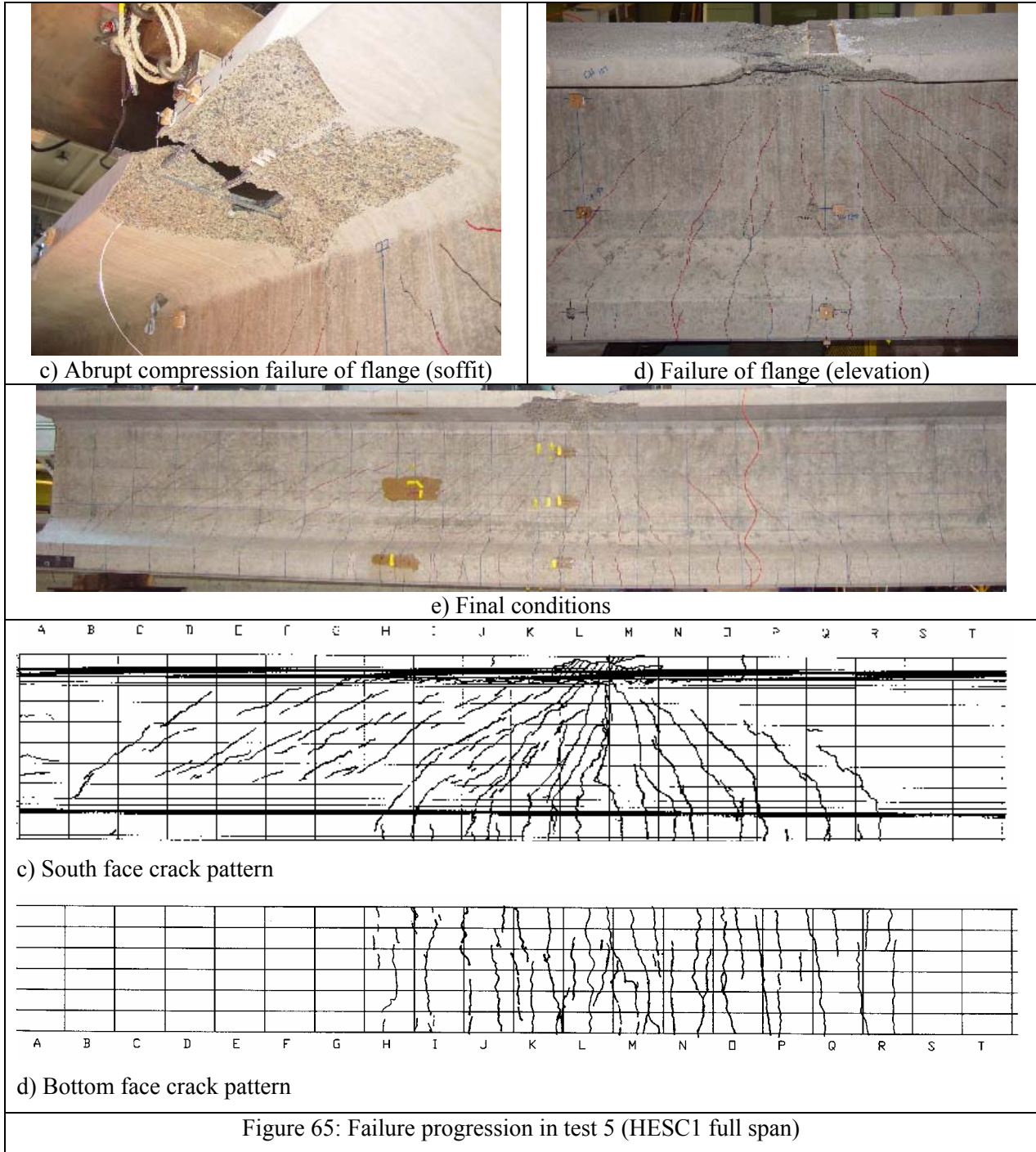
f) Abrupt shear failure of beam



13.3.9. HESC Full Span Observations (Test 5)

The fifth test was conducted on the second HESC beam. A full span was used. This test was identical to test three with the exception of the loading head. Instead of the 8-inch X 17-inch loading plate used in test 3, a 4-inch wide plate running the full width of the top flange was used. The progression of failure is illustrated in Figure 65. The failure progression was comparable to the previous tests. The beam failed due to loss of the compression flange; however, unlike test 3 no crushing of the top flange was visible until the abrupt loss of the entire flange.





13.3.10. HESC Reduced Section Observations (Test 6)

The sixth test was conducted on the previously tested HESC beam. The beam was notched and the bottom row of strand was severed. The progression of failure is illustrated in Figure 66. A single flexural crack formed at the notched section of the beam. At an elevated load level nominal shear cracks radiated from the load point. The deformation was concentrated in the primary flexural crack. A gap opening in excess of 0.5-in. was observed. The system failed due to an audible fracture of the strands.

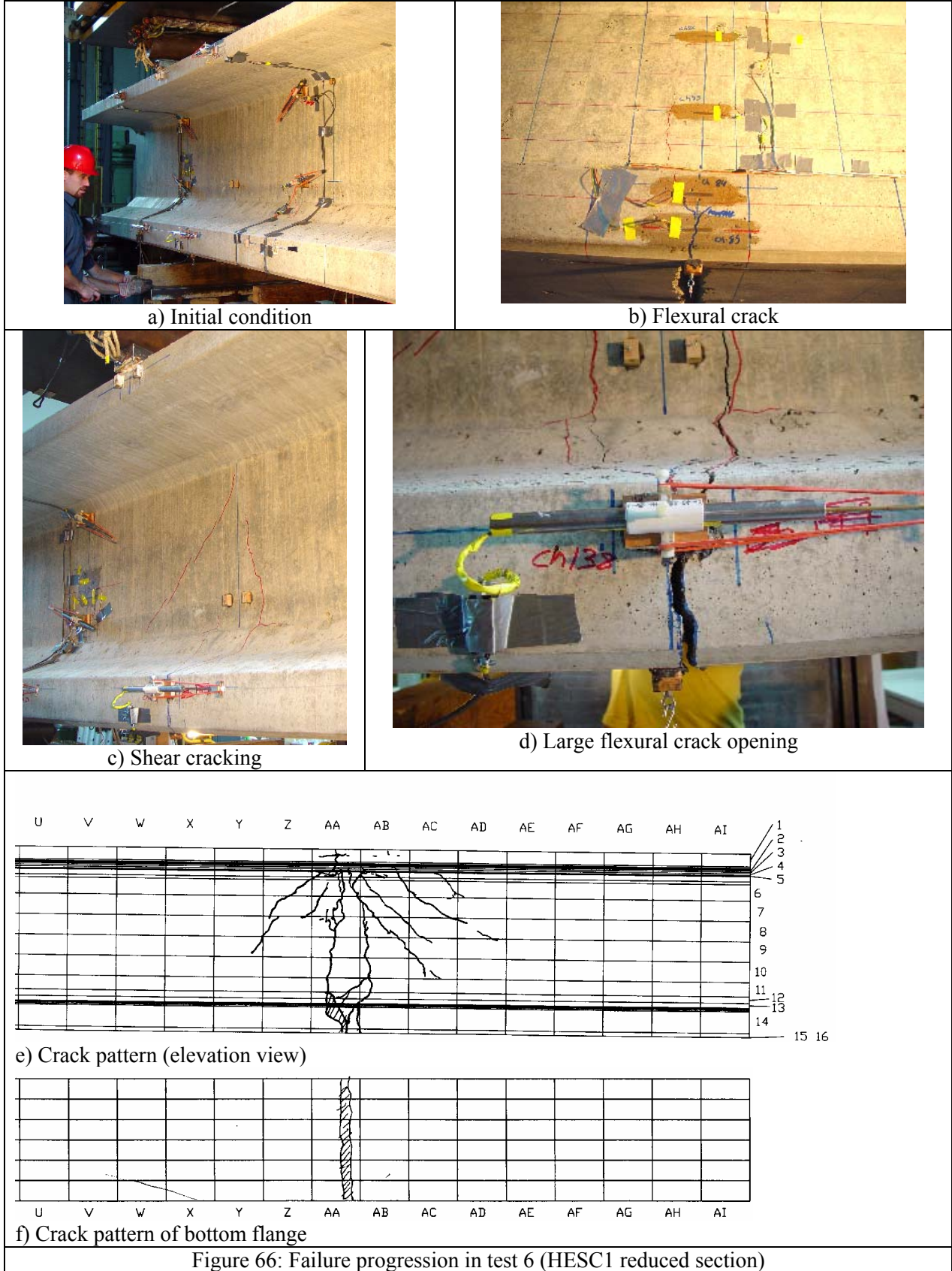
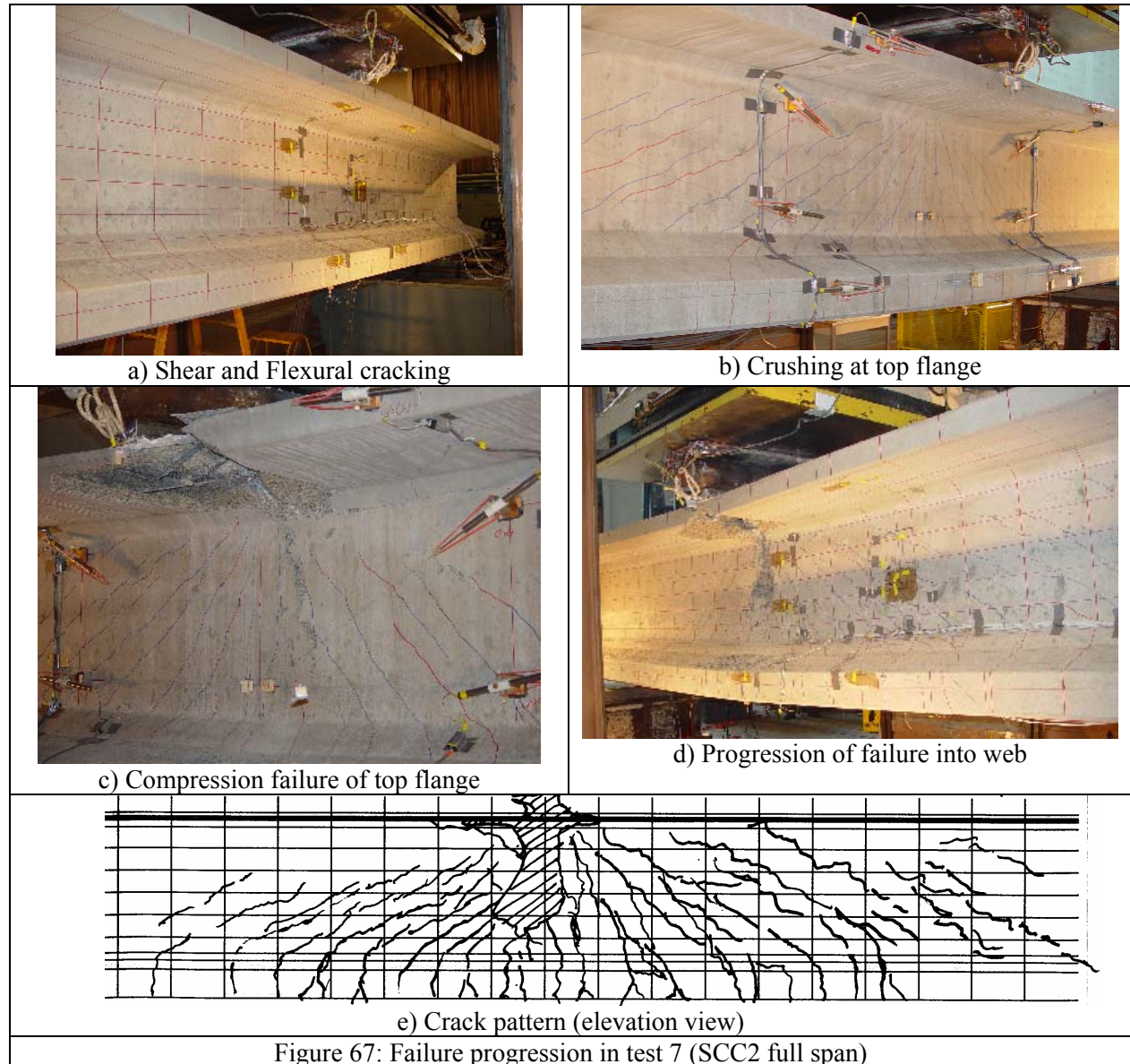


Figure 66: Failure progression in test 6 (HESC1 reduced section)

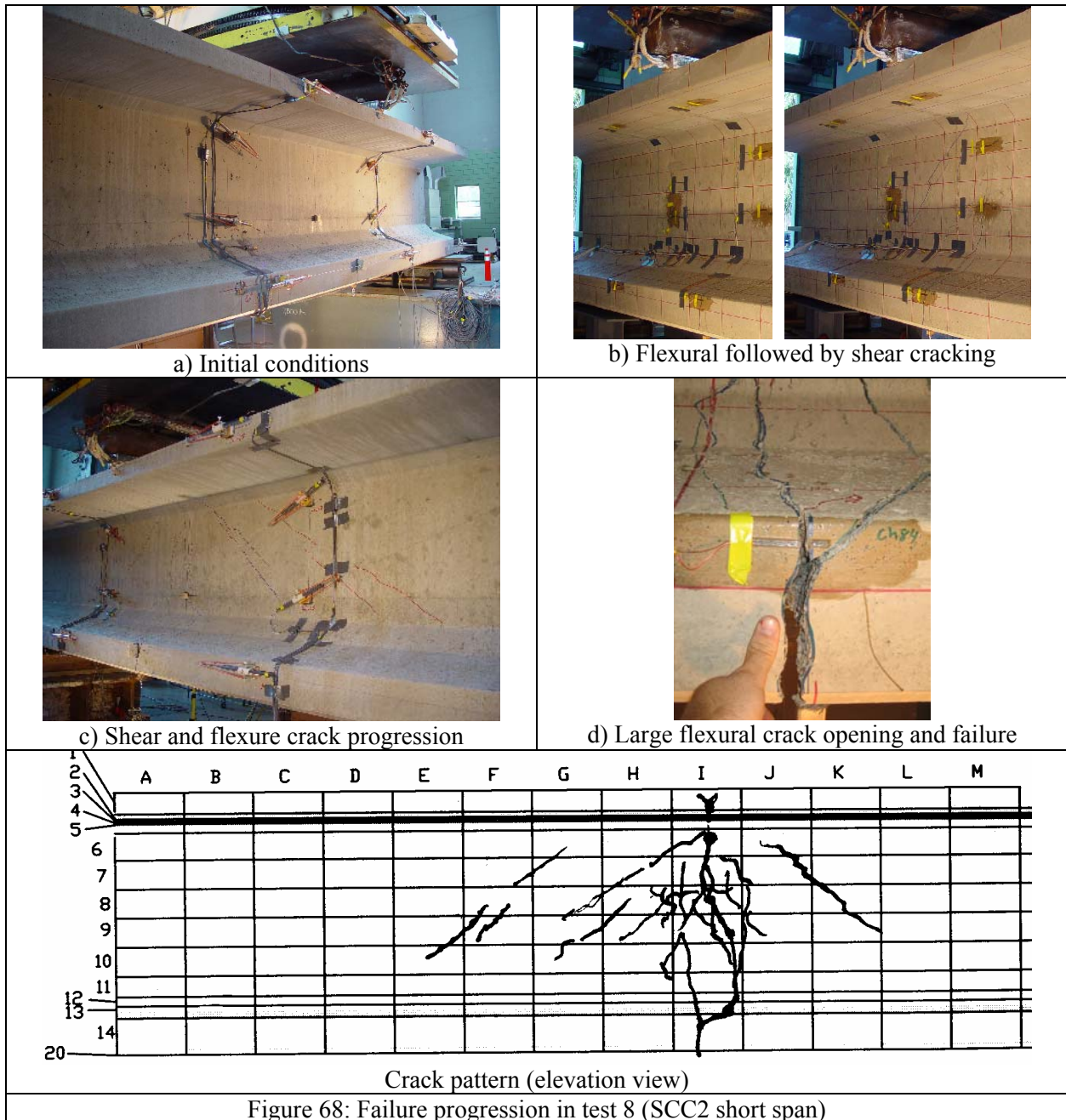
13.3.11. SCC Full Span Observations (Test 7)

The seventh test was conducted on the second SCC beam. The beam was tested over the full span. The progression of failure is illustrated in Figure 67. The beam followed the same progression of damage previously observed in the SCC and HESC full span tests. The ultimate failure was attributed to an abrupt compression failure initiating at the top flange and progressing into the web. The failure was similar to that observed for the HESC test 3.



13.3.12. SCC Reduced Section Observations (Test 8)

The final test was conducted on the previously tested SCC beam. As with test 6, the section was notched and the bottom row of strands was cut. The progression of failure is illustrated in Figure 68. The damage initiated with flexural cracking at the notched section. The flexural crack continued to grow and eventually lead to strand fracture. The response was comparable to the previously tested HESC beam.



13.3.13. Bond Slip

The slip of the strand was measured during each test. Strand slip was measured on both the end near the load point and the opposing side. The instrumentation was concentrated on the near side. No slip was measured on any of the far end transducers. Consequently only the near slip is discussed. Slip occurred in a non-symmetric manner. Some strands exhibited moderate slip while others, sometimes located adjacent to the slipping strand, exhibited none. The slip in all cases was minimal with a maximum value less than 0.05-in.

The slip versus applied load for each test is presented in Figure 69 to Figure 76. The global load versus deformation is plotted on the same graph to provide a reference. In general, slip occurred as the beam exhibited inelastic response. The level of slip was comparable between the two materials. The full span

tests exhibited moderate slip. For these tests the full development length was provided however significant shear cracking formed. It could be argued that the slip was due to compatibility with the formation of shear cracks. The most pronounced slip was observed in the short span tests on the SCC and HESC beams. In this configuration the embedment length was less than the required development length. In both the HESC and SCC only a small portion of the strands exhibited measurable slip. In all cases the load was maintained with initiation of slip. Based on these results it is unlikely that the slip lead to loss of flexural strength. The strands in the reduced section tests were stressed to fracture. In both tests no slip was measured (note, the jump at the end of test 8 is due to the energy released during fracture of the strand and not due to a physical slip). From these measurements it can be concluded that the SCC and HESC provides adequate bond characteristics to prevent slip when using a full development length.

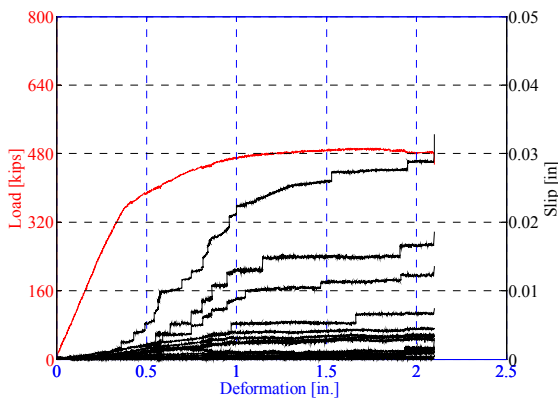


Figure 69: Bond Slip HESC full Ld (Test 3)

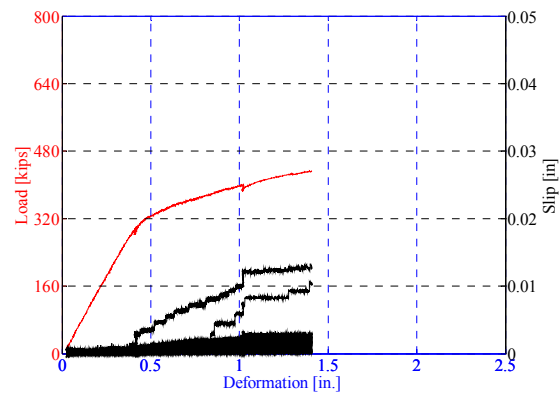


Figure 70: Bond Slip SCC full Ld (Test 1)

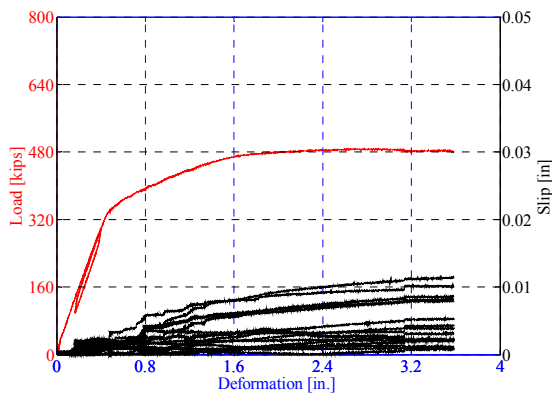


Figure 71: Bond Slip HESC full Ld (Test 5)

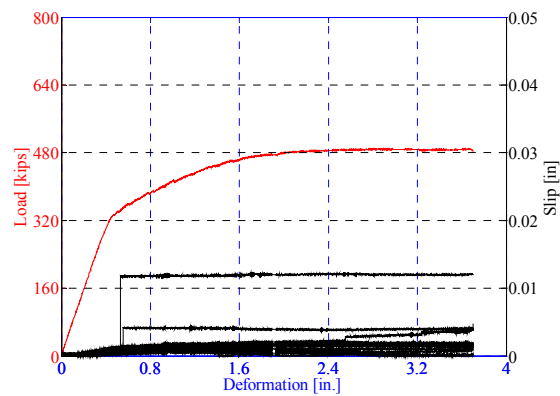


Figure 72: Bond Slip SCC full Ld (Test 7)

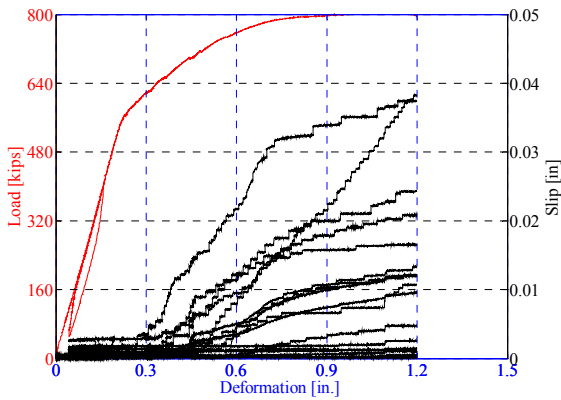


Figure 73: Bond Slip HESC 58%Ld (Test 4)

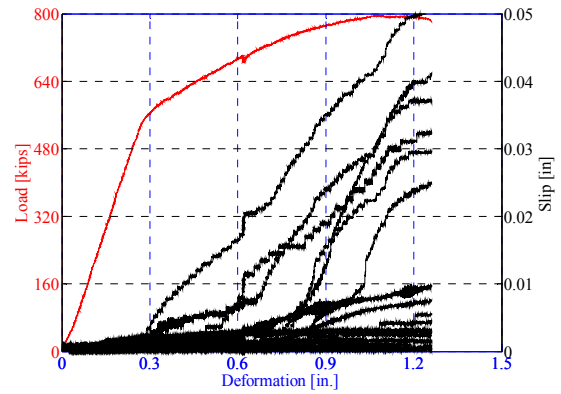


Figure 74: Bond Slip SCC 58%Ld (Test 2)

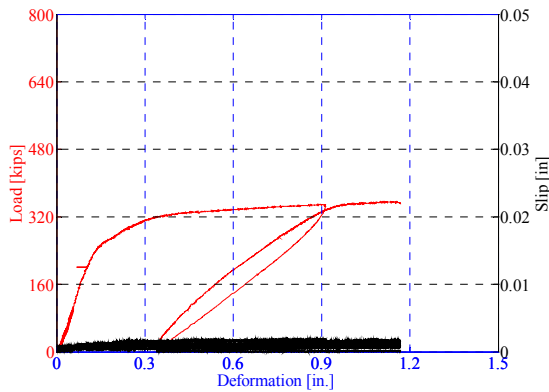


Figure 75: Bond Slip HESC Full Ld reduced section (Test 6)

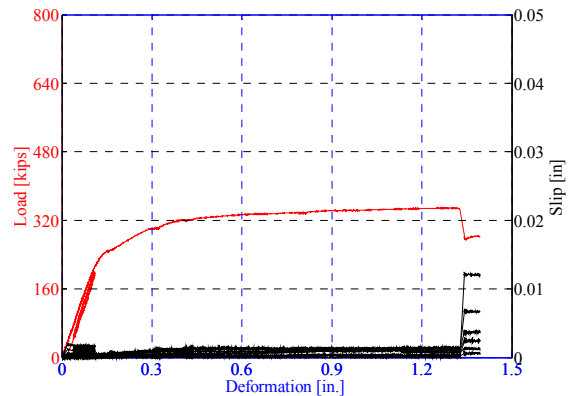


Figure 76: Bond Slip SCC Full Ld reduced section (Test 8)

13.4. Phase 2 Conclusions

The destructive testing of the bulb tee beams indicate that SCC and HESC perform well in structural applications under a variety of demands. In particular the following conclusions can be made from the discussion presented in this section:

- Use of the global elastic load deformation of the beams to compute the in-situ modulus did not provide enough repeatability to make sound conclusions. This method of evaluation may not be accurate enough for large size beams.
- The elastic modulus measured using surface mounted strain gages and the applied load indicated that the SCC had a higher in-situ modulus than the HESC. This is in support of the conclusions of the camber measurements and the strains measured during transfer of prestress.
- The apparent cracking moment exceeded conventional predictions.
- The SCC in all cases provided greater ductility than the HESC.
- The SCC and HESC exceeded the nominal design strengths for all conventional beam failure modes. The design strengths were exceeded for a shear failure mode, flexural compression failure mode, and flexural tension failure mode.
- Observed progression of damage was consistent between the SCC and HESC beams tested under the same conditions.

- Measured end slip was observed on all but the reduced beam sections. Slip occurred in a non-symmetric manner with slip on some stands and none on others.
- In all cases a minimal slip less than 0.05-in. was observed.
- Strand slip initiated with inelastic deformation of the beam. Load carrying capacity increased after slip initiated.
- Slip was observed in the beam with the full development length and the beam with the reduced development length. This can be attributed to the formation of shear cracks. It is the opinion of the authors that these cracks result in end slip due to section compatibility.
- In the reduced section tests no slip occurred. From these measurements it can be concluded that the SCC and HESC provides adequate bond characteristics to prevent slip when using a full development length.

14. PHASE 3 – STRAND TO CONCRETE BOND MECHANICS

Phase 3 was conducted to assess bond characteristics of SCC in comparison to HESC and to examine alternate bond test procedures. To examine the concrete-to-steel bond characteristics of prestressing strand a series of pullout tests on prestressed and unstressed strand and wire are conducted in combination with flexural beam tests. Three test specimen types are examined: 1) conventional large pullout block [Logan 1997], 2) short prestressed pullout blocks, and 3) flexural beam tests (Figure 77).

The large block pullout tests provide a direct evaluation of the performance of *unstressed* lifting ties in precast members. The pullout strands are oriented vertically in the block. The block is reinforced with conventional reinforcement and has no initial prestress. In a typical precast application, lifting ties are anchored in a prestressed member and consequently have a level of lateral stress acting on them. This stress helps to prevent pullout. The pullout strengths measured in the large block thus represent a lower bound of the available capacity.

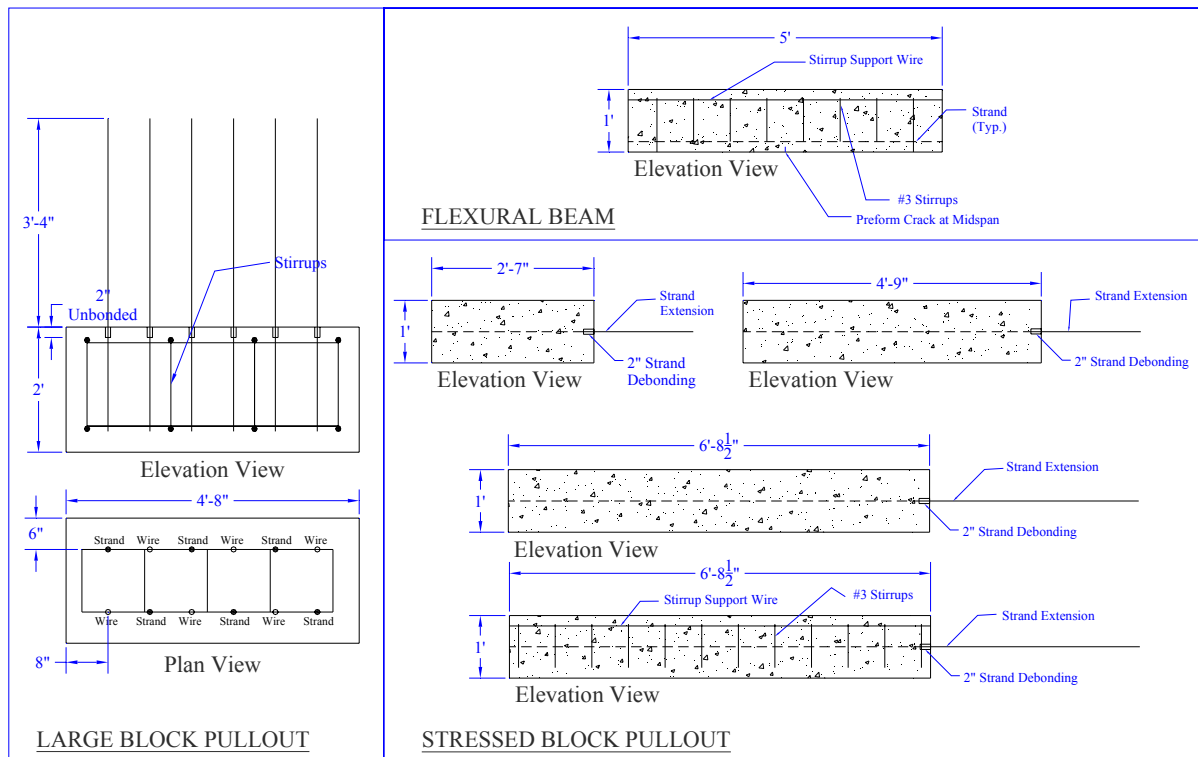


Figure 77: Test specimens

It is important to realize that the large block test does not represent the condition under which prestressing strand is most commonly used, specifically, as precast stressed longitudinal strand. In the large block test, the strands are: 1) oriented vertically, 2) unstressed, and 3) allowed to rotate as they exit the block. In a beam where the strand is horizontal, free water may collect under the strand leading to void formation [Jeanty, Mitchell and Mirza 1988]. In a vertical orientation, the strand may act as a wick to attract water and mortar. This could potentially increase or decrease the pullout strength from that of a horizontal orientation, thus making direct correlation difficult.

The lack of prestress could decrease the available pullout capacity. During release of initial prestress the strand may dilate due to Poisson's effect [Hoyer 1939] or through unwinding of the strand. At the end of the concrete member this effect will be the greatest thus allowing the strand to theoretically lock into the concrete. In an unstressed condition no locking occurs, furthermore the strand may actually contract as the strand is being pulled from the block. The contribution of this effect will be examined.

When a flexural crack opens in a prestressed beam the strand is anchored in the concrete at either side of the crack. For the crack to open one of two conditions must occur: 1) the strand must deform at the crack or 2) the strand must slip from one or both sides of the concrete. Deformation at the crack commonly occurs due to yielding of the strand. For slip to occur, however, the strand must dislocate by twisting out of the concrete. Twisting is resisted by the anchoring of the strand at the other side of the crack. In the pullout block, twist of the strand is not directly prevented due to the need for a long jack. Thus in the test, the strand can more readily slip. To examine if these conditions contribute to lower strengths, stressed block pullout and flexural beam tests are conducted on the same strand used in the large pullout block. The configurations of the specimens examined are illustrated in Figure 77.

14.1. Phase 3 Test Matrix

The research variables include strand orientation, concrete type and strand diameter. High early strength concrete and self consolidating concrete are compared. Concrete design strength of 6800 psi at 24 hours and 8000 psi at 28-days is used. Both concretes are comprised of natural silica sand and a crushed Diabase stone. For the HES mix #67 (0.75in. max) and #8 (0.375 in. max) gradations are used. For the SCC mix #8 gradation is used. Type III cement is used in combination with blast furnace slag cement. All tests are conducted after 28 days to provide consistency between results. Two strand diameters are studied: 0.5-in. special and 0.6-inch. For the stressed conditions, the strands are preloaded to an initial prestress of 0.75fpu. For the unstressed pullout tests a minimum of 5 iterations are performed per condition to determine the repeatability of the test. For the stressed conditions, three tests are performed for each variation. The test matrix is summarized in Table 45.

Table 45: Test Matrix					
Stressed Block Pullout					
Series	Concrete Type	No. Specimens	Specimen Cross Section	Specimen Length [in]	Confinement Reinforcement
SIA	SCC	3	6.5" w x 12" d	31	None
SIB	SCC	3	6.5" w x 12" d	57	None
SIC	SCC	3	6.5" w x 12" d	80.5	None
SIC-R	SCC	3	6.5" w x 12" d	80.5	12 No.3 Stirrups @ 7" o.c.
HIA	HSC	3	6.5" w x 12" d	31	None
HIB	HSC	3	6.5" w x 12" d	57	None
HIC	HSC	3	6.5" w x 12" d	80.5	None
Large Block Pullout					
Series	Concrete Type	No. Specimens	No. Specimens	Specimen Length [in]	Notes
SMS - Block S	SCC	6	As Rec'd Strand	20	1/2" Special Strand
SMW - Block S	SCC	6	Single Wire	20	Center Wire from 1/2" Sp.
HMS - Block H	HSC	6	As Rec'd Strand	20	1/2" Special Strand
HMW- Block H	HSC	6	Single Wire	20	Center Wire from 1/2" Sp.
Flexural Beam Test					
Series	Concrete Type	No. Specimens	Specimen Cross Section	Specimen Length [in]	Shear Reinforcement
SF	SCC	3	6.5" w x 12" d	60	8 No. 3 Stirrups @ 7" o.c.
HF	HSC	3	6.5" w x 12" d	60	8 No. 3 Stirrups @ 7" o.c.

14.2. Phase 3 Test Setup

Pullout tests are conducted using a hydraulic through-hole jack inline with a calibrated load cell. A loading rate of 20kips/minute is used. After yielding or slip the pressure level is maintained until load carrying capacity decreases below 80% of the max capacity. The three tests are illustrated in Figure 78.

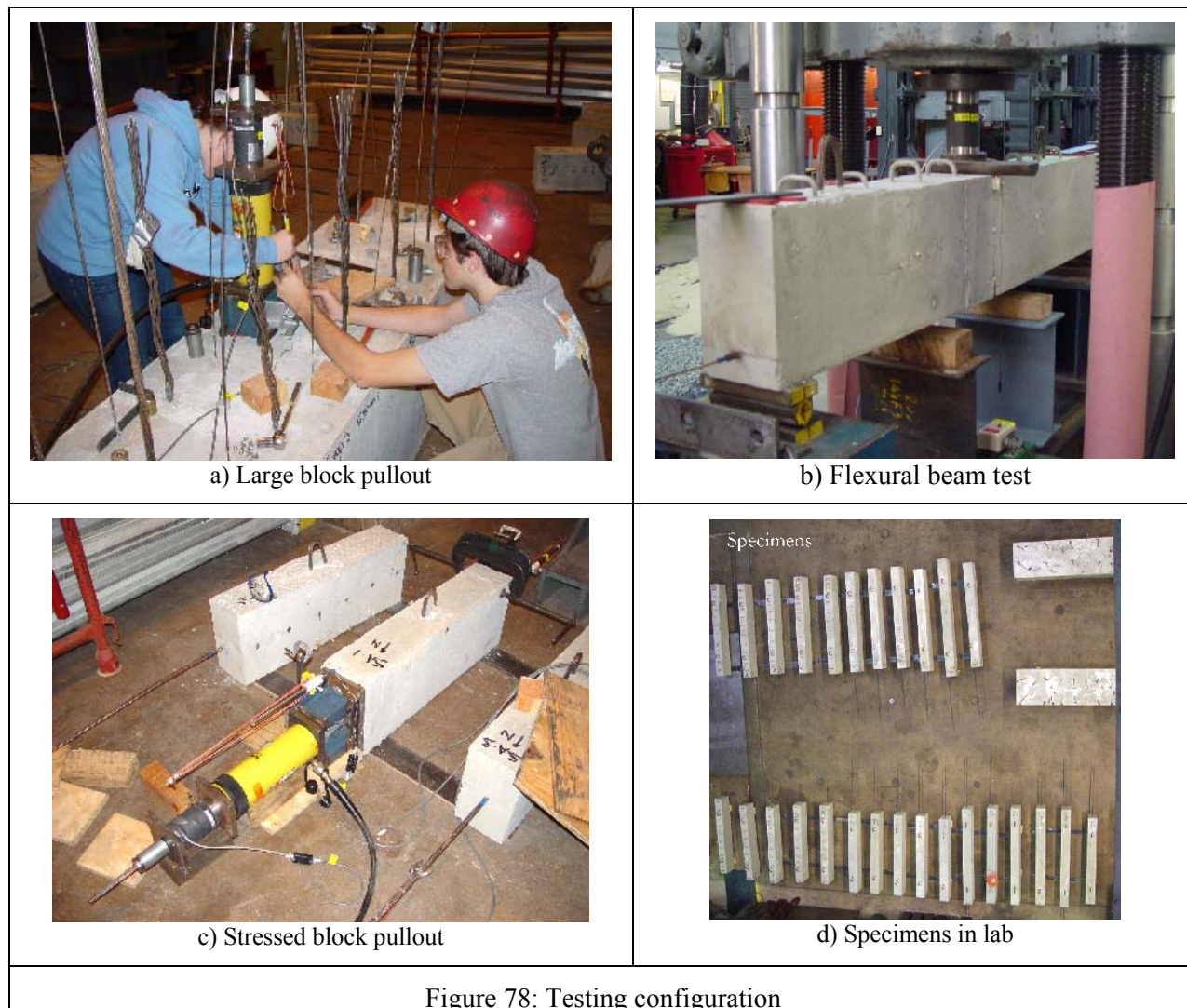


Figure 78: Testing configuration

14.3. Material Properties

The mix designs were comparable to the designs used in the bulb tee fabrication. The proportions were modified slightly to address oversights made during the initial bulb tee beam fabrication. Specifically, the SCC aggregate content was increased and the cement content was decreased, and the HESC cement content was increased. The changes made were less than 1% from the original.

14.4. Large Block Pullout Tests

Pullout tests have been completed on the large block specimens and small and medium size stressed blocks. The flexural beam tests have been completed. The long stressed blocks are being held until the results of the previously mentioned tests are thoroughly processed.

Preliminary review of the large pullout block indicates that the SCC and HESC materials provide comparable resistance to pullout. The load – slip response of the strands are presented in Figure 79. The SCC block is presented as solid lines and the HESC block as dashed lines. The response to pullout is consistent within each block and between the two concrete materials. Pullout of strand from the SCC block resulted in fracture for three of the five tests. All strands in the HESC block failed due to pullout. Preliminary results indicate that the SCC and HESC mix designs used provide comparable bond resistance.

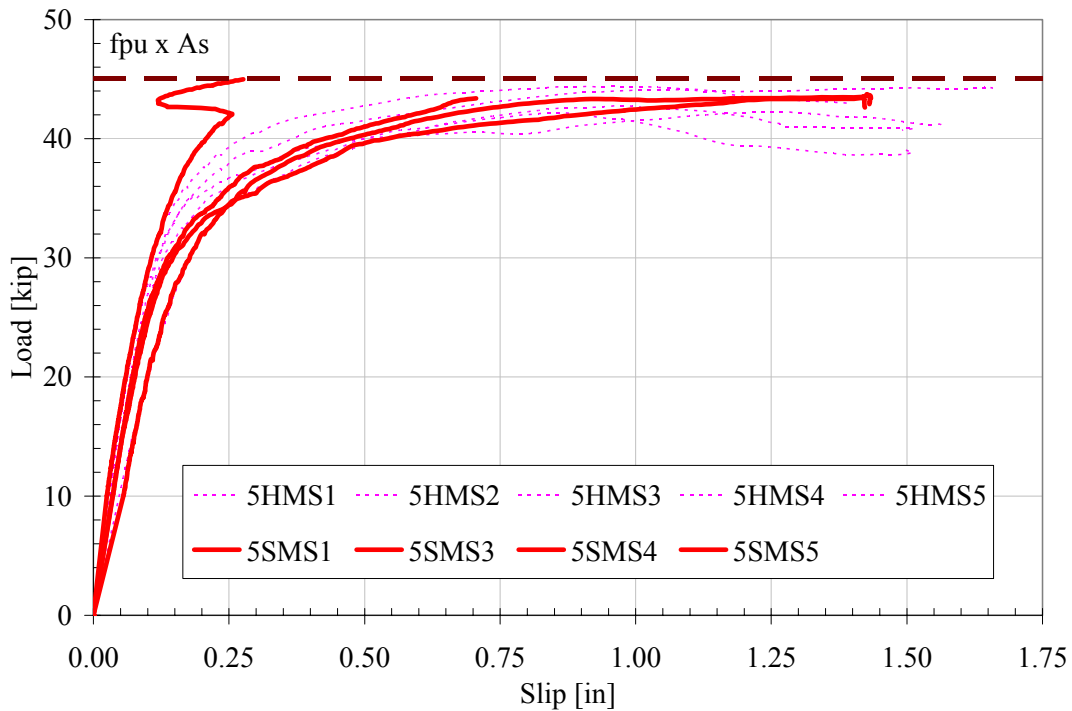


Figure 79: Load – slip response

It must be noted that the tests provide much greater consistency than the previously conducted large block pullout tests. This is most likely attributed to the age of the concrete. The original large block pullout tests were conducted when the concrete was only 25 hours old. While material tests indicate that the strength was 4000psi at the time of the pullout tests the large block may not have been fully cured. Consequently, variability in strength could be expected within the block and possibly along the strand. In the preceding tests the pullout was conducted after the concrete had achieved an age of 28-days. At this age the concrete could be assumed to have a uniform strength within the block. The variation of the pull out force in phase 3 was dramatically smaller than the variation in the first phase of testing. The consistency of the concrete properties throughout the pull out block has a great influence on the bond capacity in the pull out test.

14.5. Phase 3 Preliminary Conclusions

The results of this phase are not yet complete. Information on the relative bond strength of the various mechanisms is being investigated and will be released in a supplemental report.

15. PROJECT CONCLUSIONS

An evaluation on the use of self consolidating concrete (SCC) for structural prestressed-precast bridge beams was conducted. The study examined the material in a plastic and hardened state and the performance when used in conventional bridge bulb tee beams. To provide a baseline, the response was assessed relative to a conventional high early strength concrete (HESC) commonly used in precast bridge construction. The goals of the project were to assess the material from a mechanical and durability standpoint, to assess if the material would provide an economic advantage over conventional concretes, and to assess the performance when used in structural bridge members. These goals were achieved through a series of material tests, timed beam construction, and through ultimate load testing. Detailed conclusions can be made for each phase of the research program.

15.1. Mechanical and Durability of Concrete

The plastic and hardened concrete properties were thoroughly examined in the first phase of the research. The tests were conducted on the plastic concrete and through material testing of concrete cylinders and prisms. All hardened concrete samples were cured with the full scale beams or were match cured for the initial curing period. After this initial period, all specimens were cured according to ASTM requirements. The following conclusions can be made from the results of the first research phase:

- The SCC and HESC mix designs are typical of U.S. practice. Specifically the levels of GGBF slag cement and coarse aggregate quantities and gradations are within acceptance levels for PennDOT and most transportation authorities.
- Proportioning of the HESC and SCC mixes was well controlled. The batched weights were within 1% of the design proportions.
- Moderate levels of GGBF slag cement were used along with type III cement to reduce cost and enhance performance. The levels, 35% for HESC and 25% for the SCC, were within commonly used proportions.
- A crushed Diabase is used for coarse aggregate in both mixes. The relative hardness of the material should not compromise the structural performance of the concrete.
- The slump of the HESC was higher than the design expectations but was within the PennDOT limit of 8-inches.
- The spread of the SCC was lower than the design target, with a low of 20-in. and a high of 22.5-in. The mix however illustrated good stability and flow through reinforcement. No segregation of the mix was measured.
- The unit weights of the mixes were similar with the HESC having a marginally higher value. This can be attributed to the larger size coarse aggregate used in the mix.
- Batching temperatures were higher for the SCC due to the higher ambient temperature. The temperatures were within allowable levels.
- The time for initial set was 50 minutes longer for the SCC. The 5.2 hour and 6.3 hour setting times are within a reasonable range for precast operations.
- The time of set can be accurately predicted with a power function as detailed in section 7.5.3.
- Elevated curing temperatures on the order of 140°F were used during the initial 24 hours. This resulted in a rapid achievement of compressive strength. In addition, the initial cure resulted in a leveling of the strength up to 56-days followed by a late increase in capacity. The trends observed do not follow conventional ACI models for long-term strength gain.
- The SCC has a higher compressive strength than the HESC.

- The cylinder testing indicates that the SCC has a lower elastic modulus than the HESC. This contradicts in-situ testing.
- The tension capacities of the concretes are conservatively higher than ACI estimates. The direct tension capacity and modulus of rupture is higher in the SCC than HESC. The strengths are comparable when normalized to the square root of the compressive strength.
- The shrinkage characteristics of the concretes are less than ACI 209 estimates.
- The SCC has a marginally higher shrinkage than that of the HESC. Both shrinkage responses can be estimated by a standard formulation.
- The air contents of the plastic concretes were within design requirement of 5+/-1%.

The SCC and HESC meet all mechanical characteristics needed for use in precast prestressed beam production. The material test results indicate that both mixes should perform well when used in full scale beams.

15.2. Prestressing Strand

The strand used in the project was pre-qualified prior to fabrication of the bulb tee beams using conventional methods. The following observations were made during the prequalification process:

- Large block pullout tests of the strand resulted in an underperformance of the bond capacity when compared to recommendations available in the literature.
- Considerable variability was observed in the large block pullout tests. The test should be modified to allow for greater repeatability. This could be achieved through smaller pullout samples which would allow the concrete to cure in a uniform manner.
- The bond capacity of the strand was 31.46 kips or 1.06 kips/in² of surface area.
- A design bond stress was computed from the pullout data. A bond stress capacity of 790 psi is recommended for this group of strand.
- The average bond capacity was less than the accepted value of 37.4 kips.
- The length required for development of the full tensile strength of the strand was less than the transfer length using the average bond strength.
- The length required for development of the full tensile strength of the strand was less than the transfer length using the 5th percentile bond strength.

Based on these results and favorable past experience with the strand by the precast producer, the decision was made to go forward with use of the strand in the full scale bulb tee test program. In-situ measurement of transfer length and slip is performed and reported in the following sections. Combinations of both strand heats were used for fabrication of the beam section.

15.3. Nondestructive Assessment of Beam

Nondestructive evaluation of the beam indicates that the in-situ properties of the beam may be contrary to material test data. Conclusions made from non-destructive evaluation of the beam are summarized in the following bullets:

- The measured camber and elastic shortening of the beams indicate that the SCC is stiffer than the HESC. This contradicts the laboratory tests conducted on cylinders which indicated that the SCC was more flexible.

- The length required for transfer of initial prestress is shorter than that expected from standard PCI formulations. This indicates that the concrete to strand bond properties are within code expectations. Long term monitoring of this trend should be conducted through additional research.
- The transfer length required for both the HESC and the SCC compare well with each other. This indicates that the SCC could be expected to provide strand to concrete bond properties similar to HESC.
- The losses measured in the beam sections are less than code estimations. Furthermore, the SCC exhibits less loss than the HESC. Consequently, use of codified losses will provide a conservative estimate of the beam capacity.
- The expected shear and flexural capacities increase as a result of the as-built concrete strengths and effective prestress.

15.4. Economic Viability

The use of SCC results in a marginal increase in production costs for large scale bulb-tee construction based on the production times measured. These costs were based on the times measured for a labor crew inexperienced with the use of SCC (first time placement). It is highly likely that training would progress at a rapid rate with repeated use and in turn provide significant cost benefits. In addition the material provides comparable surface finishes to standard HESC mixes without vibration. Full adoption of SCC in the precast plant would significantly reduce the daily operation noise levels thus enhancing the work environment. Furthermore, additional costs would be recouped by eliminating the need to purchase, maintain, and use vibratory equipment. On a larger scope, the fluidity of the SCC mix would also allow architectural finishes to be incorporated directly into the structural member, allowing for greater opportunities for structural precast in the bridge market.

The limited cost-benefit study indicates that SCC has good promise in achieving savings in precast production. It is recommended that further research be conducted to comprehensively assess the savings. If the opportunity arises a long term study should be conducted in line with a plant transitioning from HESC to SCC.

15.5. Ultimate Strength of Bridge Beams

The destructive testing of the bulb tee beams indicate that SCC and HESC perform well in structural applications under a variety of demands. In particular the following conclusions can be made from the discussion presented in this report:

- Use of the global elastic load deformation of the beams to compute the in-situ modulus does not provide enough repeatability to make sound conclusions. This method of evaluation may not be accurate enough for large size beams.
- The elastic modulus measured using surface mounted strain gages and the applied load indicated that the SCC had a higher in-situ modulus than the HESC. This is in support of the conclusions of the camber measurements and the strains measured during transfer of prestress.
- The apparent cracking moment exceeds conventional predictions.
- The SCC in all cases provided greater ductility than the HESC.
- The SCC and HESC exceeded the nominal design strengths for all conventional beam failure modes. The design strengths were exceeded for a shear failure mode, flexural compression failure mode, and flexural tension failure mode.
- Observed progression of damage was consistent between the SCC and HESC beams tested under the same conditions.

- Measured end slip was observed on all but the reduced beam sections. Slip occurred in a non-symmetric manner about the section with slip on some stands and none on others.
- In all cases a minimal slip less than 0.05-in. was observed.
- Strand slip initiated with inelastic deformation of the beam. Load carrying capacity increased after slip initiated.
- Slip was observed in the beam with the full development length and the beam with the reduced development length. This can be attributed to the formation of shear cracks. It is the opinion of the authors that these cracks result in end slip due to section compatibility.
- In the reduced section tests no slip occurred. From these measurements it can be concluded that the SCC and HESC provides adequate bond characteristics to prevent slip when using a full development length.

A third research phase is underway to evaluate the contributions of various bond mechanisms on the total resistance to strand pullout. The results of this program will be presented in a supplemental report.

15.6. Summary Conclusions

The research results indicate that the self consolidating concrete studied provides mechanical characteristics that outperform current recommendations. The material test results and accompanying large-scale tests indicate that SCC is a viable material for construction of prestressed bridge beam members.

It is important to note that the research program was conducted on a particular mix design using proprietary admixtures. The conclusions drawn in the research are with respect to the mix studied. Alternate mixes should be investigated independently.

16. SCC CODE RECOMMENDATIONS

Code adoption will require three topics to be addressed:

- 1) Mechanical property estimates for design.
- 2) Quality Control Methods
- 3) Quality Assurance Methods

SCC provides adequate structural properties that meet the needs of bridge construction. As with all concretes these properties vary from batch to batch and in some circumstances may fall out of the specified levels. To address this reality, mechanical properties of SCC mixes should be verified at regular intervals and when the mix design is altered.

In general, current codes provide conservative estimates for the mechanical properties of SCC. Use of ACI estimates for tension and compression strength, elastic modulus, and creep and shrinkage under predict actual properties. Continued reliance on these estimators will result in a conservative nature to design. With greater use more appropriate estimators should be developed. An example of equations for modulus of rupture and shrinkage and creep are included within the report as an example.

Durability properties must be investigated for all new mixes through a series of freeze thaw tests. Reliance on air void characteristics may also assist with the evaluation however the results should only be used as a guide. The standard air void acceptance values were based on normal strength concrete made from type I cement. High performance concretes such as SCC do not necessarily correlate to the older air void acceptance values, therefore SCC must be examined directly through freeze thaw testing. This should be noted in any new code change.

PennDOT [Horwhat 2005] envisions that changes will be made to both Sections 714 for precast concrete and 1107 for prestressed concrete. For prestressed concrete, revisions to Section 1107.03(d) 5 Concrete would be required. The revisions would specify the additional tests required for both mixture qualification and then subsequently for production testing. Quality control during plant batching will be addressed using standardized plastic material tests. ASTM has standards which are currently being balloted for the spread test, J-ring and column segregation which would likely be referenced. Although Section 1001 or even 704 may ultimately be revised for use of SCC for cast in place applications, plant fabricated materials may precede changes to these sections.

17. FUTURE WORK

While the presented research provides a comprehensive study of SCC for use in prestressed bridge beam construction further examination of a few topics is recommended to supplement this work.

Future research should include:

- 1) The research was conducted on a particular SCC mix design. To properly assess the material, similar studies should be conducted on other SCC mix design based on different constituent proportions.
- 2) Alternate admixture chemicals should be studied to ensure that the performance gained for the tested mix is also achievable if other brands are used.
- 3) Freeze thaw resistance of the mixes must be studied in greater detail. This should involve variation in AEA content, HRWR type, and supporting hardened material tests.
- 4) Fatigue tests should be conducted to assess the potential for bond loss in SCC subjected to repeated loading.
- 5) Long term chloride permeability tests should be conducted to examine the sensitivity to corrosion when using SCC.

18. REFERENCES

ACI Committee 209, "Prediction of Creep, Shrinkage, and Temperature Effects in Concrete Structures (ACI 209R-92)," American Concrete Institute, Farmington Hills, Mich., 1998, 47 pp.

ACI 318-02, *Building Code Requirements for Structural Concrete and Commentary*. American Concrete Institute, 2002.

AASHTO LRFD, "Bridge Design Specifications," American Association of State Highway and Transportation Officials, Washington, DC, 2000.

AASHTO "T96-02 Method of Test for Resistance to Degradation of Small-Size Coarse Aggregate by Abrasion and Impact in the Los Angeles Machine," American Association of State Highway and Transportation Officials, Washington, DC, 2001.

---. "T259 Method of Test for Resistance of Concrete to Chloride Ion Penetration," American Association of State Highway and Transportation Officials, Washington, DC, 2000.

Assaad, J., Khayat, K., H., Daczko, J., "Evaluation of Static Stability of Self Consolidating Concrete," ACI Materials Journal, V.101, No.3, May – June, 2004, pp 207-215.

ASTM International. "C31/C31M-00 – Standard Practice for Making and Curing Concrete Tests Specimens in the Field," West Conshohocken, PA. 2000.

---. "C39/C39 – Compressive Strength of Cylindrical Concrete Specimens," West Conshohocken, PA: 2004.

---. "C78 – Flexural Strength of Concrete (Using Simple Beam with Third-Point Loading)," West Conshohocken, PA: 2000.

---. "C131/C131M – Standard Test Method for Resistance to Degradation of Small-Size Coarse Aggregate by Abrasion and Impact in the Los Angeles Machine," West Conshohocken, PA: 2001.

---. "C138/C138M – Standard Test Method for Density (Unit Weight), Yield, and Air Content (Gravimetric) of Concrete," West Conshohocken, PA: 2001.

---. "C143/C143M – Standard Test Method for Slump of Hydraulic Cement Concrete," West Conshohocken, PA: 2003.

---. "C403/C403 M – Standard Test Method for Time of Setting of Concrete Mixture by Penetration Resistance," West Conshohocken, PA: 2002.

---. "C457 – Microscopical Determination of Parameters of the Air-Void System in Hardened Concrete," West Conshohocken, PA: 1998.

---. "C469 – Static Modulus of Elasticity and Poisson's Ratio of Concrete in Compression," West Conshohocken, PA: 1994.

---. "C496 – Splitting Tensile Strength of Cylindrical Concrete Specimens," West Conshohocken, PA: 1996.

---. "C512 – Creep of Concrete in Compression," West Conshohocken, PA: 1994.

---. "C666 – Resistance of Concrete to Rapid Freezing and Thawing," West Conshohocken, PA: 1997.

---. "C1064/C1064M – Standard Test Method for Temperature of Freshly Mixed Portland Cement Concrete," West Conshohocken, PA 2001.

---. "C1202 – Standard Test Method for Electrical Indication of Concrete's Ability to Resist Chloride Ion Penetration," West Conshohocken, PA: 2003.

Attigbo, E.K., Nmai, C.K., and Gay, F.T., "Air-Void System Parameters and Freeze-Thaw Durability of Concrete Containing Superplasticizers - A Summary of Research Findings," *ACI Concrete International, Construction*, Vol. 14, No. 7, July 1992, pp. 57-61.

Chan, Y., Chen, Y., Liu, Y., "Development of Bond Strength of Reinforcement Steel in Self-Consolidating Concrete," *ACI Structural Journal*, V. 100, No.4, July-Aug., 2003, p.490-498.

Commonwealth of Pennsylvania Department of Transportation, "PA Test method 623- Method of Test for Air Content of Hardened Concrete," www.dot.state.pa.us, June 2003.

Commonwealth of Pennsylvania Department of Transportation, "Publication 408/2003 - Specifications," www.dot.state.pa.us, October 2004.

Commonwealth of Pennsylvania Department of Transportation, "Publication #34 – Bulletin #14 Approved Aggregate Producers 2004 Edition," Harrisburg, PA, January 2004.

Commonwealth of Pennsylvania Department of Transportation, "PennDOT LRFD P/S Concrete Girder Design and Rating Program, PSLRFD Version 2.0," Harrisburg, PA, September 2002.

Daczko, J., A., "Stability of Self-Consolidating Concrete, Assumed or Ensured?," Conference Proceedings: First North American Conference on the Design and Use of Self-Consolidating Concrete, Master Builders, November 12-13, 2002.

Geiseler, J., Kollo, H., and Lang, E., "Influence of Blast Furnace Cements on Durability of Concrete structures," *ACI Materials Journal*, V.92, No.3, May-June 1995, pp.252-257.

Goodier, Chris I. "Development of self-compacting concrete," *Proceedings of the Institution of Civil Engineers, Structures & Buildings* 156. Issue SB4, Nov 2003, pp. 405-414.

Goodspeed, C. H., S. Vanikar, and R. A. Cook, "High-Performance Concrete Defined for Highway Structures," *Concrete International*, 1996, Feb, Vol. 18, No. 2, pp. 62-67

Hoyer, E. and Friedrich, E., 1939, :Beitrag Zur Frage der Haftspannung in Eisenbetonbauteilen ("Contribution to the question of Bond Stress in Reinforced Concrete Elements"), *Beton und Eisen*, V. 38 Mar. 1920 pp.107-110 (in German).

Huo, X. S., Al-Omaishi, N., and Tadros, M. K., "Creep, Shrinkage, and Modulus of Elasticity of High-Performance Concrete," *ACI Materials Journal*, V.98, No.6, Nov.-Dec. 2001, p.440-449.

Jeanty, P. R., Mitchell, D., and Mirza, S. M., 1988, "Investigation of Top Bar Effects in Beams," *ACI Structural Journal*, Vol.85, No.3, May-June, pp.251-257.

Khayat, K., H., Assaad, J., "Air-void Stability in Self-consolidating Concrete," *ACI Materials Journal*, V.99, No.4, July - August, 2002, pp 408-416.

Khayat, Kamal. "Viscosity-Enhancing Admixtures for Cement-Based Materials – An Overview," *Cement and Concrete Composites*, no 20, 1998, pp 171-88.

Kosmatka, S., H., Panarese, W., C., "Design and Control of Concrete Mixtures," 13th Edition, Portland Cement Association, Skokie, Ill, 1990, p.205..

Logan, D., R., 1997, "Acceptance Criteria for Bond Quality of Strand for Pretensioned Prestressed Concrete Applications," *PCI Journal*, V. 42 No.2, Mar-Apr., pp. 52-90.

New Jersey DOT, "Standard Specifications for Road and Bridge Construction," 2001, <http://www.state.nj.us/transportation/eng/specs/Road&Bridges/English/EnglishStandardSpecifications.htm>

PCI FAST Team, "Interim Guidelines for the Use of Self-Consolidating Concrete in Precast/Prestressed Concrete in Precast/Prestressed Concrete Institute Member Plants," TR-6-03, PCI, April 2003, pp.88.

- Precast / Prestressed Concrete Institute. "Precast Prestressed Concrete Bridge Design Manual," Chicago: 1997.
- Precast / Prestressed Concrete Institute FAST Team, "Interim Guidelines for the Use of Self-Consolidating Concrete in Precast/Prestressed Concrete in Precast/Prestressed Concrete Institute Member Plants," TR-6-03, PCI, April 2003, pp.88.
- Popovics, S., 1971, "Physical Aspects of the Setting Time of Portland Cement Concrete," Journal of Materials, JMLSA, Vol.6, No.1, March, pp.150-162.
- Seamus F. Freyne, Bruce W. Russell, and Thomas D. Bush, Jr., "Heat Curing of High-Performance Concrete Containing Type III Cement," ACI Materials Journal, V.100, No.6, Nov.-Dec. 2003, p.449-454.
- Shi, C., Stegemann, J., A., and Caldwell, R., J., 1998, "Effect of Supplementary Cementing Materials on the Specific Conductivity of Pore Solution and Its Implications on the Rapid Chloride Permeability Test (AASHTO T277 and ASTM C1202)," ACI Materials Journal, Vol.95, No.4, July, 1998, p.389-394.
- Siebel, E., 1989. *Air-Void Characteristics and Freezing and Thawing Resistance of Superplasticized Air-Entrained Concrete with High Workability*. Proceedings of the Third CANMET/ACI International Conference on Superplasticizers and Other Chemical Admixtures in Concrete, Oct, Ottawa, Canada; Ed. by V. M. Malhotra; American Concrete Institute, Detroit, MI, pp. 297-319. (ACI SP-119)
- Sivasundaram, V., Malhorta, V., M., "Properties of Concrete Incorporating Low quantity of cement and High Volumes of Ground Granulated Slag," ACI Materials Journal, V. 89, No.6, Nov.-Dec. 1992, p. 554-563.
- West Virginia DOT Division of Highways, "Standard Specifications Roads and Bridges," 2000. Charleston, West Virginia, 2000.
- Zia, P., Ahmad, S., and Leming, M., "High-Performance Concretes A State-of-Art Report (1989-1994)," FHWA-RD-97-03, <http://www.tfhrc.gov/structur/hpc/hpc2/contnt.htm> Accessed October 2004.